

GEOLOGY OF THE POTTERDOAL DEPOSIT, MUNRO TWP., ONTARIO

**GEOLOGY, PETROLOGY AND GEOCHEMISTRY OF THE POTTERDOAL
Cu-Zn DEPOSIT, KIDD-MUNRO ASSEMBLAGE , MUNRO TOWNSHIP,
ONTARIO**

By

MARK STEVEN EPP, B.Sc. (Hons)

A Thesis

Submitted to the School of Graduate Studies

in Partial Fulfillment of the Requirements

for the Degree

Master of Science

McMaster University

(c) Copyright by Mark Steven Epp, September 1997

Abstract

The Potterdoal volcanogenic massive sulphide deposit is hosted by a tholeiitic/komatiitic succession located in northern Munro Township, Ontario. An integrated surface and drill core study of this property was undertaken to document the three dimensional structure and stratigraphy of the deposit. Petrography focused on mineralogical changes associated with the hydrothermal alteration within specific units. Several geochemical methods were used to determine the effects of hydrothermal alteration (as quantified by elemental mobility) as well as source magma affinities and tectonic setting. Based on this information, a model for ore genesis was developed.

The Potterdoal deposit is hosted by volcanic rock of an iron tholeiite affinity, emplaced within an ocean floor rifting environment. The chemistry of the tholeiites shows similarities to that of large deposits like Kidd Creek, but lacks the felsic component of bimodal volcanism. It is suggested that felsic volcanics are absent because the local crust did not achieve sufficient thickness to allow partial melting of lower crustal material.

The deposit consists of a stockwork zone overlain by an extensive massive sulphide lens which lies along a scarp structure defined in the paleosurface. Stockwork mineralization is narrowly confined to conduits within a fault breccia in the footwall Ore Flow gabbro, and widens into an overlying tectonic breccia. Sulphide paragenesis

appears to be controlled by the thermal solubilities of the sulphide minerals, and consists of pyrite, sphalerite, pyrrhotite and chalcopyrite in both stockworks and the massive sulphide lens. The lens occurs at the top of the tectonic breccia near the paleo-seawater interface, and formed by direct replacement of the tectonic breccia. The lens locally exhibits ore grade base metal values (i.e. combined Cu and Zn content of at least 3%), and shows an upward and outward gradation from chalcopyrite to sphalerite-dominated ore. These features suggest that exhalation of the hydrothermal system was focused into local vent sites.

Mass change associated with the hydrothermal alteration envelopes surrounding Ore Flow fault breccia conduits involve loss of Si, Ca, Na and Sr, and gain of Fe, Mg, K, Cu and Zn. These changes are attributed to fluid-rock reactions which are consistent with hydrothermal alteration associated with other VMS deposits,

The genetic model suggested for the Potterdoal deposit involves a hydrothermal system driven by heat from the intrusion of the Munro-Warden Sill at a high stratigraphic level. The relatively small size of the deposit is probably due to the rapid cooling of the sill, which shortened the life-span of the hydrothermal system. The primary source of metals was the upper portion of the Munro-Warden Sill, as indicated by the high degree of pervasive hydrothermal alteration of this part of the gabbro.

Drill core information has also revealed the importance of the Buster Fault in the construction of the currently exposed Potterdoal stratigraphy. Thrusting subparallel to bedding along the Buster Fault during the Kenoran compressional event (~ 2.6 Ga) was

responsible for the local repetition of tholeiitic flows, and has effectively removed the deep footwall rocks originally associated with the Potterdoal mineralization.

Acknowledgments

I would like to express my greatest gratitude to Dr. James H. Crocket, for providing me with a fascinating project, giving me guidance when I needed it, letting me run with it once I had figured things out, and for showing me lots of patience during the prolonged period it took me to finish.

I would like to thank Dr. Dave Good, whose wide ranging discussions provided me with a focus for my thesis work. I would also like to thank Dr. Paul M. Clifford, who helped me grasp some of the finer points of Archean volcanology.

Numerous discussions at the early stages of this project with Dr. J. Andy Fyon of the O.G.S. and Dr. C. Tucker Barrie of the G.S.C. is also gratefully acknowledged.

Permission for access to the drill core and the Potterdoal property was graciously provided by Granges Inc. and Buster McChristie. Extremely helpful information was also provided by Granges Inc. Project Geologists Todd Keast and Heather Miree.

Much thanks is given to Jack Whorwood for his expert photographic services and assistance, Len Zwicker for his abundant thin section work, and Dave “Junior” Leng for his assistance out in the bug and bear infested climes of northeastern Ontario.

I would finally like to thank my friends, Jodie Smith, Richard McLaughlin, Trevor Bohay and Tim Schwartz, for the endless coffee breaks, multi-disciplinary discussions, soup lunches and Q.O.L.’s.

This research was financially supported by the Natural Sciences and Engineering Research Council grant provided through Dr. James H. Crocket.

This work is dedicated in loving memory to my father, Wayne Andrew John Epp,
who taught me independence and dedication, and filled me with the wonder
of the north.

... There's gold and it's haunting and haunting;
It's luring me on as of old;
Yet it isn't the gold that I'm wanting
So much as just finding the gold.
It's the great, big, broad land 'way up yonder,
It's the forests where silence has lease;
It's the beauty that thrills me with wonder,
It's the stillness that fills me with peace.

(From Robert Service's 'The Spell Of The Yukon')

Table of Contents

	Page
Abstract	iii
Acknowledgments	vi
Dedication	vii
Table Of Contents	viii
List of Figures	x
List of Tables	xi
List of Photographic Plates	xi
Chapter 1: Introduction and Objectives	1
1.1 Introduction	1
1.1.2 Previous Academic Work	3
1.1.3 Location and Access	5
1.1.4 Mining History	7
1.2 Objectives	8
Chapter 2: Field and Laboratory Methodologies	9
2.1 Field Work	9
2.2 Petrology	10
2.3 Geochemistry	11
2.3.1 Sample Preparation	11
2.3.2 Instrumental Neutron Activation Analysis	12
2.3.3 X-Ray Fluorescence Analysis	15
2.3.3.1 Analysis Of Major Oxides	16
2.3.3.2 Analysis of Trace Elements	17
Chapter 3: Regional and Local Geology	19
3.1 Regional Setting	19
3.2 Local Structure	23
3.3 General Lithologies	25
3.4 Metamorphism	29

	Chapter 4: Mine Site Geology	30
4.1	Mine Site Stratigraphy	30
4.2	Structure and Associated Rock Textures	37
4.2.1	The Buster Fault	37
4.2.2	Three-Dimensional Diamond Drill Model and The Fault Scarp Structure	42
4.2.3	Tectonic Breccias	52
4.2.4	Fault Breccias	52
	 Chapter 5: Petrography of Major Stratigraphic Units	54
5.1	Introduction	54
5.2	Upper Munro-Warden Sill	56
5.3	Theo's Flow Tholeiites	58
5.4	Ore Flow Tholeiites	58
5.4.1	Ore Flow Gabbro	58
5.4.2	Ore Flow Basalts	65
5.5	Sedimentary Rocks	67
5.6	Komatiites	71
	 Chapter 6: Sulphide Petrography and Associated Alteration	76
6.1	Sulphide Mineralization	76
6.2	Stockwork Mineralization	77
6.3	Sulphide Lens Mineralization and The Vent Proximal Setting	82
6.4	Hydrothermal Alteration and Metal Source	87
6.4.1	Progressive Alteration of The Ore Flow Gabbro	88
6.4.2	Metal Source	94
	 Chapter 7: Geochemistry	96
7.1	Introduction	96
7.2	Major Element Discriminator Plots	99
7.3	Trace Element Discriminator Plots	101
7.4	Rare Earth Elements	104
7.5	Mass Balance Of Progressive Hydrothermal Alteration	111
	 Chapter 8: Discussion	116
8.1	Tectonic Setting	116
8.2	Ore Deposit Model -- A Genetic Summary	117
8.3	Comparison Of The Potterdoal Deposit with the Potter Mine Deposit ..	122

	Chapter 9 : Conclusions	128
9.1	Genetic Summary Of The Potterdoal Deposit	128
	References	130
Appendix A	Sample Descriptions and Locations	134
Appendix B	Precision and Accuracy Calculations For XRF and INAA Data	139

List of Figures

Figure		Page
1-1	Location of Munro Township within the Abitibi Greenstone Belt	4
1-2	Field mapping locations Within Munro Township	6
3-1	Geology map of the northwest Black River-Matheson area	20
3-2	Two stratigraphic sub-divisions for the rocks of the Munro Township area	21
3-3	Geochronologic sub-division of southwestern Abitibi Subprovince	22
3-4	Regional aeromagnetic map of the Munro Township area	24
3-5	Regional geologic map of the Munro Township area	26
3-6	Location map of the main gabbroic sills	28
4-1	Composite stratigraphic section of the Potterdoal deposit	31
4-2	Surface geology of the Potterdoal deposit	32
4-3	Isoclinal folding model for the McCool Hill syncline	38
4-4	Model for structural repetition within the Potterdoal map area	41
4-5	Geological cross sections constructed from surface drilling	44
4-6	Surface geology map overlying the cross sections shown in Figure 4-5	45
4-7	Three dimensional structural model of the Potterdoal stratigraphy	46
4-8	Stereo net plot defining the sub-surface fault scarp structure	48
4-9	Detailed structural map overlying the sub-surface fault scarp	50
6-1	Sulphide paragenesis diagram	78
6-2	Drill intersection longsection for the Potterdoal sulphide lens	83
6-3	EDS elemental spectrum K-feldspar grains	92
7-1	Jensen cation plot	100
7-2	Tholeiitic/calc-alkaline volcanic affinity plot	102
7-3	Ti-Zr-Y Pearce plot	103
7-4	Ti-Zr-Sr Pearce plot	105

7-5	Normalized rare earth element profiles for various units	106
7-6	Y vs. Zr plot	108
7-7	Zr/Y vs. Y diagram	110
7-8	Mass change diagrams for increasingly altered Ore Flow gabbro	112
8-1	Conceptual model of the Potterdoal deposit	118
8-2	Geology map of the Mangan showing	125
A-1	Potterdoal area surface sample location map	137

List of Tables

Tables		Page
2-1	Irradiation schedule for INAA	14
5-1	Petrographic description of rock units	55
7-1	Geochemical composition of surface and drill core rock samples	97
7-2	Recommended average rare earth element chondrite values	107
A-1	Abbreviated diamond drill logs showing sample locations	138
B-1	Precision and accuracy calculations for XRF data	140
B-2	Precision and accuracy calculations for INAA data	142
B-3	Precision calculations for triplicate samples	143

List of Photographic Plates

Plates		Page
1-1a	The Kidd Creek Mine located northeast of Timmins, Ontario.....	2
1-1b	The Potterdoal Mine, Northern Munro Twp, Ontario.....	2
4-1	Tectonic breccia consisting of tuffaceous and cherty fragments.....	36
4-2a	The surface expression of the Buster Fault.....	40
4-2b	The Buster Fault intersected in core.....	40
4-3	Sheared massive sulphide ore with rotated clast.....	43
4-4	Outcrop of Ore Flow gabbro showing stepped erosional surfaces.....	51

4-5	Ore Flow gabbro with mineralized, flat dipping joints.....	51
5-1	Leucogabbroic phase of the Munro-Warden Sill in outcrop.....	57
5-2	Munro-Warden Sill leucogabbro showing hydrothermal vein networks.....	57
5-3	Photomicrograph of Munro-Warden Sill leucogabbro.....	59
5-4	Pillow structures located within Theo's Flow.....	59
5-5	Ore Flow gabbro in outcrop.....	61
5-6	Flow top breccia found along the top of the Ore Flow gabbro.....	61
5-7a	Fault breccia exposed on surface.....	62
5-7b	Fault breccia in core showing incipient brecciation.....	62
5-7c	Strongly developed fault breccia in core.....	62
5-8	Photomicrograph of the least altered Ore Flow gabbro.....	64
5-9	Transitional phase between Ore Flow gabbro and basalt.....	66
5-10	Variolitic pillows at the western most end of the Ore Flow.....	66
5-11a	Photomicrograph of Ore Flow basalt showing plumose textured plagioclase.....	68
5-11b	Photomicrograph of Ore Flow basalt showing dendritic clinopyroxene.....	68
5-12	Photomicrograph of graphitic chert.....	70
5-13	Core samples showing framboidal pyrite nodules within graphitic cherts.	70
5-14a	Crystal tuff in outcrop, showing fine rhythmic layering.....	72
5-14b	Core sample of crystal tuff.....	72
5-14c	Photomicrograph of graded bedding within tuff.....	72
5-15	Weathering habit of peridotitic komatiites.....	73
5-16	Polygonal jointing in peridotitic komatiites.	73
5-17a	Photomicrograph of peridotitic komatiite.....	75
5-17b	Photomicrograph of picritic komatiite.....	75
6-1	Tectonic breccias with sulphide veinlets.....	81
6-2	A vertical drill core transect of the sulphide ore lens.....	81
6-3a, b	Relict replacement textures of tectonic breccia fragments.....	84
6-4a, b, c	Reflected light photomicrographs of a vertical transect through a massive sulphide ore zone.....	86
6-5	Core samples showing progressive hydrothermal alteration of Ore Flow gabbros.....	89
6-6a, b, c	Photomicrographs showing progressive hydrothermal alteration of Ore Flow gabbros.....	90
6-7	Photomicrograph of epidote in hydrothermally altered fractures.....	93

Chapter 1

Introduction and Objectives

1.1 Introduction

Within the Abitibi Greenstone Belt, empirical observation has associated major volcanogenic massive sulphide (VMS) deposits with hydrothermally altered Archean felsic volcanics (Spence and De Rosen-Spence, 1975; Franklin et al., 1981; Lydon, 1988). This observation has led to the discovery of numerous large deposits including the Kidd Creek, Noranda, Mattagami and Kamiskotia camps. However, there are some VMS deposits which do not conform with this historically noted felsic volcanic association. These deviant deposits have been conspicuously noted in the literature (Fyon et al., 1992; Barrie et al., 1993), but have received only minimal study due to their relatively small size. The stratigraphic association of these deposits is dominated by mafic, tholeiitic to komatiitic assemblages, with little or no felsic component present. Some deposits of this nature are interpreted to occur within stratigraphic and temporally equivalent rocks of the considerably larger Kidd Creek deposit (Plate 1-1a), and appear to have formed within a related tectonic environment.

Plate 1-1a The Kidd Creek Mine located northeast of Timmins, Ontario.

Plate 1-1b The Potterdoal Mine, Northern Munro Twp, Ontario. The fenced off area encloses the original inclined shaft, which was subsequently open pitted.

a)



b)



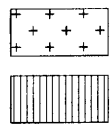
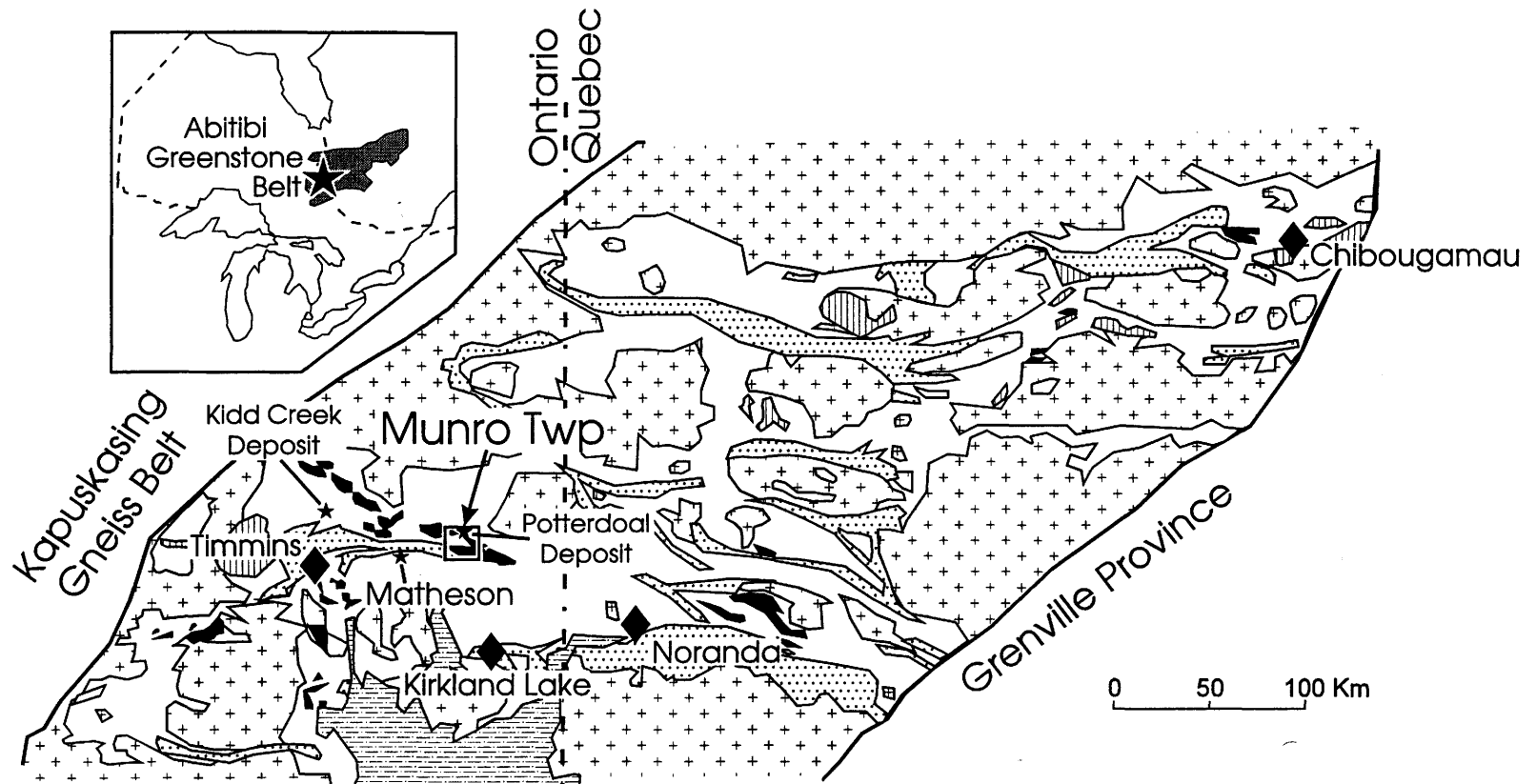
The long abandoned Potterdoal Mine (Plate 1-1b) is one of these mafic associated deposits, and is located in north-central Munro Township, approximately 39 km by road east of the nearest town of Matheson, Ontario (Figure 1-1).

1.1.2 Previous Academic Work

A large body of academic research has been performed on the rocks of the Munro Township area; however as previously stated, very little of this work was focused on the local base metal deposits. Initial mapping of the Munro Township area was completed in 1912, after several small gold deposits were discovered in the southwestern corner of the township. The first comprehensive work describing the geology of the Munro area was undertaken by Jack Satterly (1952). In this study, Satterly determined the dominant structural feature of the township to be a large, east-west trending syncline, referred to as the Munro Syncline, which runs across the northern half of the township. Most of the following work then concentrated on petrologic studies, which examined the layered intrusives and especially the komatiitic flows for which Munro Township is world known (MacRae, 1963, 1969; Pyke et al., 1973; Fleet and MacRae, 1975; Arndt, 1975; Arndt et al., 1977; Arth et al., 1977; Arndt and Nesbitt, 1982, 1984). A re-interpretation of the local scale regional geology west of Lake Abitibi was most recently compiled by Robert Johnstone in 1991. Johnstone's study contains the most ambitious and thorough coverage of structural geology and tectonic setting of the Munro Syncline structure.

Similar to the petrologic studies, most economically oriented studies have been concentrated on the "Kambalda type" nickel, PGE and gold potential of komatiitic and

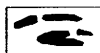
Figure 1-1 Location of Munro Township within the Abitibi Greenstone Belt (modified from Goodwin and Ridler, 1970). Locations identified by large diamonds indicate major gold and base metal mining camps within the Abitibi Subprovince.



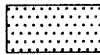
Granitic Rocks



Mafic Intrusions



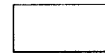
Ultramafic Rocks



Archean Sediments



Proterozoic Sediments



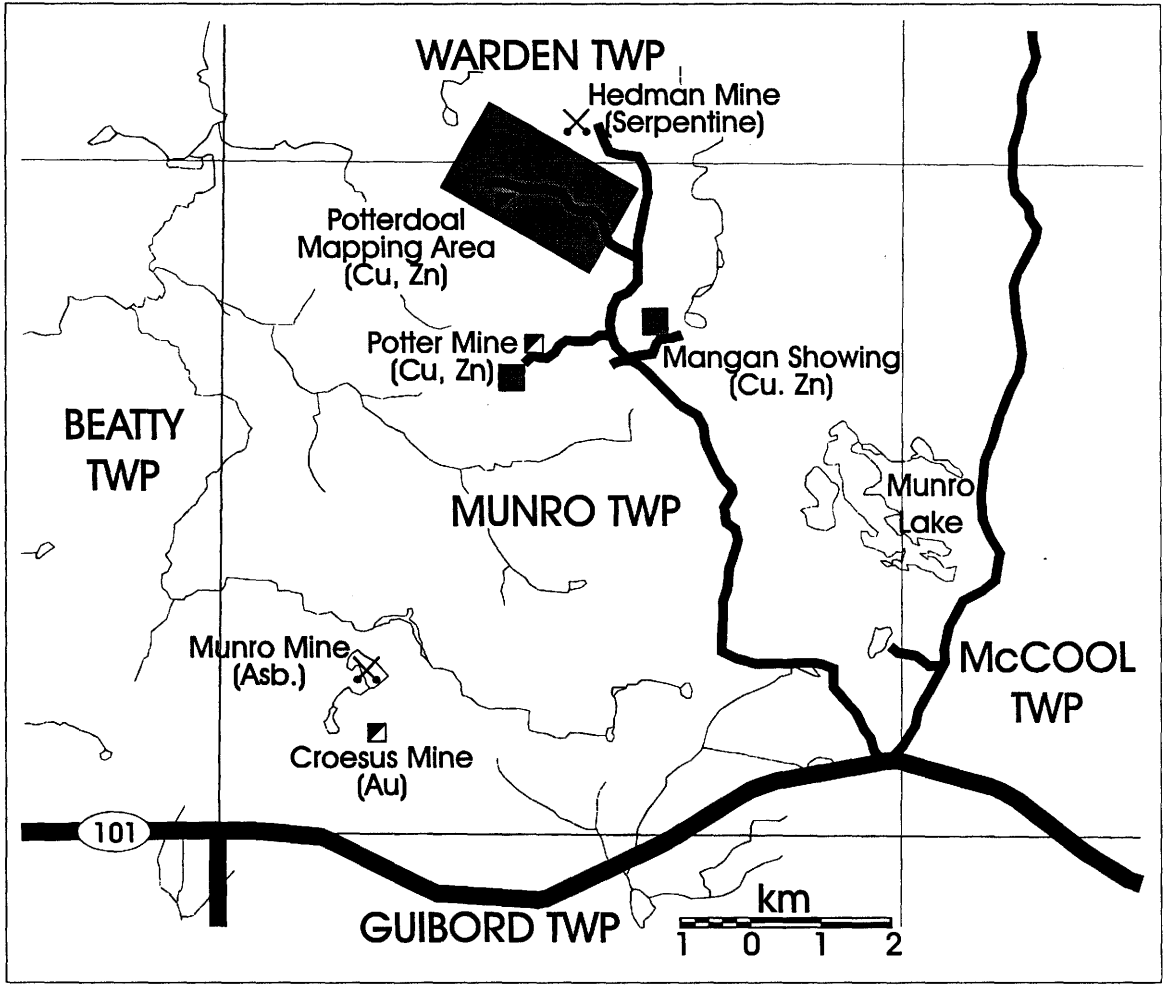
Volcanic Assemblages

layered flow units (Pyke, 1976; Arndt, 1976; MacRae and Crocket, 1977; Stone and Crocket, 1993). Some work has also been done on the peridotite-associated talc-serpentine-asbestos deposits located in southwestern Munro Township and in the north in Warden Township. The only previous study to directly examine a mafic associated VMS deposit was performed by Paul Coad (1976). Coad's masters thesis study concentrated on the petrology, alteration and sulphide replacement at the Potter Mine, in central Munro Township (Figure 1-2). This copper-zinc dominated ore system was shown to be associated with a volcanic breccia (hyaloclastite) horizon which directly overlies a thick, differentiated gabbroic sill. Most recently, some of the discussion covered within this thesis is currently in press (Epp and Crocket, in press).

1.1.3 Location and Access

The Potterdoal Mine is located in greenstones of Munro Township (Figure 1-1 and 1-2) situated in northeastern Ontario. The township is situated 19 km east of the town of Matheson and approximately 50 km north of the Kirkland Lake area. Access to the township was attained from Highway 101, which runs eastward from Matheson to the Ontario-Quebec border (Figure 1-2). Highway 101 runs roughly along the southern boundary of Munro Township, and access to the northern parts of the township was made by using the Hedman Mine access road (the Hedman Mine is a current producer of industrial serpentine). This all season gravel road cuts north-northwestward from the southwest corner of the township, and provides convenient access to the north central region of the township. The main field area for this thesis (highlighted in Figure 1-2) is

Figure 1-2 Field mapping locations Within Munro Township.



located at the end of a small, poorly maintained gravel road, which leads westward from the Hedman Mine gate (approximately 1 km south of the northern Munro Township boundary).

1.1.4 Mining History

The discovery of the original surface showing of the Potterdoal deposit was made by Paul Doal of Matheson in 1926. In 1927, 660 feet of diamond drilling was performed, and a 28 ton bulk sample taken. The massive sulphide bulk sample returned grades of 15.22% copper, 4.15% zinc, 2.70 ounces per ton silver, and 0.045 ounces per ton gold (Ontario Dept. of Mines, 1927). Mining began in earnest in 1928 and continued to 1930, concentrating on a sheared sulphide lens approximately 8 feet wide and dipping steeply to the north. An inclined shaft was driven down on the ore lens to a depth of 125 feet, and a vertical shaft was sunk to 250 feet to the northwest of the showing. A total of 2577 tons of high grade ore, grading approximately 11% copper, were eventually shipped for refining in Noranda (Dept. of Energy, Mines and Resources, 1974). The property then lay dormant until 1979, when Amax Minerals remapped, ran various surface geophysical surveys and drilled with limited success (Bath, 1990). In 1991, Granges Inc. re-examined the property, performing more geophysical surveys and diamond drilling, which resulted in the discovery of a high grade sulphide lens in a structure concordant to the steep south dipping bedding (Cotnoir, 1993).

1.2 Objectives

Recent drilling on the Potterdoal property, graciously provided by Granges Inc., permits an opportunity to incorporate subsurface data into the further study of this poorly understood deposit type. In this thesis, we will (1) define the stratigraphy, petrology and structure around the Potterdoal Mine, (2) characterize the chemistry of stratigraphic units associated with the Potterdoal deposit, (3) examine the chemistry of the progressive footwall alteration associated with an ore-forming hydrothermal system, (4) discuss base metal distribution within the ore system, and (5) propose a model for the ore deposit. Chemical characterization of these rocks includes major and trace elements determined by X-ray fluorescence (XRF) analysis, and rare earth elements determined by instrumental neutron activation analysis (INAA).

Comparison of the Potterdoal and Potter Mine deposits was undertaken to examine local variations of sulphide occurrences. Even though these two deposits are interpreted to be stratigraphically equivalent (Johnstone, 1991, Granges Staff, pers. comm., 1993), there are significant differences in the stratigraphic location and rock type associations of their respective sulphide mineralization.

Chapter 2

Field and Laboratory Methodologies

2.1 Field Work

Field work was performed during the summers of 1994 and 1995. Initially, remapping of several areas covered by 1:5000 and 1:2500 scale maps supplied by Granges Inc. was performed to become familiar with the regional geologic units and stratigraphic relationships within the Munro Township area. Detailed mapping at 1:1000 scale was then focused on areas surrounding known mineral occurrences. The most significant of these sites are the Potterdoal and Potter mine sites, as well as the area in the direct vicinity of the Mangan showing (see shaded areas on Figure 1-2). Mapping at most locations was somewhat facilitated by the presence of old cut line grids, put in during the winter of 1990 and set out at a 100 metre spacing. The usefulness of these cut lines was locally limited due to the degree regrowth of the local bush as well as the deterioration of the line pickets. Base lines for the cut line grids were put in parallel to the dominant structural trend in the Munro Twp area. The result of this is that the grid line north deviates 30 degrees east of true north, and it important to note that all mapping was performed on this skewed grid system.

During the collection of field samples for geochemical analyses and specimen petrology, a concerted effort was made to collect fresh unweathered samples. Where fresh samples were difficult to prepare in the field, large samples (2 to 3 kilograms) were collected and subsequently cleaned back at the McMaster University sample preparation room. Samples taken from diamond drill core were typically very fresh and clean, and therefore did not require any further preparation.

The re-logging of 7,000 metres of core from the Potterdoal property and 1000 metres from the Mangan showing was performed with special emphasis on stratigraphic and structural correlation. Numerous core samples were also collected for chemistry because of their freshness and better representation of stratigraphic units which are poorly exposed on surface. Evidence from these two areas was compared with core information from the Potter Mine property. Unfortunately, the majority of the core storage on the Potter Mine property had been vandalized, so only general rock types and mineralization styles could be observed.

2.2 Petrology

Samples for thin section work were obtained from both surface and diamond drill core rock samples. Suites of thin sections were selected to provide representative collections of all major stratigraphic rock units, progressive hydrothermal alteration, and progressive sulphide mineralization. Samples showing no significant sulphide mineralization were prepared as regular thin sections through the Geology Department's thin section services at McMaster University. Samples containing minor to massive

sulphides were prepared as polished thin sections at the Toronto University thin section facilities run by Mr. George Taylor. Examination of thin section work was done using a Leitz transmitting/reflecting microscope so that the inter-relationship of primary minerals, hydrothermal alteration and sulphide mineralization could be directly studied. For some cases where mineral identification was in question an Energy Dispersive Spectrometer (EDS) attachment for an electron microscope (Philips 515 high resolution scanning electron microscope, Brockhouse Institute for Materials Research, McMaster University) was used to provide semi-quantitative evidence of elemental abundances within the mineral grain. The elements present and their relative proportions were used in combination with optical properties to more positively identify the mineral in question.

2.3 Geochemistry

2.3.1 Sample Preparation

Initial preparation of field samples for geochemical analysis involved the removal of all weathering effected surfaces from 0.5 to 1.0 kilogram rock samples. This was done using a hydraulic splitter with high carbon steel cutting blades. Then, approximate 0.5 kilogram portions of each sample were sent to Activation Laboratories in Ancaster, Ontario where crushing, using jaw and cone crushers, and then pulverization to a less than 150 mesh powder, using a low chromium “soft steel” shaker mill were carried out.

2.3.2 Instrumental Neutron Activation Analysis (INAA)

Trace elemental determinations by INAA were a major portion of the laboratory work performed for this thesis. This work was generally based on analytical procedures developed by Jacobs et al. (1977), as well as on procedures specifically developed for the gamma-ray spectrometry instrumentation located within the Geology Department at McMaster University.

Pulverized samples (<150 mesh) of approximate 500 milligram aliquots (± 2 mg) were weighed into polyethylene vials, capped and then sealed using an electric soldering iron. All handling of the vials was done with steel tongs and latex glove to prevent Na contamination from hands. The samples, along with three international reference standards (BHVO-1, MRG-1 and SCo-1; Hawaiian basalt, Mont Royal gabbro and Cody shale, respectively), were labeled with a permanent marker and then bundled between two plastic, 6 cm diameter petri dishes. Three sets of samples, each containing a common triplicate sample, were then submitted to the McMaster Nuclear Reactor (MNR) for irradiation.

Each sample set underwent two separate irradiations in the RIFLS (Reactor Irradiation Facility for Large Samples) facility of the MNR. During irradiation, the sample bundles were rotated to allow for even neutron flux across all samples. The first irradiation consists of a one hour duration, 2 megawatt-hour (MWH) epithermal irradiation. An epithermal irradiation refers to a lower energy neutron spectrum flux (~ 0.4 eV to 1.0 MeV) produced by shielding the sample bundle with a cadmium sleeve. This irradiation was used for quantitative determination of the short lived isotopes ^{140}La

and ^{153}Sm , with half-lives of 40.2 h and 46.5 h respectively, and ^{45}Sc (half-life of 83.8 d). Gamma-ray spectra were measured after a 3 to 5 day decay time, with counting times ranging between 3,600 to 7,200 seconds. The second irradiation consists of a 3.5 hour duration, 7 MWH thermal irradiation. No cadmium shielding was used for the thermal irradiations, allowing the full neutron energy spectrum to bombard the sample bundle. Two separate gamma-ray spectral counts were performed after thermal irradiations. The first was performed after 14 days decay time, with 3,600 to 7,200 second counting times, allowing the quantitative determination of Nd, Lu, Th and Yb. The second gamma-ray spectral count was performed after 50 to 60 days decay time, counting for 14,400 to 28,800 seconds, and gives quantitative determinations of Ce, Hf, Cs, Tb, Ta, Eu and Co. A list of the spectral energy levels used to calculate abundances of each element for epithermal and thermal irradiations is summarized in Table 2-1.

Gamma-ray spectra were collected from an Aptec Engineering Ltd. multichannel analyzer (MCA), coupled with an Aptec model 6300 spectroscopy amplifier. The spectroscopy amplifier was connected to an intrinsic coaxial germanium crystal detector (Canberra Industries Ltd., Meriden, Connecticut) cooled by liquid nitrogen and shielded by a four inch thick lead housing. The detector geometry consists of a thin beryllium window and closed end coaxial, with an active facing window area of 19.8 square centimetres. The detector has a quoted relative efficiency of 23%, with a resolution of 1.90 keV at 1.33 MeV and a peak to Compton ratio of 47.1 : 1. Display and statistical processing of spectral counts were performed by the Aptec proprietary analyzer software package, version 5.3, release 4 for Windows 3.1 (copyright 1989-1994, Aptec

Table 2-1: Irradiation schedule for specific elements, determined by instrumental neutron activation analysis.**Epithermal Irradiation: 2 MWH irradiation with cadmium shielding****Decay Time Following Epithermal Irradiation: 3 to 5 days****Counting Time: 7,200 seconds**

Nuclide	Target Element	Product Isotope	Half-life	Spectral Energy (keV)
La	140La	139La	40.23 h	1595.0 and 487.9
Sm	153Sm	152Sm	46.7 h	69.6 and 103.6
Sc	46Sc	45Sc	83.9 d	890.8

Thermal Irradiation: 7 MWH irradiation at least 14 days after epithermal irradiation**First Thermal Count****Decay Time Following Thermal Irradiation: 7 to 10 days****Counting Time: 7,200 seconds**

Nuclide	Target Element	Product Isotope	Half-life	Spectral Energy (keV)
Nd	147Nd	146Nd	10.99 d	91.5
Lu	177Lu	176Lu	6.71 d	208.6
Yb	175Yb	174Yb	4.19 d	396.5

Second Thermal Count**Decay Time Following Thermal Irradiation: 50 to 60 days****Counting Time: 14,400 to 28,800 seconds**

Nuclide	Target Element	Product Isotope	Half-life	Spectral Energy (keV)
Ce	140Ce	139Ce	32.5 d	145.8
Tb	160Tb	159Tb	72.4 d	300.0
Hf	181Hf	180Hf	42.5 d	483.3
Cs	134Cs	133Cs	2.05 y	606.0
Rb	86Rb	85Rb	18.66 d	1076.01
Ta	182Ta	181Ta	155.1 d	1223.3
Eu	152Eu	151Eu	12.2 y	1409.6

(Modified from Walker, Kirouac and Rourke, 1977)

Engineering Ltd.). All samples utilized a 16,384 channel calibration, which gave an approximate 0.1 keV channel width resolution. Counting “dead times” were kept below 5%, and if found to be greater than 5%, the sample in question was allowed to decay for an additional period of time to bring down the dead time.

Detection limits determined by Schwartz (1995), for similar INAA procedures performed on felsic rocks, quoted limits of 0.5 ppm for all rare earth elements. Since the majority of rocks analysed in this study were of mafic to ultramafic composition, the bulk concentrations of rare earth elements were substantially lower, with some elements having concentrations less than 0.5 ppm. Due to significantly lower background noise level relative to the felsic rocks, the analysed mafic and ultramafic rocks of this study can attain detection limits significantly lower than 0.5 ppm. Spectral peaks showing peak to background areas greater than 2:1 to 4:1 can be considered real values (Jacobs et al., 1977; pers. comm. James Crocket, 1997), allowing lower detection limits down to values of 0.2 ppm. The extremely low concentrations of rare earth elements in the standards as well as the bulk of the analysed samples lead to relatively high precision errors, however, for most elements precision error was kept significantly below 10%.

2.3.3 X-Ray Fluorescence Analysis

X-ray fluorescence spectrometry (XRF) analyses for major and trace elements were performed at the University of Western Ontario XRF Laboratory. The methods

used by for the determination of the various elements was outlined in a communication from Dr. Charles Wu (University of Western Ontario), and are summarized below.

2.3.3.1 Analysis Of Major Oxides

Major element analyses are reported as oxides, and included SiO_2 , TiO_2 , Fe_2O_3 , MnO , MgO , CaO , K_2O , Na_2O and P_2O_5 , each expressed as a relative percentage. Values for the “loss on ignition” (LOI) were determined by finding the relative loss of mass which occurred when 1.000 gram of pulverized sample was roasted at 1000°C for 2 hours.

XRF analyses were performed on fused disks which were prepared following a similar method to that described by Norrish and Hutton (1969), and involved the mixing of 1.00 grams of pulverized sample, combined with 5.00 grams of the Norrish formula flux (containing LaO which acts as a heavy absorber). This mixture was fused at 1000°C for 20 minutes, poured into pre-heated molds and then allowed to cool.

Analyses were performed on a Phillips PW-1450 automatic sequential spectrometer, which utilized a side-window Rh-target X-ray tube. A 45 keV / 50 mA potential was applied to the X-ray tube to excite the samples. All analytes were measured on spectra K-lines on a gas flow proportional counter. The resulting spectral profiles were then processed using in-house software run on a desk top personal computer. Calculation of nominal oxide concentrations were then determined relative to a “super standard” monitor prepared by Dr. K. Norrish. Further correction for inter-element and

flux matrix effects was obtained from an iteration process using coefficients provided by Dr. Norrish.

Reference standards used included the CANMET Canadian Certified Reference Materials Project (CCRMP) standard “MRG-1”, the USGS standard “PCC-1”, and the Geological Survey of Japan standard “JB-1A”. These standards were randomly run as unknowns to check the quality of data during sample analyses. Quoted detection limits for XRF analysis of major oxides was 0.01 wt%. Precision errors of less than 1% were obtained for Si, Ti, Al, Fe, Mg and Ca, less than 3% for Mn, K and Na, and 7% for P.

2.3.3.2 Analysis of Trace Elements

Trace elements were analyzed using an XRF methodology and include Nb, Zr, Y, Sr, Rb, Ba, Ga, Pb, Zn, Cu, Ni, Co, Cr and V. Element determinations were performed on whole rock pressed powder pellets. These pellets were made by combining 6.0 grams of pulverized sample with a boric acid backing, and 3 to 4 drops of a 2% polyvinyl alcohol solution binding agent. This mixture was then transferred to a loose-sleeve type briquetting press and pressed for five minutes under 10 tons of pressure.

Analysis of trace elements used both the Rh- and W-target tubes with a tube voltage of 60 keV at 40 mA. A combination of a scintillation detector and flow proportional counter was used for the measurement of spectral intensities. Mass absorption coefficients were then calculated from the RhK_a and WK_B Compton peak

intensities as described by Willis (1989) and Nesbitt *et al.* (1976). Spectral profiles were then finally corrected using pre-calculated interference factors.

A comprehensive set of 24 international rock standards were utilized to calibrate the determination of this diverse set of elements. In addition, randomly selected duplicate samples were also run to insure the accuracy and precision of the results. This method provides quoted detection limits of 2 ppm for Nb, Zr, Y, Sr and Rb, and 5 ppm for Ba, V, Cr, Co, Ni, Cu, Zn and Pb.

Chapter 3

Regional and Local Geology

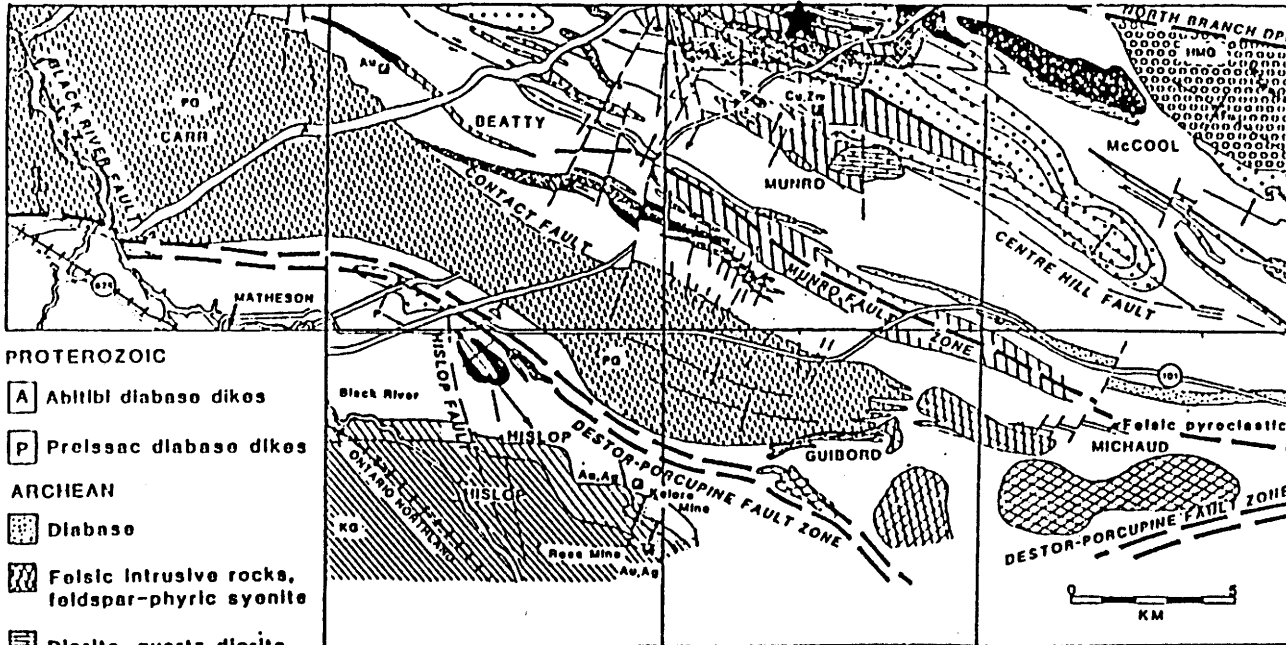
3.1 Regional Setting

The Potterdoal Mine lies between splays of the Destor-Porcupine Fault system within the central southwestern Abitibi subprovince (Figures 1-1 and 3-1). The Destor-Porcupine Fault splays shown on Figure 3-1 include the main Destor-Porcupine Fault to the south, the Contact Fault, the Munro Fault Zone, and the North Branch Fault not shown just north of the township. Recent stratigraphic correlation work indicates that host rocks for the deposit belong to the Kidd-Munro assemblage (Jackson and Fyon, 1991). Most previous work in the area has utilized an older but very similar stratigraphic correlation, which is presented in Figure 3-2 and was based on the geochronological correlation performed by Corfu et al., 1989 (Figure 3-3). For the sake of consistency, the newer stratigraphic correlation scheme was used throughout this work.

The Kidd-Munro assemblage shows a narrow range of extrusion dates between 2717 ± 2 to 2714 ± 2 Ma (Barrie et al., 1988; Corfu et al., 1989), and generally strikes east-west from north of Timmins to just southwest of Lake Abitibi, where the Potterdoal deposit is located. Within the Munro Township area, the mafic tholeiitic to komatiitic Kidd-Munro assemblage is conformably underlain by the older (2730 ± 1.5 to 2713 ± 2

Figure 3-1 Generalized geology map of the northwest Black River-Matheson area (Johnstone, 1991).

Potterdoal Deposit



PROTEROZOIC

- A** Abitibi diabase dikes
- P** Preissac diabase dikes

ARCHEAN

- D** Diabase
- F** Felsic intrusive rocks, feldspar-phyric syonite
- Dl** Diorite, quartz diorite
- G** Gabbro
- KG** Kinojevia Group(KG) tholeiitic lavas
- SR** Stoughton-Roquemaure Group
- U** Upper felsic horizon, calcalkalic tuff and tuff breccia intercalated with tholeiitic lavas and felsic sills

- PL** Peridotitic and basaltic komatiite lavas
- T** Tholeiitic lavas, minor interflow sediments
- L1** Layered flow (tholeiitic)
- L2** Layered flow (basaltic komatiite)
- Per** Peridotite
- Gill** Gabbro sill

- PG** Peridotite-pyroxenite-gabbro sills
- PGP** Gabbro portion
- PGT** Porcupine Group(PG), medial to distal turbidites, deep water feldspathic arenite, wacko and argillite
- HMG** Hunter Mine Group(HMG), calcalkalic dacite and andesite lavas and flow breccias, felsic block and ash deposits, lapilli and crystal tuff units-McCool Twp, calcalkalic rhyolite and dacite lavas and flow breccia.-Beatty and Munro Twps

Figure 3-2 Old and new stratigraphic sub-divisions for the rocks of the Munro Township area.

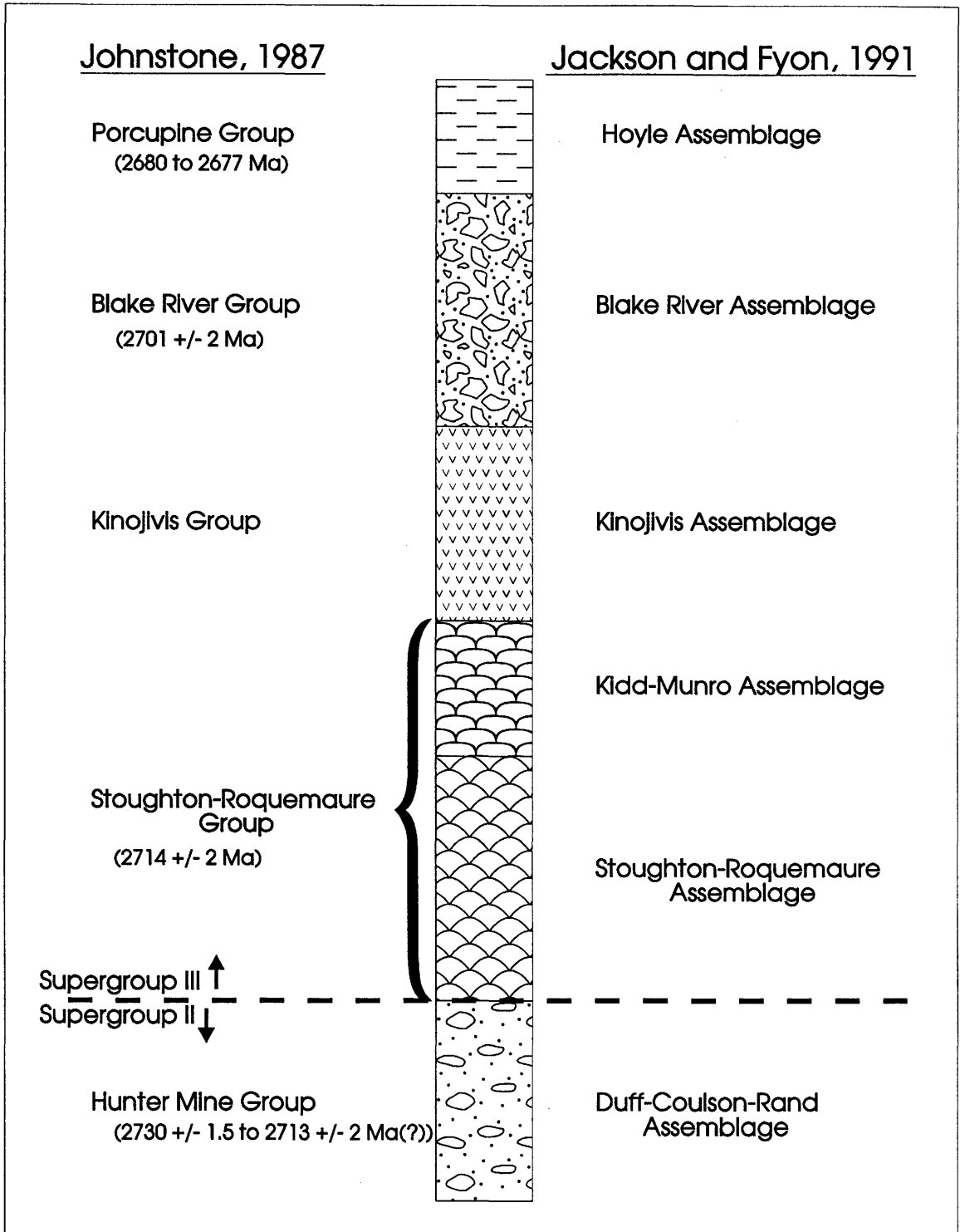
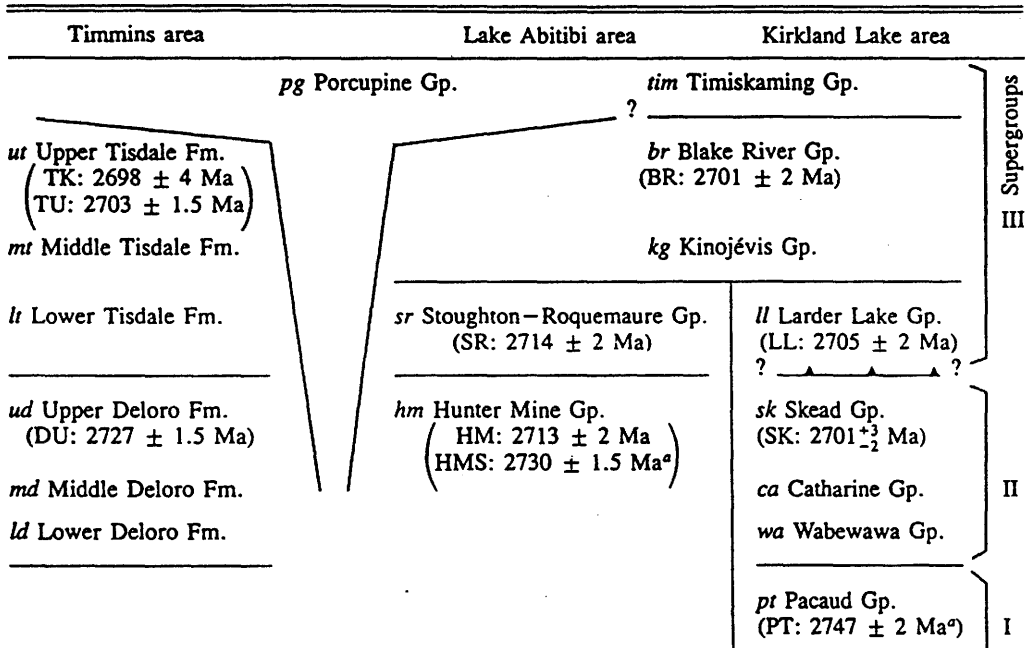


Figure 3-3 Geochronologic sub-division of stratigraphic section within the southwestern Abitibi Greenstone Belt prepared by Corfu et al., 1989. Rocks on the Munro Township area are shown in the central column.



NOTES: Stratigraphic subdivision from MERQ-OGS (1983). Formations (Fm.) as defined by Pyke (1982) for the Timmins area correspond to groups (Gp.) in the other areas (Jensen and Langford 1985).

^aFrom Mortensen (1987a, and personal communication, 1987).

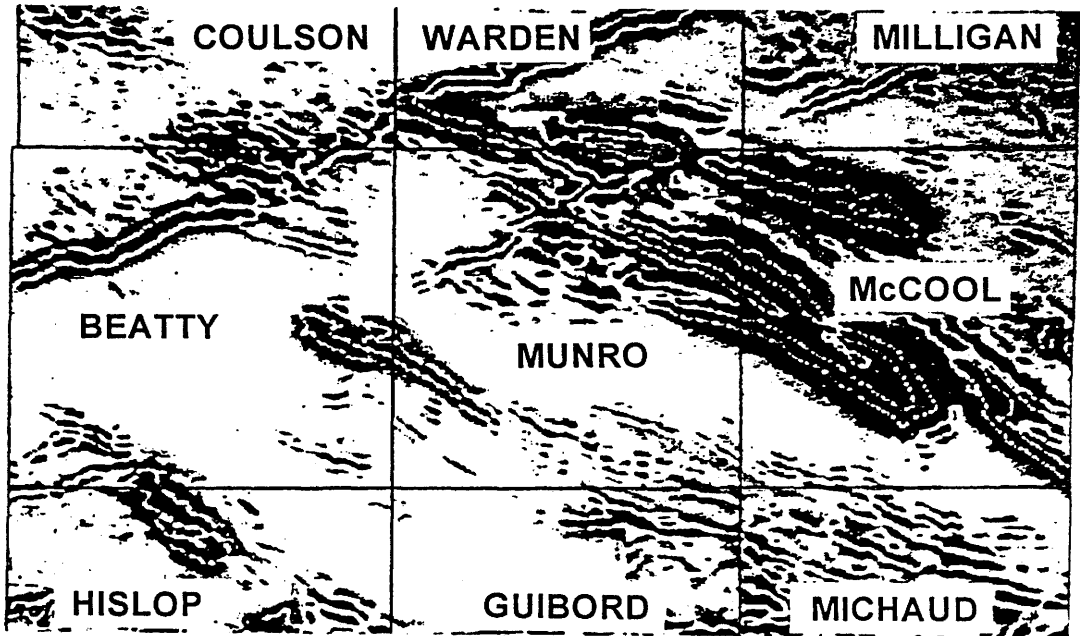
Ma) calc-alkalic Duff-Coulson-Rand assemblage to the north, and is in fault contact with younger (2680 to 2677 Ma) turbiditic sediments of the Hoyle assemblage to the south (Jackson and Fyon, 1991; Corfu et al., 1989; Corfu et al., 1991).

3.2 Local Structure

The most significant structure affecting the geology of Munro Township area is a tight, shallowly west-north-westward plunging synclinal structure, referred to as the McCool Hill Syncline (Johnstone, 1987). This structure is located in the northern half of the township, and is clearly seen on a regional aeromagnetic map (Figure 3-4), which also shows the fold closure in the adjacent McCool Township. This syncline folds a laterally extensive stratigraphy consisting of alternating units of Fe to Mg tholeiitic basalts, basaltic to peridotitic komatiites, and tholeiitic to peridotitic sills. The komatiitic flows contain a large relative proportion of magnetite, and are the main rocks which strongly defined the magnetic profile of the syncline.

The majority of the rocks in the township show no penetrative fabric, even though the local stratigraphy has been subjected to intense synclinal folding. Some authors have suggested that the less competent units like the serpentized peridotite sills may have taken up most of the strain, leaving the remaining units relatively unaffected (pers. comm., J.A. Fyon, 1995). Since these sills are poorly exposed and only make up a few percent of the total stratigraphy, the intense deformation along these sills is not generally evident.

Figure 3-4 Regional “total field” aeromagnetic map of the Munro Township area. Darker shade indicates higher magnetic intensity (Johnstone. 1987).

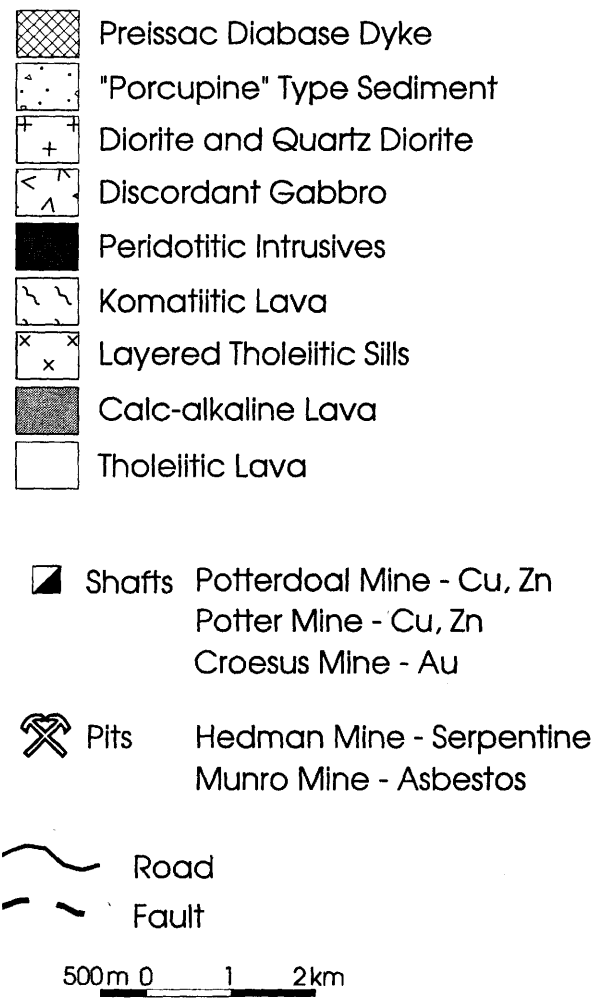
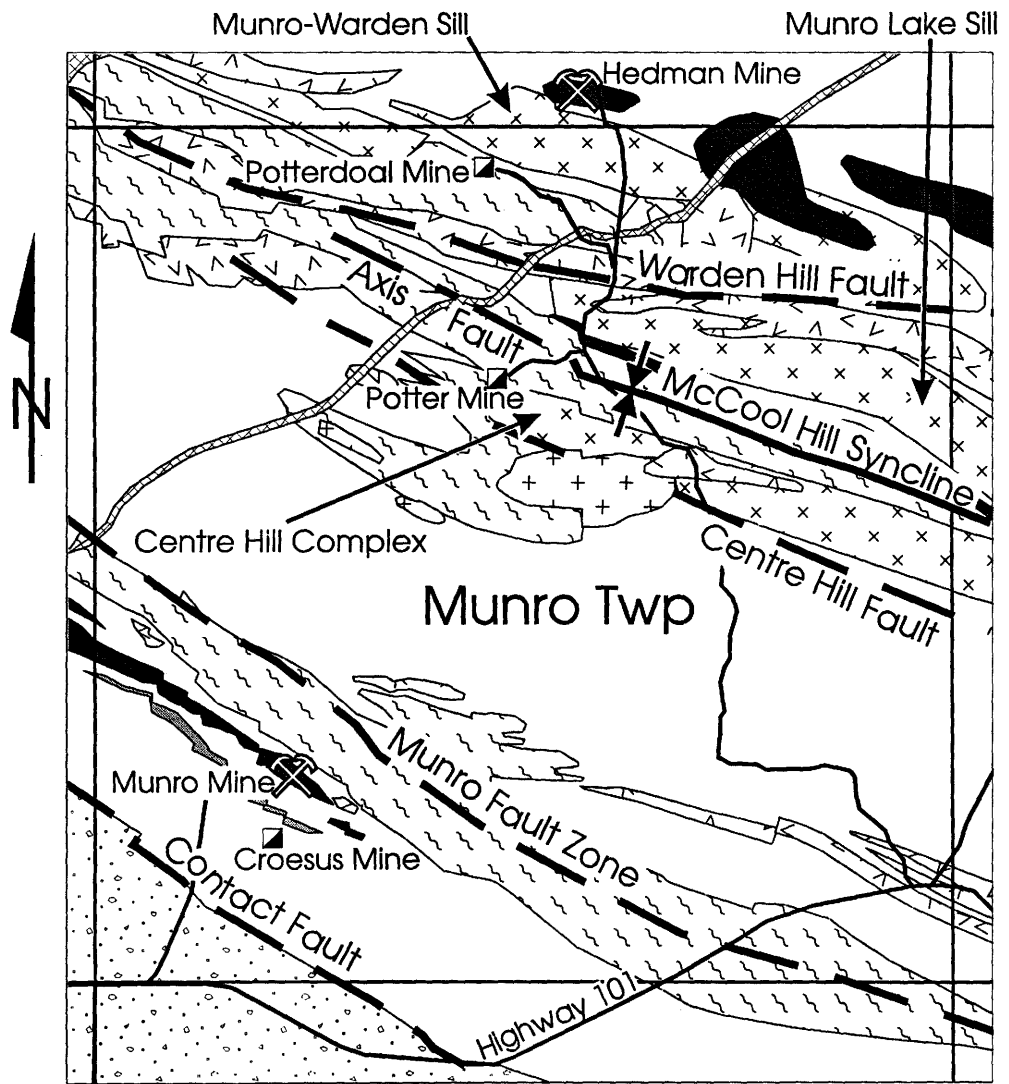


The degree and complexity of faulting in the township is high, owing to the close proximity of several major splays of the Destor-Porcupine Shear system (Johnstone, 1991). However, these fault splays generally tend to show a subvertical to steep southward dip, and trend approximately parallel to bedding in a northwest- to west-northwest direction (Figure 3-5). This fault symmetry is consistent with thrusting related to the ~2.6 Ga Kenoran compressional event (convergent in a north-south direction), suggesting that the fault splays were formed at that time. The Warden Hill and Centre Hill faults, situated in northern Munro Township (Figure 3-5), are also thought to be related to the Kenoran compressional event. However, these faults are associated with bedding plane slip during the isoclinal folding of stratigraphy located in northern half of the township.

3.3 General Lithologies

Tholeiitic basalt flows are the dominant rock type in the township, accounting for about 50% of the stratigraphy. These tholeiitic units consist of pillowed to massive flows of from 1 to 20 m thickness, interlayered with several thicker flows, generally 90 to 120 m thick (Johnstone, 1987). These thicker flows are often layered, grading from peridotitic bases to gabbroic tops, and are represented in the field area by Theo's Flow (Arndt, 1977). Komatiitic flows generally appear sheet-like and range in thickness from approximately 1 to 5 m. Thicker komatiitic flows typically show polygonal jointing, whereas thinner flows may show the delicate flow top spinifex textures for which Munro Township is well known.

Figure 3-5 Regional geologic map of the Munro Township area (Modified from Johnstone, 1991).

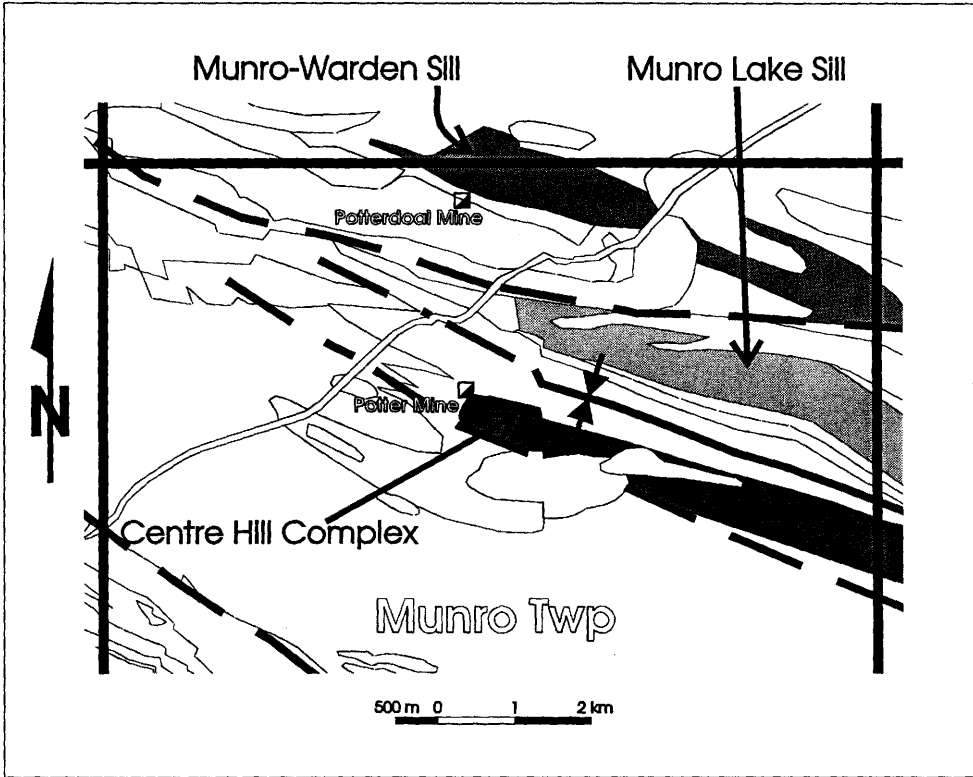


Minor amounts of interflow chemical sediments and crystal tuff also occur at irregular intervals within the stratigraphy, and only rarely reach thicknesses of up to 3 to 4 m. Chemical sediments are represented by thin (~ 1 m) laminated graphitic chert horizons, which often contain abundant framboidal pyrite nodules. Crystal tuff units consist dominantly of well sorted, subhedral to broken plagioclase grains, and show both normal and inversed centimetre scale bedding, indicative of a possible distal air-fall origin.

A thick (800 to 1400 m), differentiated, synvolcanic tholeiitic sill is found tightly folded, around the core of the McCool Hill Syncline (Fig. 3-6). The two main limbs are referred to as the Munro Lake Sill to the north, and the Centre Hill Complex to the south. Another sill, referred to as the Munro-Warden Sill, is also found further to the north, and is interpreted as a faulted repetition of the Munro Lake Sill across the Warden Hill Fault (Johnstone, 1987). These sills were emplaced at very shallow depths, and appear to have locally breached the seafloor interface. The main evidence supporting the theory that these sills breached the seafloor is the presence of an extensive breccia caps (the "hyaloclastite" unit of Coad, 1976) which immediately overlies the exposed sill.

Large, discordant gabbroic dykes intrude along some of the late bedding-subparallel faults, formed during folding of the above stratigraphy. There are also two late sets of diabase dykes produced by separate rifting events. The older swarm (2.63 Ga, Gates and Hurley, 1973) are the Matachewan olivine diabase dykes, which are generally small (~ 40 to 70 m wide), have a north trend, and are fairly numerous. Pressiac dykes represent a younger swarm (2.14 Ga, Fahrig and West, 1986) of thicker (~ 150 m wide),

Figure 3-6 Simplified map of northern Munro Township showing the location of the main gabbroic sills.



northeast-trending dykes of a quartz diabase composition, and are much less common than the Matachewan dykes.

Extrusive rocks in the southwestern corner of the township represent the lowest portion of local Kidd-Munro assemblage, and contain two thin calc-alkaline flows intercalated with thick tholeiitic flows. These calc-alkaline rocks may represent the only example of bimodal tholeiitic volcanism in the Munro Township, or may indicate a slight temporal overlap of tholeiitic dominated "Kidd-Munro" volcanism with the older, underlying calc-alkaline "Duff-Coulson-Rand" volcanism (Johnstone, 1987).

3.4 Metamorphism

Jolly (1980) discussed the variations of metamorphic grade in the southwestern Abitibi Belt, noting that Munro Township lies within an area dominated by a sub-greenschist, prehnite-pumpellyite facies. The average metamorphic grade appears to be slightly higher (i.e. low greenschist) in the southwest corner of the township, probably due to the proximity to two major faults which acted as conduits for fluid movement (Arndt, 1975). Contact metamorphism is also noted around intrusives such as the synvolcanic sills in the northern half of the township. These kilometre-thick sills have prograded the surrounding rocks to lower greenschist.

Chapter 4

Mine Site Geology

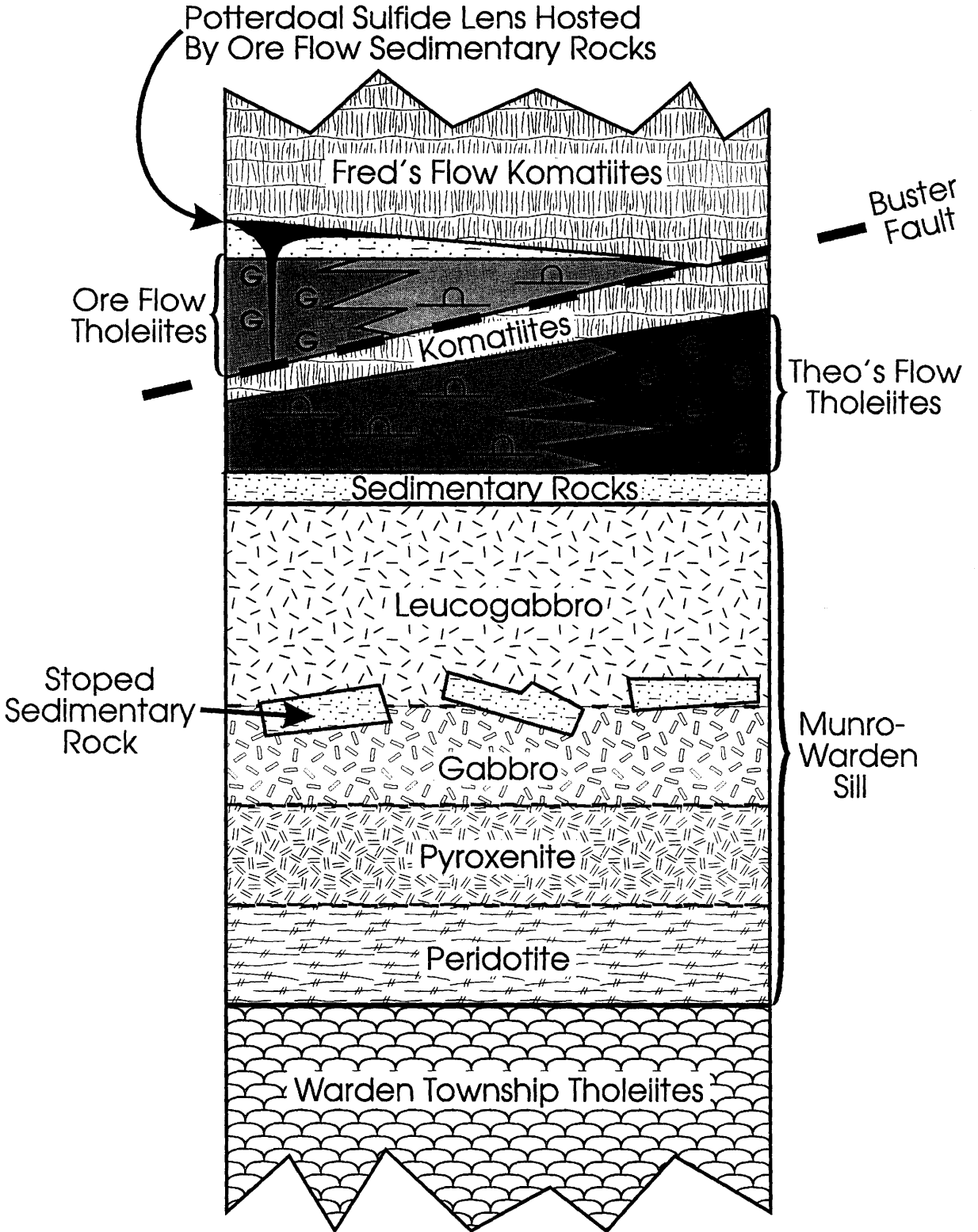
4.1 Mine Site Stratigraphy

The Potterdoal deposit lies along the north limb of the McCool Hill Syncline, and shows toppling directions towards the south. Stratigraphic units dip moderately steeply at about 70° towards the south. A composite stratigraphic section showing the setting of the Potterdoal deposit is presented in Figure 4-1. Stratigraphic units defined in Figure 4-1 have been generalized from the geology of the field map area shown in Figure 4-2. Thicknesses of some units in the stratigraphic section have been exaggerated for the sake of clarity, and actual thicknesses will be provided in the following discussion of each unit.

The Warden Township tholeiites constitutes the base of the Potterdoal stratigraphy. These tholeiites occur as a thick unit of mainly pillowed flow basalts, and generally have a Mg-tholeiitic affinity. These rocks were not studied in detail during this project, as they exhibited no direct relationship to the ore forming system.

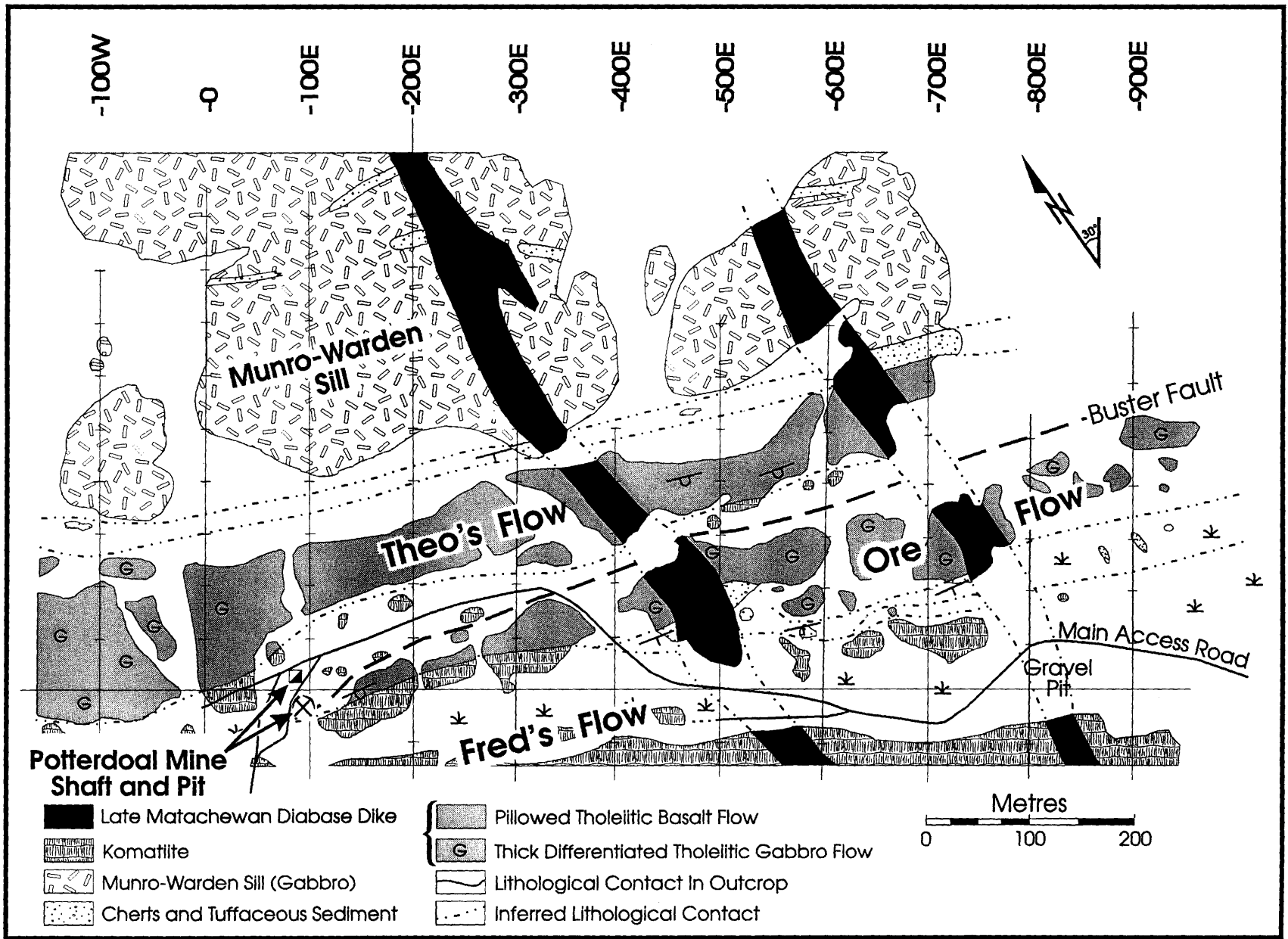
The unit overlying the Warden Township tholeiites is the Munro-Warden Sill, which straddles the boundary between Munro and Warden townships. This sill can be subdivided into four distinct phases with a peridotite base overlain by pyroxenite, gabbro,

Figure 4-1 Composite stratigraphic section of the Potterdoal deposit. Thickness of some units within the stratigraphic section have been exaggerated for clarity. Actual thicknesses are provided in the discussion of each unit. The portions of the tholeiitic flows designated by “G” represents coarse grained, massive gabbros, which laterally grade into pillowed flows, designated by “d”.



(No scale implied)

Figure 4-2 Surface geology of the Potterdoal deposit.



and finally capped by a thick leucogabbro. The sill has an approximate thickness of 900 metres within the study area, but thins towards the west, apparently due to faulting (Johnstone, 1991). It contains a nearly continuous series of large, bedded, cherty to tuffaceous blocks (some as large as 20 m by 50 m), lying near the internal gabbro-leucogabbro transition. These blocks are interpreted as stoped hanging wall fragments since bedding orientations within the individual blocks varies significantly ($\sim 30^\circ$ from sill trend), and the blocks do not appear to be restricted to a specific horizon within the sill.

A chert and crystal tuff unit of a few meters in thickness occurs above the Munro-Warden Sill. This horizon appears to have been important in controlling the emplacement of the Munro-Warden Sill, as it can be traced for a significant distance (approximately 500 m) along the top of the sill. The upper contact of the sill is typically very irregular against the overlying sedimentary rocks. The upper portion of the sill also contains many small sedimentary rock xenoliths (1 to 10 cm) which have been stoped off and partially assimilated, indicating that roof stoping was an active process.

A tholeiitic unit, referred to as Theo's Flow, conformably overlies the sedimentary horizon (Arndt, 1977). This unit is a thick differentiated flow, approximately 130 m in thickness, in the western end of the map area. The flow grades laterally towards the east into pillowed lavas, and thins to approximately 80 m in thickness. The differentiated portion of Theo's Flow has been extensively studied by Arndt et al. (1977), and is interpreted as a rapidly extruded lava pond, showing a well developed flow top breccia. The exact location of the transition from a thick differentiated flow to pillowed lavas is uncertain. However, lava tube structures have been noted running parallel to the present

horizontal erosional surface around line 100E, and there are indications of moderately thick sheeted flows further towards line 0 (refer to Figure 4-2). This interpretation of a lateral transition in Theo's Flow differs from that originally proposed by Arndt et al. (1977), who suggested that the massive differentiated unit to the west and pillowed flow units to the east were originally unrelated, and were later juxtaposed by faulting.

A thin band of interlayered peridotitic and picritic komatiites conformably overlies Theo's Flow. This unit was probably much thicker than present exposure indicates and was truncated by the bedding-subparallel fault structure known as the Buster Fault (Cotnoir, 1993). This fault is responsible for an important small-scale stratigraphic repetition of tholeiitic and komatiitic units observed within the map area. The Buster Fault was first recognized in the 1991 surface mapping by Granges Inc. field geologists, and then was defined underground by the 1992 drill program (reference from original Granges Inc. field maps, and Cotnoir, 1993).

The unit above the Buster Fault has been designated the "Ore Flow" for the purposes of this study, since it forms the immediate footwall rocks to the Potterdoal deposit. The Ore Flow unit has a maximum thickness of about 80 m in the eastern part of the map area, but thins to the west and eventually pinches out against the Buster Fault. Due to the removal of the lower portion of the Ore Flow by the Buster Fault, the original thickness is uncertain. However, the flow thickness must have been greater than the 80 m exposed in the map area. Like Theo's Flow, the Ore Flow shows a lateral transition from a massive gabbroic flow to sheeted flows, and finally variolitic pillowed flows. However, the transition from massive to pillowed flows occurs from east to west, opposite to the

comparable trend noted for Theo's Flow. The gabbroic phases of the Ore Flow shows no indication of differentiation similar to Theo's Flow, but does become somewhat more felsic towards the interior of the massive flow. Despite the differences in flow morphology, both the Ore Flow and Theo's Flow are thought to represent tholeiitic units from the same stratigraphic level, which were faulted into their present positions. Evidence for this interpretation is taken from drill sections and from the general similarity of the komatiites which cap both tholeiitic flows.

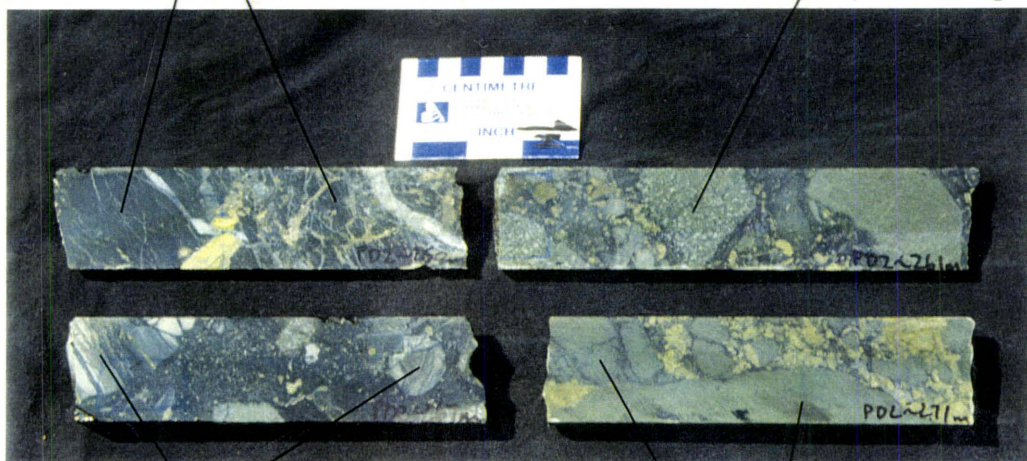
A second interlayered graphitic chert and crystal tuff horizon, which reaches thicknesses of up to 4 m where undisturbed, overlies the Ore Flow tholeiite. Locally these sedimentary rocks are found as thickened chaotic breccias which also include fragments of the underlying Ore Flow basalts and gabbros. This breccia is referred to as the "tectonic breccia", and is a very important unit since it is the primary host rock for the main sulphide mineralization. The tectonic breccia occurs in what was probably a paleotopographic low along the top of the Ore flow (the formation of this breccia will be discussed later). Plate 4-1 shows a transect through typical tectonic breccia, found within the PD2 diamond drill hole. Note the wide variation fragment types and degree of angularity which are characteristic of tectonic breccias within the Potterdoal area.

Locally in the west end of the map area, a thin fragmental flow unit of basaltic komatiite occurs interlayered with the undisturbed sedimentary rocks overlying the Ore Flow. These fragmental rocks are texturally and chemically comparable to those which host the Potter Mine sulphide deposit, approximately 2.4 km to the south of the Potterdoal deposit (Figure 3-5). A previous study had categorized very similar fragmental

Plate 4-1 Tectonic breccia consisting predominantly of tuffaceous and cherty fragments, but can also contain gabbroic fragments.

Graphitic Chert Fragments

Coarse Grained Gabbro Fragments



Laminated Tuff Fragments

Medium Grained Gabbro Fragments

rocks at the Potter Mine as olivine basalt hyaloclastite, where they locally form the primary matrix of sulphide mineralization (Coad, 1976). However, since this rock type is volumetrically insignificant in the Potterdoal stratigraphy and is not associated with the ore mineralization, it will not be considered further.

Capping this stratigraphy is the second series of komatiitic flows referred to as Fred's Flow (Arndt, 1977). Within the map area, Fred's Flow is a thick series of sheeted flows (~ 2 m thick each); however, a few hundred metres to the west, Fred's Flow becomes a 120 m thick differentiated flow (Arndt et al., 1977). This unit appears not to have been effected by the hydrothermal system which emplaced the deposit, and apparently played no major role in the localization of the deposit.

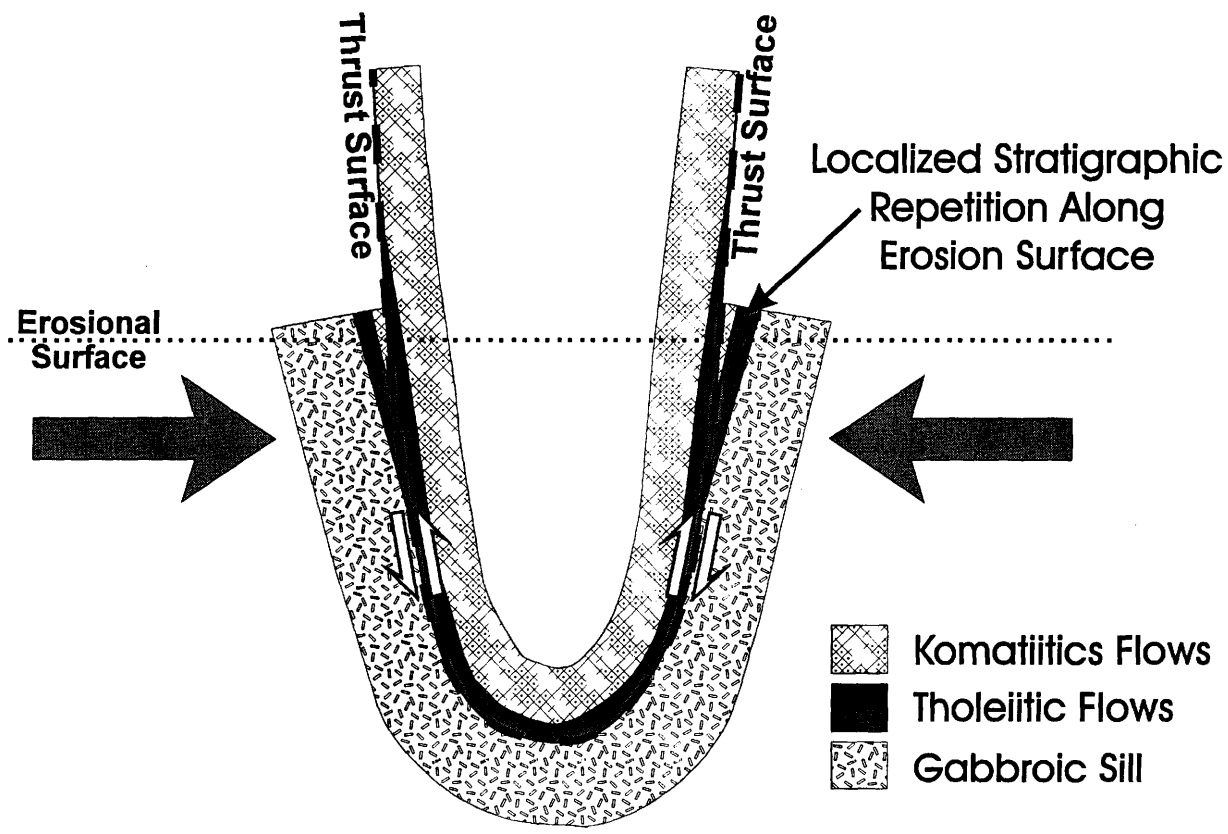
Two late north-trending Matachewan olivine diabase dykes cut the entire stratigraphy of the map area (Figure 4-2). These dykes are 45 to 55 m wide, show strong tangential cooling fractures along their margins, and have little or no obvious contact metamorphic aureoles. The more western dyke coincidentally cuts the thickened sedimentary breccia package precisely where the ore lens, as defined by drill core data, would have projected to surface (between lines 400E and 600E overlying the Ore Flow, see Figure 4-2), and consequently obscures any surface exposure of the ore lens.

4.2 Structure and Associated Rock Textures

4.2.1 The Buster Fault

As briefly discussed in the stratigraphic summary, the Buster Fault played an important role in the arrangement of stratigraphic units presently exposed at surface. This

Figure 4-3 Diagrammatic model of the isoclinal folding of the McCool Hill syncline, showing localized repetitions of stratigraphy produced by low angle, bedding sub-parallel thrust faulting associated with flexural slip.

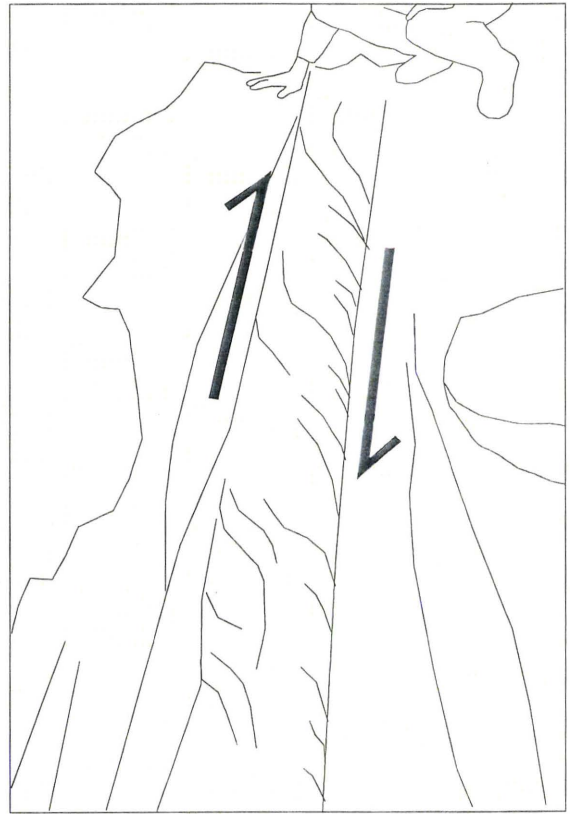


narrow, west-northwest trending fault zone was formed by bedding-subparallel flexural slip during isoclinal folding of the McCool Hill Syncline, and is diagrammatically shown in Figure 4-3. Folding is thought to have occurred primarily during the Kenoran compressional event, approximately 55 Ma after formation of the stratigraphic section. Surface shear kinematics of the north limb slip-fault indicate a minor dextral horizontal shear sense (Plate 4-2a), whereas drill core data indicates strong vertical reverse thrusting (i.e. south side over north side, Plate 4-2b). These observations agree well with structural features expected to form along the north limb of a shallowly plunging west-northwest isoclinal structure, such as the McCool Hill Syncline. Another feature compatible with flexural-slip folding is the observed repetition of stratigraphically equivalent units, which involves translation of a tholeiitic unit along shallowly ramped (bedding-subparallel) faults, followed by upturning and erosion. This is seen in the map area as a northern "tholeiite and capping komatiite" sequence, repeated on the south side of the Buster Fault by another sequence of "tholeiite and capping komatiite". The tholeiitic components involved in this structural repetition north and south of the Buster Fault are Theo's Flow and the Ore Flow respectively (Figure 4-4). An important result of this thrust faulting is that the original footwall rocks to the ore-hosting Ore Flow have been removed. However, since both flows are interpreted to be stratigraphically equivalent, the undisturbed footwall rocks to Theo's Flow are interpreted to be similar to those of the Ore Flow. Thus, the Munro-Warden Sill gabbros found within the map area may be equated with the dislocated footwall rocks of the Ore Flow.

Plate 4-2a The Buster Fault showing C and S fabrics indicating dextral horizontal shear sense along the flat erosion surface.

Plate 4-2b The Buster Fault intersected in core, looking westward. The hole was drilled northward at a 45° angle dip from horizontal, and indicates reverse thrusting (i.e. south over north), highlighted by the black lines.

a)



b)

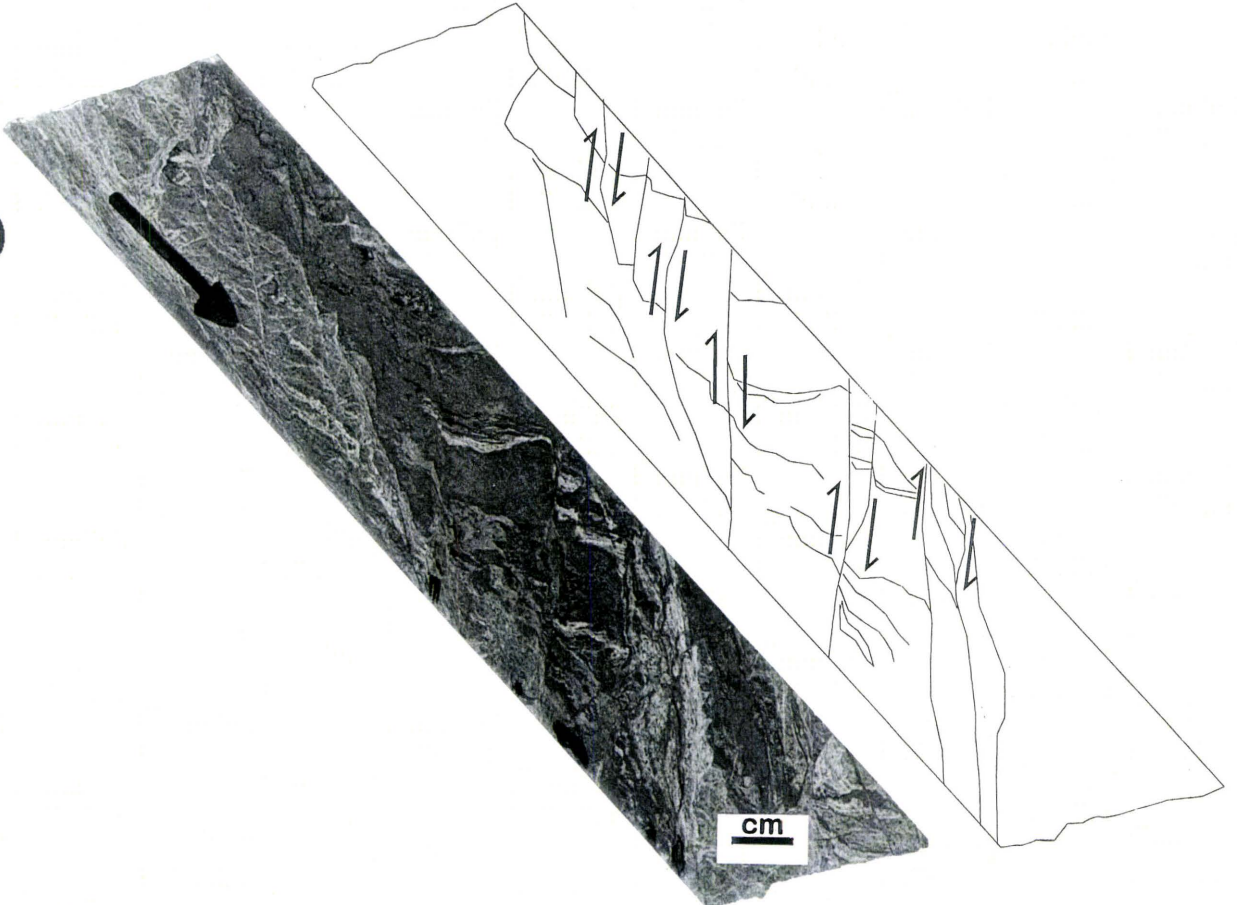
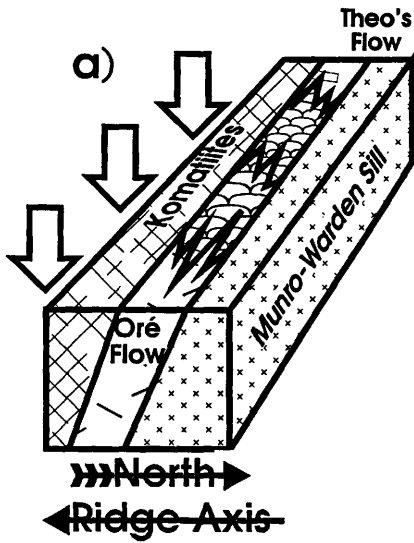
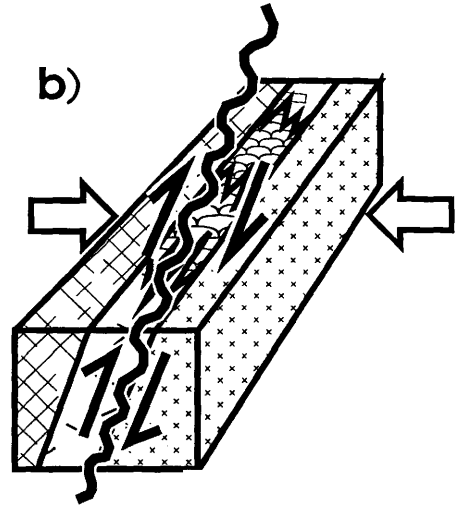


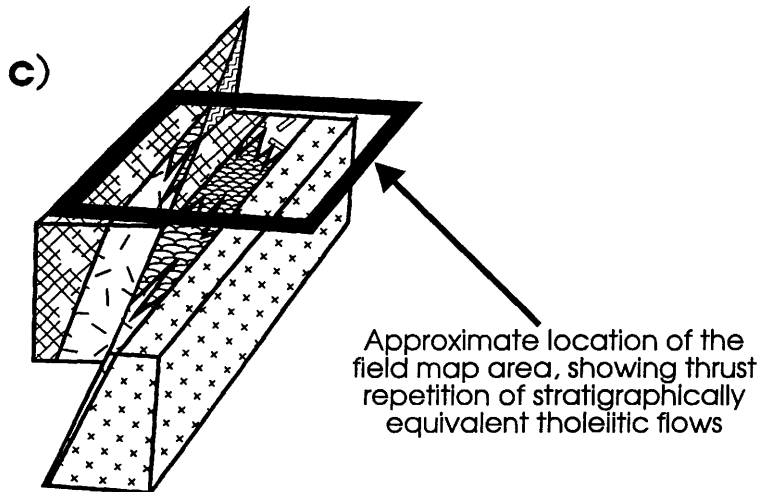
Figure 4-4 Structural repetition within the Potterdoal map area caused by isoclinal folding related thrust faulting.



Tilting of stratigraphy caused by ridge axis subsidence



Initiation of bedding sub-parallel thrust faults associated with tight isoclinal folding induced by the Kenoran compressional event



Approximate location of the field map area, showing thrust repetition of stratigraphically equivalent tholeiitic flows

A profound change in the character of the Potterdoal ore lens has also been noted between lines 100E and 200E in the western end of the map area (Figure 4-2). Surface and drill data suggest that the Buster Fault exits the competent footwall volcanic rocks and cuts into the massive sulphide horizon at this location (Figure 4-5). This has resulted in a highly tectonized segment of massive sulphides showing a steep ($\sim 80^\circ$) dip to the north and extending from about 0 to 150E along the map grid. An example of the sheared massive sulphide ore is shown in Plate 4-3, displaying shear banded laminations and a rotated, chalcopyrite rich cherty fragment. All historical mining of the Potterdoal deposit occurred within this northward dipping, sheared ore lens. The north dip of this lens has led to some confusion in the past, since all local stratigraphy shows a southward dip, and is probably responsible for the lack of success obtained by earlier drill programs. Subsequent drilling in 1992 eventually found the eastward extension of the unsheared ore lens which lies conformably along the southward dipping stratigraphy.

4.2.2 Three-Dimensional Diamond Drill Model and The Fault Scarp Structure

Extensive drilling by Granges Inc. has provided sufficient subsurface information for the construction of geologic cross section shown in Figure 4-5. Combined with surface map data (Figure 4-6), a three-dimensional model was also constructed, showing the subsurface geological structure within the map area hosting the newly discovered ore lens (Figure 4-7). The most striking feature observed in this simplified subsurface model is an asymmetric trough structure referred to as the "fault scarp". This fault scarp occurs along the top of the Ore Flow, and becomes progressively deeper along an east to west

Plate 4-3 Sheared massive sulphide ore with rotated clast, obtained from the Potterdoal inclined shaft pit.



Figure 4-5 Geological cross sections constructed from surface drilling.

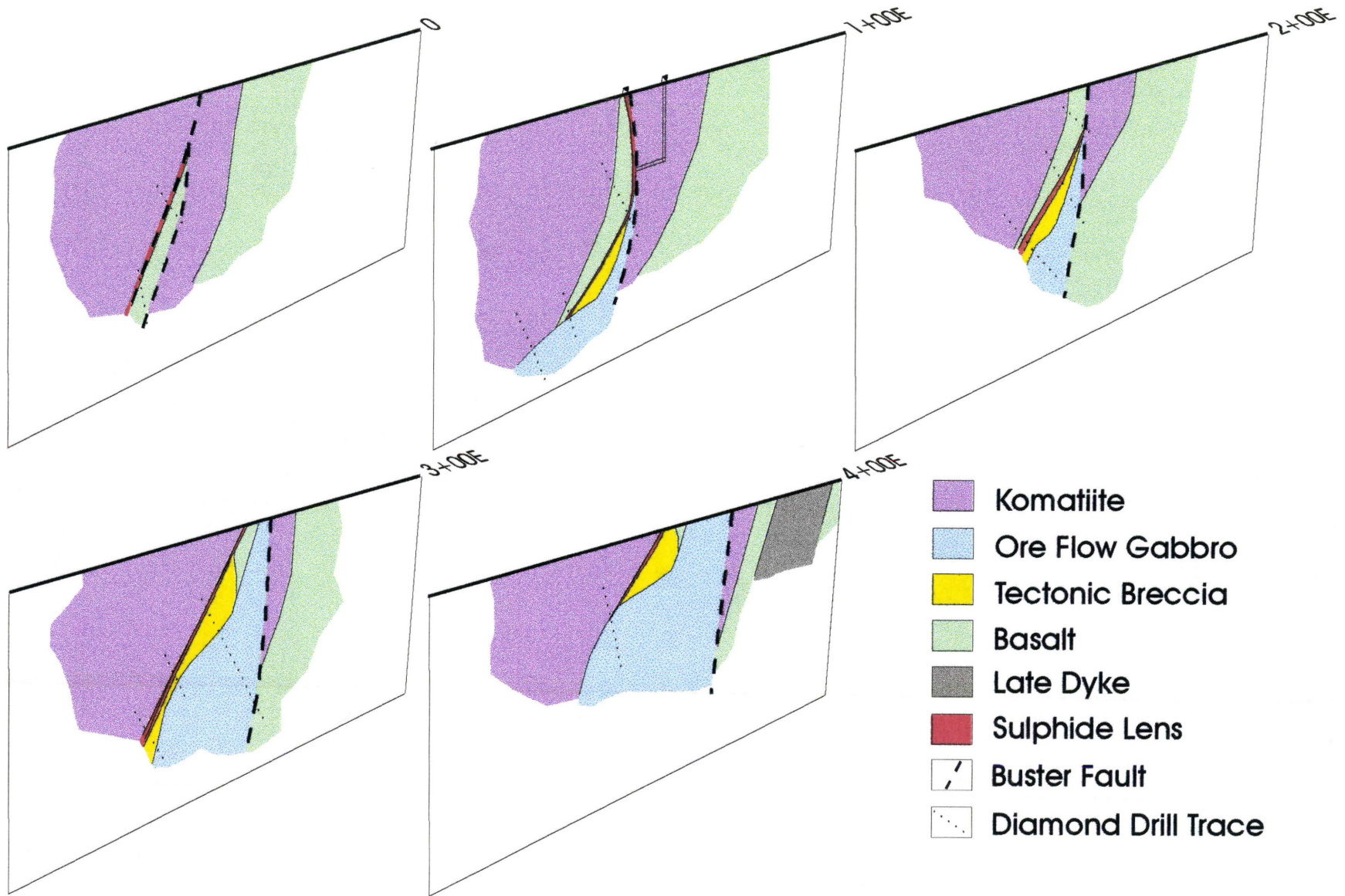


Figure 4-6 Surface geology map for area overlying the cross sections shown in
Figure 4-5

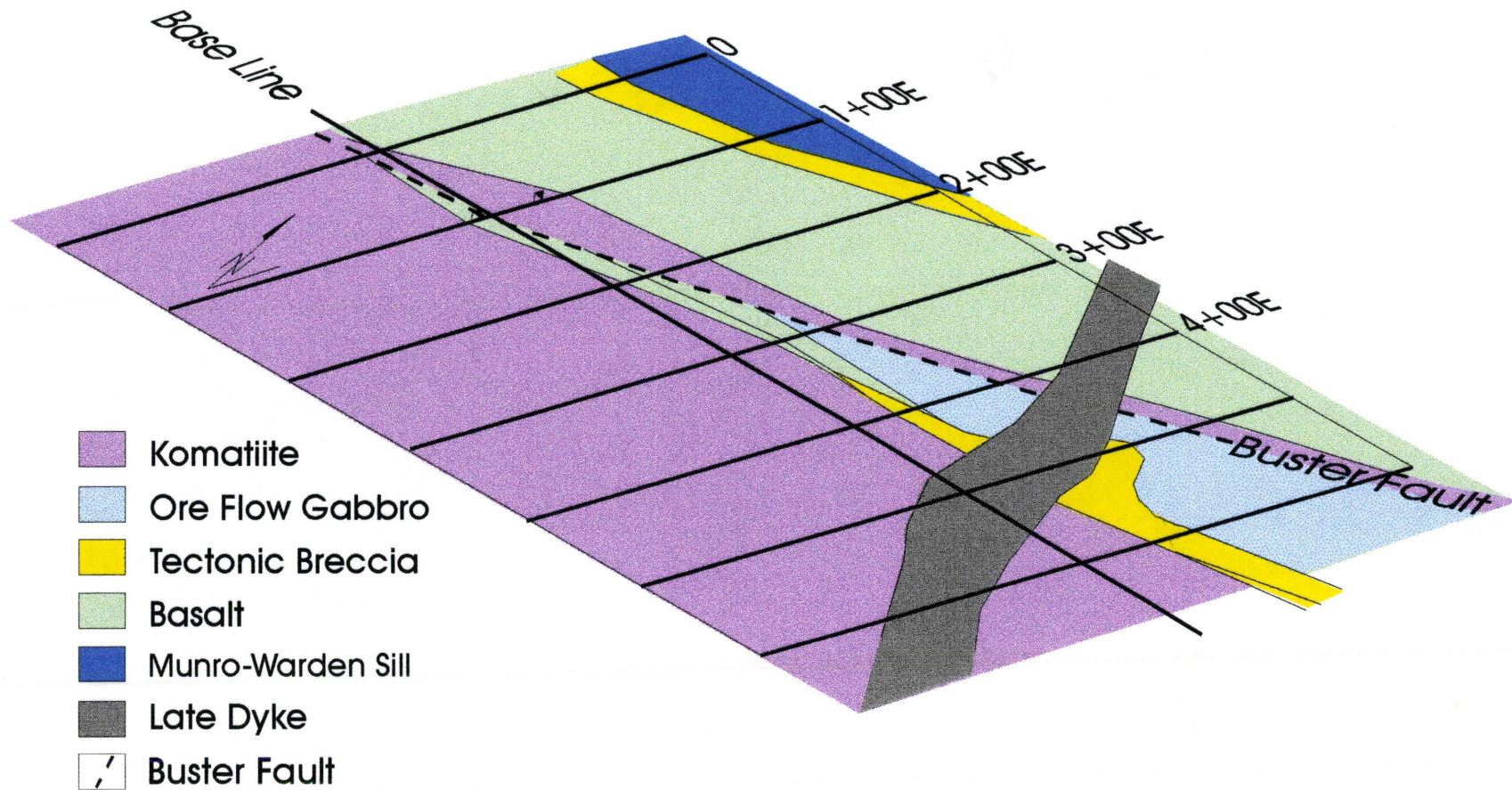
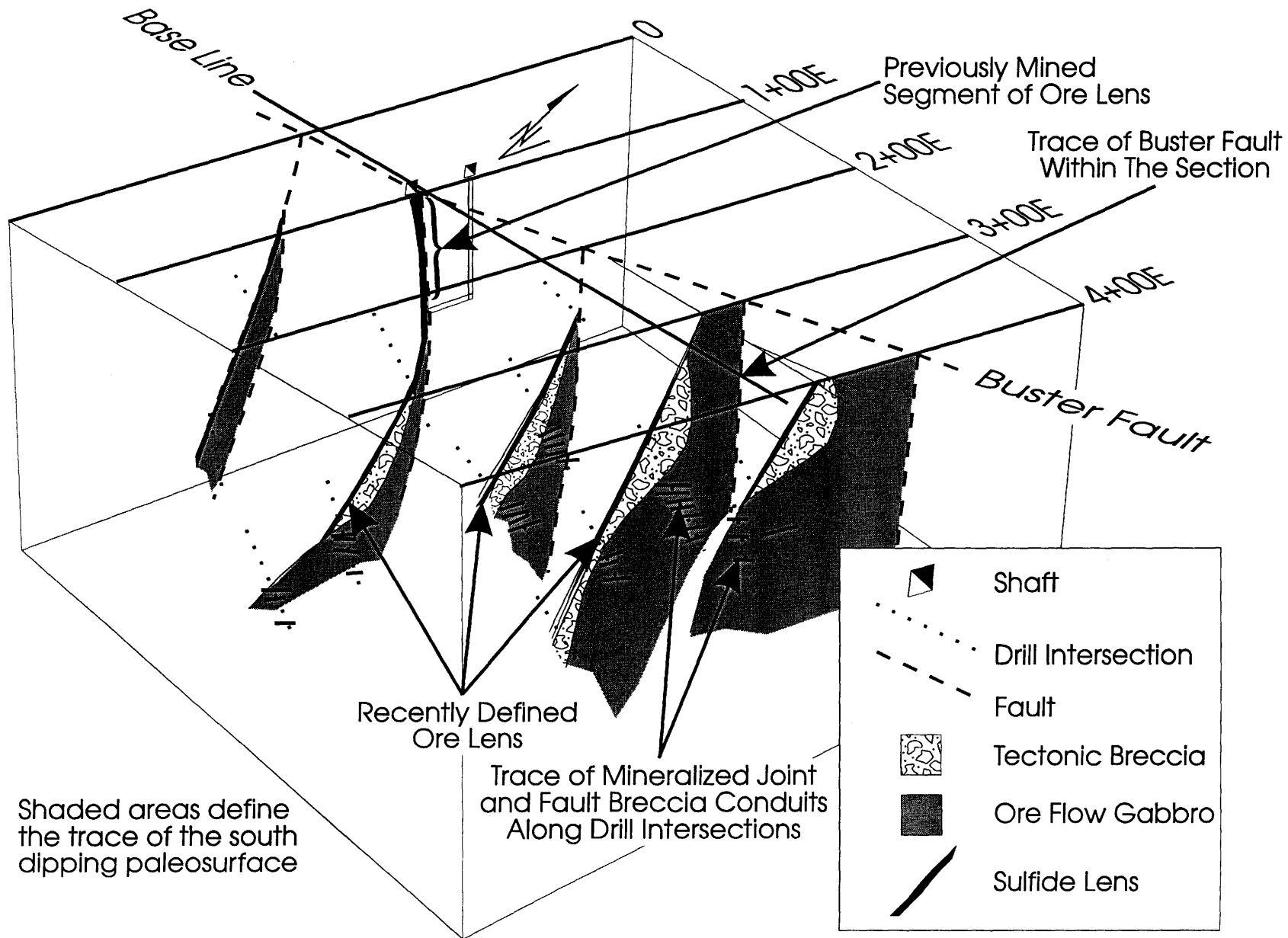


Figure 4-7 Three dimensional structural model of the Potterdoal stratigraphy, compiled from diamond drill hole information.



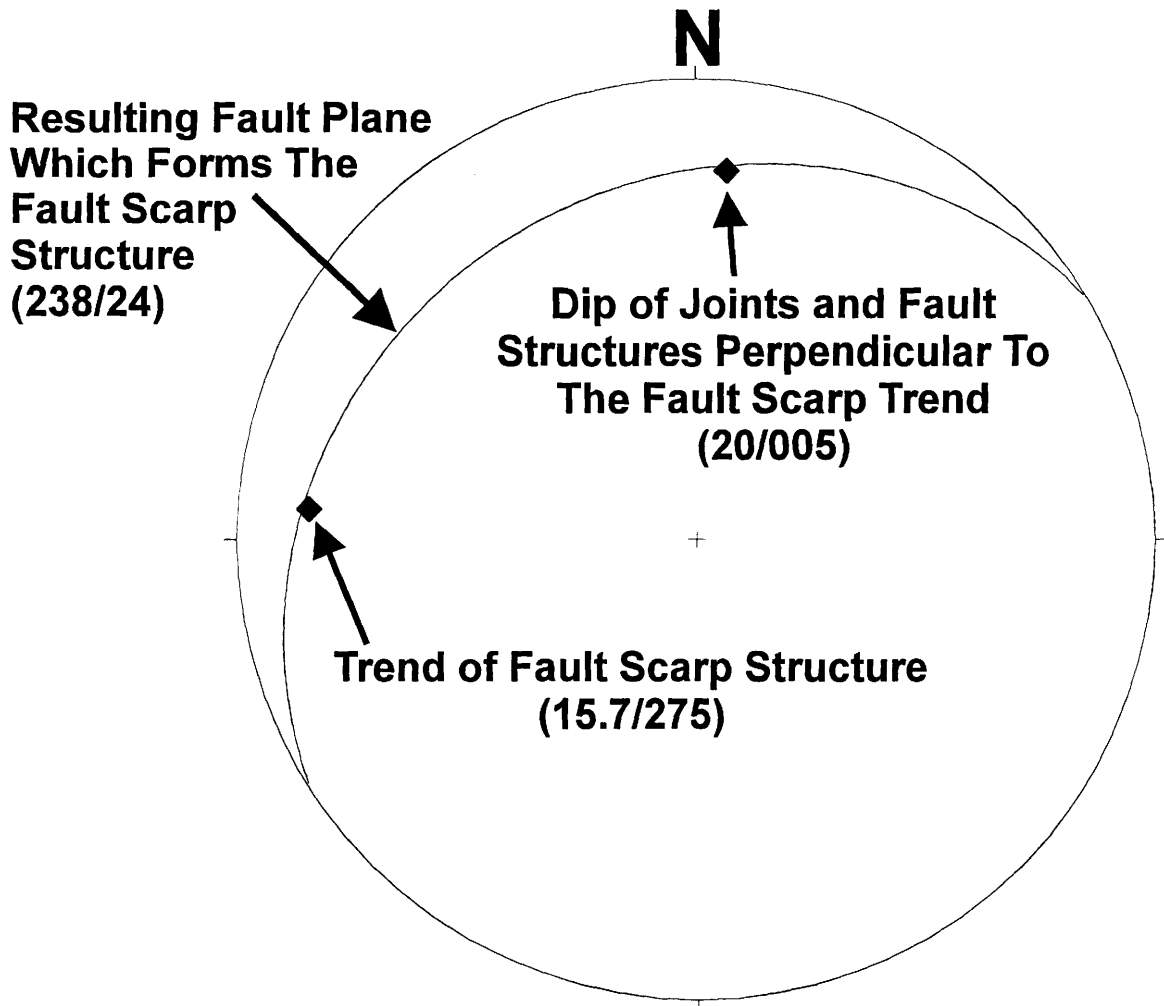
transect. Abundant joints and small shears within Ore Flow gabbros underlie the steep eastern margin and trough of the fault scarp structure, and have been interpreted to be oriented subvertically relative to the paleotopography (as defined by bedding).

The abundance of fault and joint structures within drill core of the Ore Flow gabbros had been somewhat troubling, since no expression of these structures were readily evident in surface mapping during the first field season. In an attempt to locate these structures in outcrop, a stereo net study was undertaken, using the available structural data. From the three-dimensional drill model, the trend of the fault scarp structure was determined ($16^{\circ}/275^{\circ}$). Then from seven drill holes, 43 core angle measurements of fault and joint structures within the Ore Flow gabbro were measured. These measurements were then corrected for drill hole dip and the rotation required to align the fault and joint structures parallel to the trend of fault scarp. From this, an averages

estimated fault dip perpendicular to the fault scarp structural trend was determined to be approximately 20° (represented by the trend $20^{\circ}/005^{\circ}$). This data was then plotted on a stereo net (Figure 4-8), and the two linear points were joined along a great circle. This great circle represents the plane of the fault and joint structures which make up the fault scarp, and is defined by a strike and dip of $238^{\circ}/24^{\circ}$.

Considering the three-dimensional model, this structural information was projected to surface and was found to be associated with the depression mapped along the top of the Ore Flow, between lines 400E to 600E (Figure 4-2). These projected joint and fault structures would outcrop as shallow, northwest dipping structures within the Ore

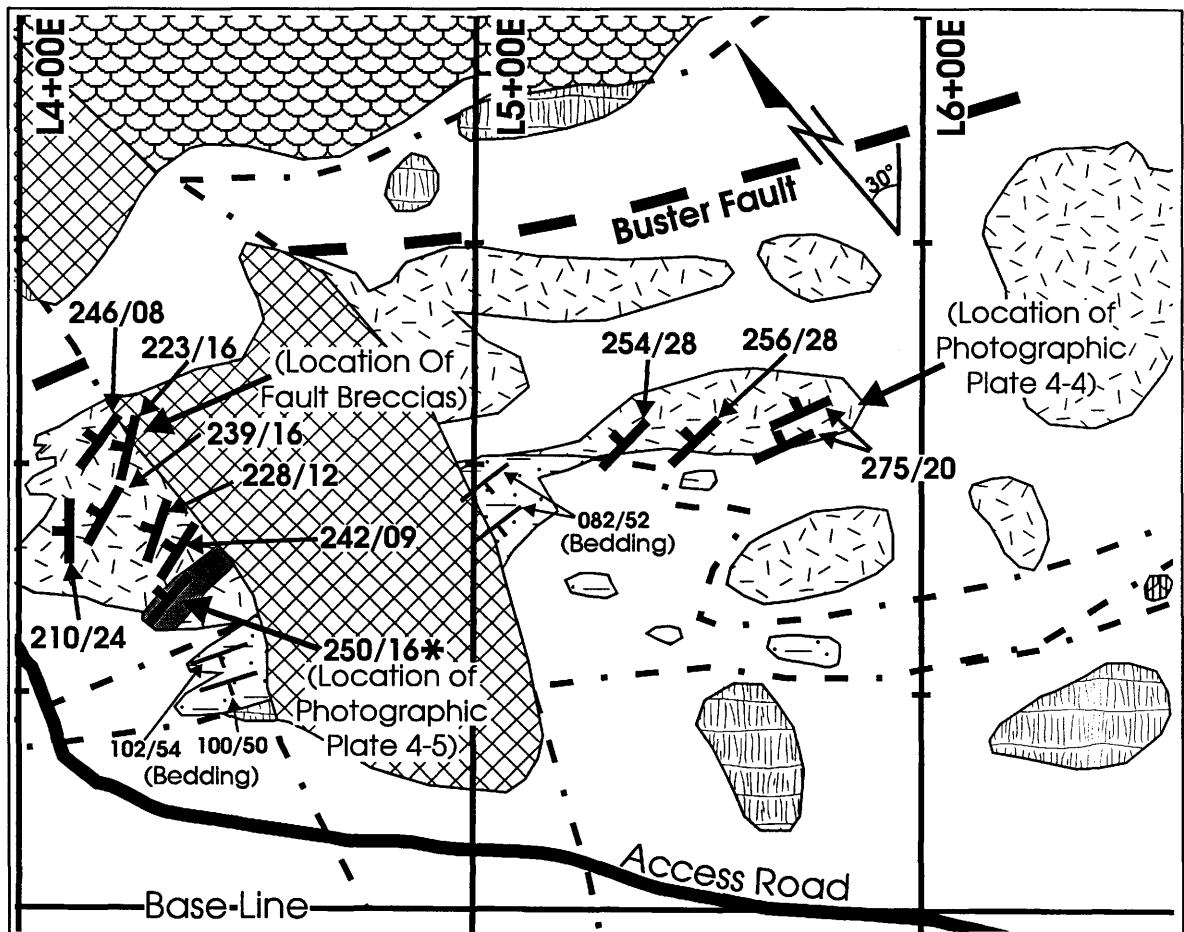
Figure 4-8 Stereo net plot defining the planar orientation of fault and joint structures which formed the sub-surface fault scarp structure



Flow gabbros. Prepared with this information during the second field season, a more detailed examination of the map area where the fault scarp structure outcrops was performed. This mapping is presented in Figure 4-9, and shows numerous shallow dipping joint sets, all generally trending to the north to the northwest. Previously, many of these important flat structure were overlooked due to their tendency to become preferred erosional surfaces. However, in more strongly jointed areas, a stepped habit of erosion surfaces (as seen in Plate 4-4, location shown on Figure 4-9) accentuates the appearance of the joint system. Once these joint and fault structures were recognized on surface, localized associations with “bleaching” alteration and sulphide mineralization within the Ore Flow gabbros were also noted (Plate 4-5), confirming the link these structures have with the ore forming hydrothermal system. A rare surface expression of a rock texture referred to as “fault breccia” (which is abundantly obvious in drill core) was also located in outcrop using the three-dimensional data. This rock type will be discussed further, later on in this chapter.

In summary, the structural analysis of joint structures noted in drill core was extremely helpful in recognizing several structurally related features in outcrop. Joint measurements collected at eight separate locations along the Ore Flow gabbro provided an average planar orientation of $245^{\circ}/18^{\circ}$. This very closely approximates the stereo net derived joint orientation of $238^{\circ}/24^{\circ}$, which was used to help recognize these structures in outcrop.

Figure 4-9 Detailed surface structural map showing the location and orientation of joints and faults related to the sub-surface fault scarp structure. (The structural measurement noted with an asterisk indicated an average measurement along a mineralized undulating fault).



0 25 50 Metres

- | | | | | | |
|---|---------------------------------|--|--------------------------------|--|-----------------------------|
|  | Matachewan Dyke |  | Komatiites |  | Ore Flow Tholeiitic Gabbros |
|  | Cherts and Tuffaceous Sediments |  | Theo's Flow Tholeiitic Basalts | | |

Plate 4-4 Outcrop of Ore Flow gabbro showing stepped erosional surfaces caused by flat, northwest dipping joints. (Photograph taken looking towards the northeast. Note hammer for scale).

Plate 4-5 Outcrop of Ore Flow gabbro showing pale “bleached” alteration and oxidized sulphide mineralization in association with flat northeast dipping joints. (Photograph taken looking towards the north. Note



4.2.3 Tectonic Breccias

The fault scarp discussed above is interpreted to have formed during the intrusion of the footwall Munro-Warden Sill. The angular chert and tuffaceous dominated “tectonic breccias” which fill the fault scarp structure (Plate 4-1), appear to have been created during seismic activity and fault movement associated with the formation of the fault scarp. This brecciation process has been discussed by Sillitoe (1985), and it is important to note that no crustal-scale tectonic process is implied by the term “tectonic breccia”. These tectonic breccias and the underlying fault scarp structures are very important since they respectively acted as the principal mineralization site and hydrothermal conduit for the ore-forming hydrothermal system.

4.2.4 Fault Breccias

Another rock type related to local structure are the fault breccias. These breccias were first observed in drill core (Plate 5-7b and 5-7c) locally developed along fault and joint systems associated with the fault scarp structure. Fault breccia consists of various sized rounded clasts (1 to 50 cm) in a milled chloritic matrix and occurs at varying depths solely within the gabbroic phase of the Ore Flow. Due to the relatively fragile chloritic nature of fault breccia textures (as compared to the enclosing massive Ore Flow gabbros), it appears that fault breccia textures are rarely preserved in outcrop. The only outcropping of fault breccias found (Figure 5-7a), is located just east of line 400E (Figure 4-9), and is thought to have been saved from glacial erosion by its fortuitous positioning

on the leeward side of the erosional resistant Matachewan dyke. The exact process of formation of this rock texture will be discussed in following chapters.

Chapter 5

Petrography of Major Stratigraphic Units

5.1 Introduction

Detailed petrographic study primarily focused on stratigraphic units directly affected by the ore-forming system. For this reason, the underlying Warden Township basalts, the lower portions of the Munro-Warden Sill, the differentiated section of Theo's Flow, and the bulk of the overlying Fred's Flow komatiites were not included in detailed examination. Excellent petrographic descriptions of these unit can be found in Johnstone (1987), Arndt et al. (1977) and MacRae (1969). A petrographic summary of important units within the map area is presented in Table 5-1, and include the upper Munro-Warden Sill, the sheeted to pillowed phases of Theo's Flow, the gabbroic and pillowed phases of the Ore Flow, the graphitic chert and tuffaceous sedimentary rocks, and the immediate capping rocks of the Fred's Flow komatiites. The petrographic data contained in this table have been averaged from several slides of each rock type, and thus shows the typical mineral composition range for each unit within the map area. Exact mineral proportions of each unit is not directly stated in the following mineralogical discussion, so reference to Table 5-1 should be made for this information.

Table 5-1: Petrographic descriptions of significant units associated with the Potterdoal mineral occurrence.
Each unit description was averaged from several thin sections which may range in the degree of alteration (from sub-greenschist to lower greenschist grades) depending upon the specific rock unit.

Mineral	% Volume	Grain Size	Description
Upper Munro-Warden Sill			
-Weak to moderately altered massive gabbro:			
Plagioclase	40 to 50%	0.25 to 1 mm	intergranular to tabular, ghostly, sericitized
Clinopyroxene	10 to 30%	0.1 to 0.5 mm	corroded, intergranular
Chlorite	5 to 30%	~ 0.05 mm	irregular, radiating, locally pseudomorphs pyroxene (mainly prochlorite, some penninite)
Quartz	2 to 15%	0.5 to 1 mm	irregular grains
Leucosene	Trace amounts	0.25 to 0.5 mm	skeletal to anhedral (pseudomorphed after titanite)
Adularia	Trace amounts	0.25 to 0.5 mm	irregular to subhedral grains
Theo's Flow			
-Fresh gabbroic textured massive flow:			
Clinopyroxene	~ 55%	0.5 to 2 mm	intergranular
Plagioclase	~ 35%	0.1 to 0.5 mm	intergranular to tabular
Olivine	~ 5%	~ 0.5 mm	subhedral, equant grains
Chlorite	~ 5%	< 0.1 mm	fibrous to radiating (mainly prochlorite)
Ore Flow			
-Weakly altered tholeiitic gabbro:			
Plagioclase	~ 40%	0.5 to 2 mm	tabular intergranular, sericitized (anorthosite)
Clinopyroxene	10 to 40%	0.25 to 1.0 mm	tabular, weakly corroded (augite)
Chlorite	5 to 35%	0.1 to 0.25 mm	lath shaped, locally pseudomorphs clinopyroxene (both prochlorite and penninite)
Quartz	5 to 10%	~ 0.5 mm	irregular grains
Adularia	~ 0 to 4%	0.25 to 0.75 mm	irregular grains
Leucosene	~ 0 to 1%	~ 0.25	subhedral pseudomorphs after titanite
-Weakly to moderately altered pillowed tholeiitic basalt:			
Plagioclase	30 to 60 %	0.05 to 1 mm	irregular to acicular (locally plumose)
Clinopyroxene	5 to 35%	0.05 to 1 mm	tabular to plumose
Chlorite	25 to 50%	< 0.05 to 0.3 mm	irregular, pseudomorphed after clinopyroxene
Calcite	~ 0 to 7%	< 0.05 to 3 mm	irregular, polygranular to continuous grains
Quartz	~ 0 to 4%	< 0.05 to 0.1 mm	irregular grains, dominantly amorphous silica
Sulfides	~ 0 to 3%	0.1 to 0.3 mm	irregular to subhedral overgrowths (predominantly pyrite and pyrrhotite)
(Calcite and silica found primarily along fractures and within amygdules.)			
Sediments			
-Fresh graphitic cherts:			
Pyrite	5 to 70%	0.1 to 25 mm	subhedral to framboidal
Quartz	20 to 85%	< 0.01 mm	granular, annealed silica
Graphite(?)	~ 2 to 20%(?)	<< 0.01 mm	irregular, "dusty" graphitic carbon
Calcite	~ 0 to 10%	~ 0.1 mm	irregular to subhedral rhombs
-Fresh to moderately altered crystal tuff:			
Plagioclase	50 to 70%	0.05 to 0.5 mm	broken tabular to irregular annealed
Quartz	~ 2 to 5%	0.2 to 0.3 mm	large irregular grains
Adularia	~ 1 to 15%	0.05 to 0.3 mm	irregular grains
Chlorite	2 to 40%	~ 0.03 mm	irregular to fibrous (replaced glass)
Sulfides	~ 1 to 3%	0.02 to 3 mm	irregular to subhedral to corroded framboidal
Calcite	~ 0 to 30%	< 0.1 mm	irregular
(Finer grained samples show significant recrystallization of plagioclase and quartz.)			
(Sulfides consist of pyrite replace by pyrrhotite, and trace amounts of sphalerite and chalcopyrite.)			
Komatiites			
-Moderately altered peridotitic komatiites:			
Olivine	70 to 90%	0.25 to 1 mm	subhedral, equant to tabular (now altered to mainly antigorite)
Clinopyroxene	5 to 15%	0.25 to 0.5 mm	tabular to intergranular, mildly corroded
Chromite/Magnetite	2 to 5%	0.05 to 0.5 mm	subhedral octahedrons
Chlorite	~ 0 to 10%	0.2 to 0.5 mm	irregular bladed (mainly prochlorite)
-Moderately altered picritic komatiites:			
Clinopyroxene	55 to 65%	0.1 to 0.4 mm	tabular intergrowth
Olivine	20 to 25%	0.2 to 0.3 mm	anhedral equant to irregular
Chlorite	15 to 25%	~ 0.01 mm	fibrous to irregular
Opaques	~ 1%	0.05 to 0.1 mm	subhedral octahedrons to irregular (chromite and magnetite?)

(Note: Clinopyroxene and chlorite in all rocks examined above typically show an inverse modal abundance relationship, since chlorite is generated primarily by the breakdown of the clinopyroxene.)

The degree of alteration of each unit varies depending on several factors, such as the thickness of extrusive units, average primary grain size, proximity to late sills, and degree of exposure to late hydrothermal activity. However, as previously noted, metamorphic alteration rarely exceeds lower greenschist facies.

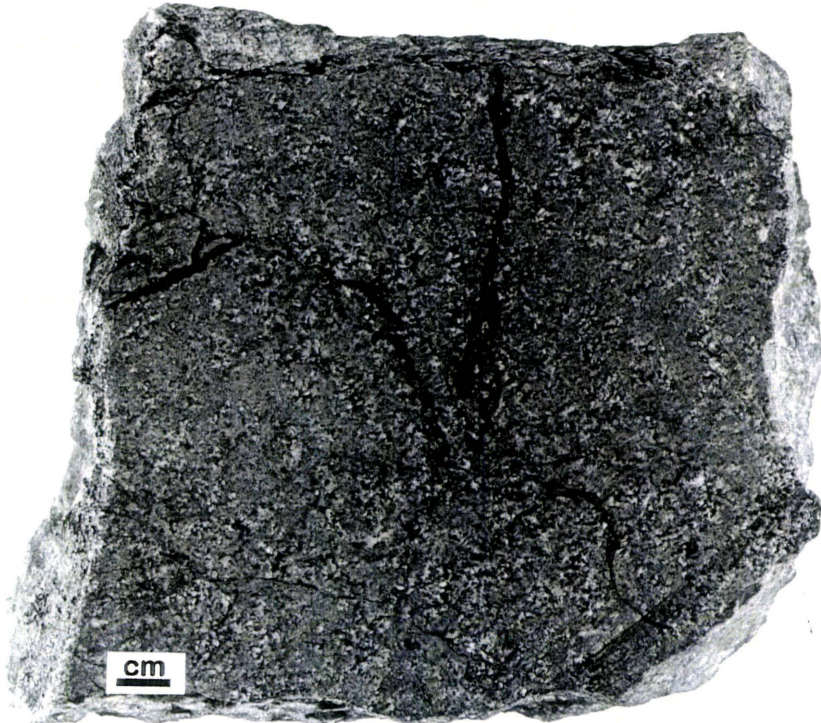
5.2 Upper Munro-Warden Sill

The upper portion of the Munro-Warden Sill consists of a tholeiitic gabbro grading to leucogabbro. Outcroppings of the leucogabbro (Plate 5-1) typically have a mottled pale green colour and show indistinct, irregular grain boundaries, indicating a pervasive alteration. Plate 5-1 also shows an irregular shaped patch of oxidized sulphides which are typically associated with joint systems which transect the Munro-Warden Sill at high angles ($\sim 70^\circ$ to 90°). The strong association of these sulphides to joint structure and locally pervasive alteration suggests that the upper portion of the Munro-Warden Sill was exposed to the effects of a convecting hydrothermal system.

A slabbed specimen of the leucogabbroic phase of the sill, shown in Plate 5-2, again shows the pervasive "non-distinct" grain margins of mafic minerals and a network of dark, randomly oriented fractures. When observed in thin section, these fractures are characterized by the replacement of all minerals by a hydrothermal chlorite referred to as penninite (penninite is readily distinguished from other chlorite species by its anomalous "Berlin blue" birefringence; Kerr, 1977; p. 443-445). In the remainder of the rock, extensive replacement of clinopyroxene by prochlorite and penninite, as well as pervasive sericitization of plagioclase, has occurred (Plate 5-3). Locally, large quartz and K-

Plate 5-1 Leucogabbroic phase of the Munro-Warden Sill in outcrop, showing mottled pale green appearance, indistinct mineral grain boundaries and a large patch of oxidized sulphides.

Plate 5-2 Cut slab of Munro-Warden Sill leucogabbro which shows a network of dark, randomly oriented fractures formed by hydrothermal alteration.



sericitization of plagioclase, has occurred (Plate 5-3). Locally, large quartz and K-feldspar grains are noted and appear to be secondary minerals, owing to their higher abundance in more intensely altered gabbros. Judging from the degree of alteration seen within the upper Munro-Warden Sill, late stage mineral reactions probably took place under conditions of high water-rock ratios is supported.

5.3 Theo's Flow Tholeiites

Theo's Flow was examined along the transitional sheeted to pillowed flow section which locally underlies the main sulphide lens. The sheeted flows, located in the central-western portion of the map area, average several metres in thickness and are characterized by a fine-grained microgabbroic texture (primarily ophitic textured). Eastward from the sheeted flows, the flow becomes much more distinctly pillowed (Plate 5-4), and attains a homogenous aphanitic internal texture with thick chloritic pillow rinds. In thin section, the flow rocks of Theo's Flow are relatively fresh with only minor chloritic (prochlorite) alteration of pyroxene, moderately sericitized, fine grained plagioclase and minor subhedral, equant olivine phenocrysts. The presence of these olivine grains makes the Theo's Flow basalts easily distinguishable from other flow basalts within the map area.

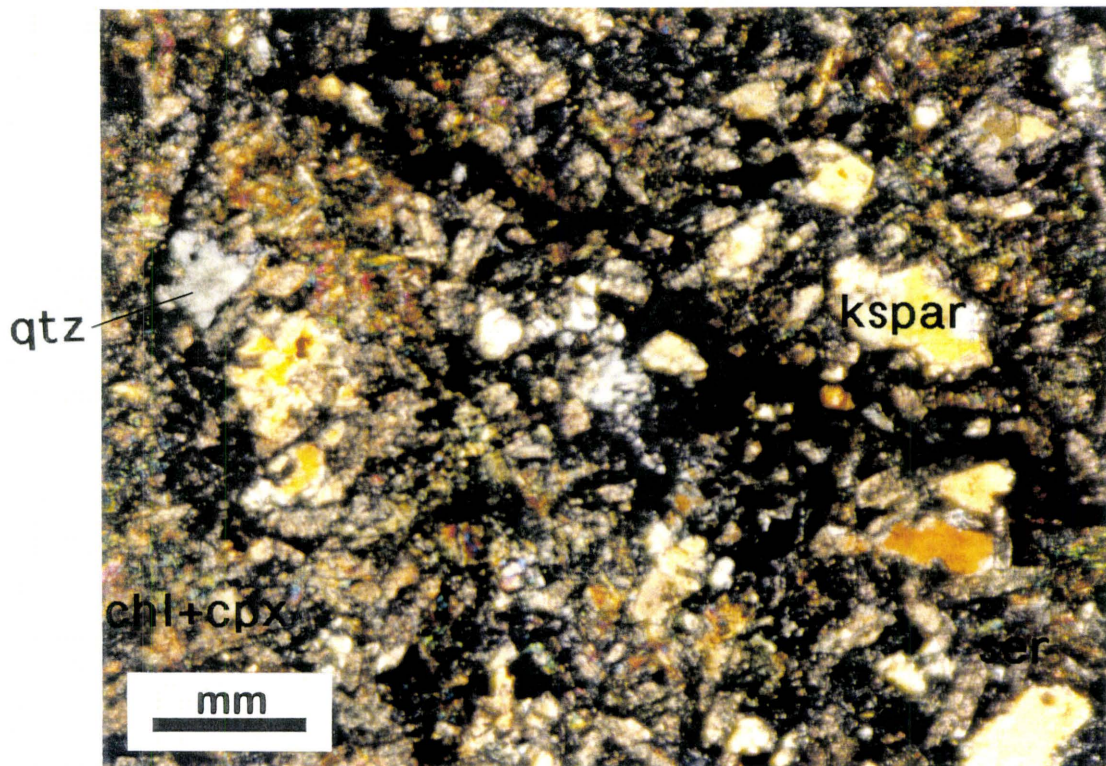
5.4 Ore Flow Tholeiites

5.4.1 Ore Flow Gabbro

Petrographic study of the Ore Flow includes both the massive gabbroic and pillowed phases of the flow. The Ore Flow gabbro appears massive and fairly featureless

Plate 5-3 Photomicrograph of Munro-Warden Sill leucogabbro containing a ground mass of sericitized plagioclase and chloritized clinopyroxene, with larger secondary grains of quartz, K-feldspar and opaque magnetite-ilmenite. (Sample photographed under cross polarized light).

Plate 5-4 Pillow structure located within the eastern extension of Theo's Flow.



in outcrop (Plate 5-5), leading to the original interpretation of the flow as a late discordant gabbro dyke (Satterly, 1952). This interpretation was subsequently accepted by later mapping (MacRae, 1965; Johnstone, 1987). However, recent evidence indicates the presence of a chilled, vesiculated flow top breccia overlying the massive flow (Plate 5-6), and a conformable contact with the overlying chert and tuff horizon has been noted in drill core. When combined with surface evidence for a lateral, east-west gradation from massive to pillowed flow habit, the re-interpretation of this unit as an extrusive volcanic unit in a seafloor environment is more probable.

The Ore Flow gabbro comprises the immediate footwall rocks to the main sulphide lens, and therefore has been locally subjected to extensive hydrothermal activity during ore formation. Evidence of this is limited in surface exposure, but is suggested by the presence of sulphides associated with joints within the gabbro (Plate 5-5) and by the poorly preserved fault breccias (Plate 5-7a). The strongest evidence for the ore-forming hydrothermal system comes from drill core, where distinct zones of hydrothermal alteration are seen to be narrowly confined (within 1 to 4 m) around fault and joint structures. It is suggested that these structures efficiently channeled the local hydrothermal flow, since gabbros more than a few metres from these highly altered structures exhibit mineral assemblages compatible with the regional metamorphic grade. The most intense alteration is typically associated with the fault breccias characterized by rounded fragments of various sizes (1 to 50 cm) in a milled chlorite-rich matrix (Plate 5-7b and 5-7c). Fault breccias were observed to occur locally only along fault structures which transect the Ore Flow gabbro. Similar fault breccia textures have not been

Plate 5-5 Ore Flow gabbro in outcrop. The Ore Flow gabbro generally appears massive and fairly featureless in outcrop, but locally contains sulphide mineralization commonly associated with joint systems (note the 40 cm long sulphide stained patch just below the hammer).

Plate 5-6 Flow top breccia found along the top of the gabbroic phase of the Ore Flow.



Plate 5-7a Fault breccia exposed on surface. Note well rounded clasts (positively weathered) in a chloritic matrix (negatively weathered). This eroded view lies along the plane of a fault in which the fault breccia formed. Owing to the relatively soft nature of the fault breccia's chloritic matrix, these breccias are rarely preserved along the erosion surface.

Plate 5-7b Fault breccia in core showing the progressive formation of incipient brecciation.

Plate 5-7c Strongly developed fault breccia in core showing well rounded "milled" fragments in a finely ground flour matrix.

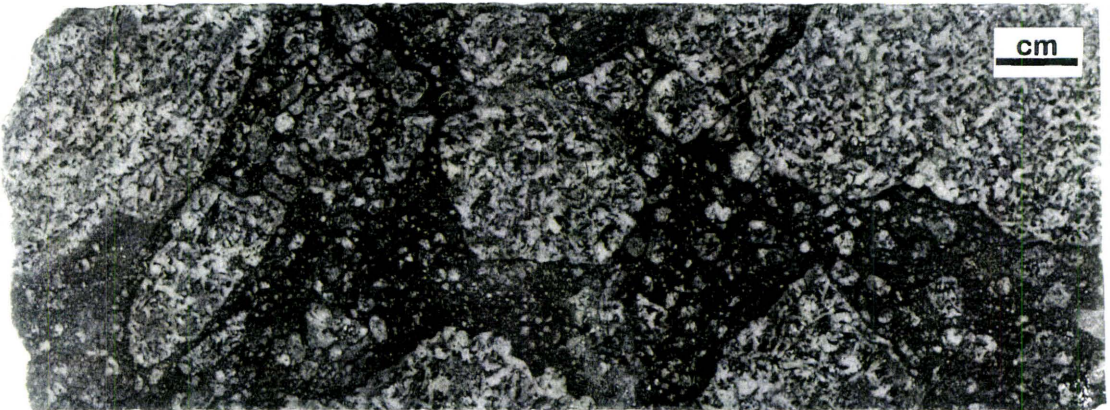
a)



b)



c)

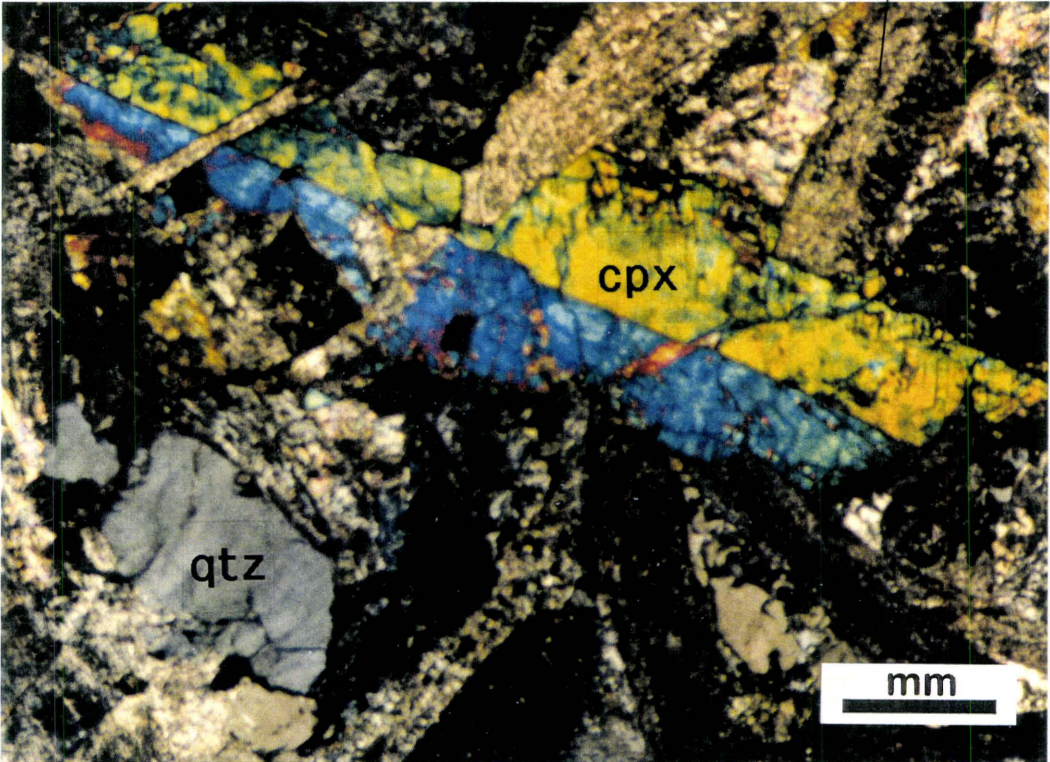


observed cutting other rock types in either outcrop or drill core. The chloritic alteration and the presence of incipient brecciation along these joint and fault systems suggests that the fault breccias formed by hydraulic fracturing along pre-existing fault and joint structure, which then liberated and milled rock fragments within highly pressurized fluid conduits.

Least altered Ore Flow gabbro specimens examined in thin section were generally medium to coarse grained and showed weak to moderate alteration (Plate 5-8). Plagioclase and clinopyroxene occurred in roughly equal proportion, and showed mutually impinging grain contacts, implying contemporaneous crystallization. Plagioclase grains showed a moderate degree of alteration to sericite, but retained enough remnant twinning to indicate that original plagioclase compositions ranged from bytownite to anorthite (biaxial negative and $2V$ values between 60° to 70°). Pyroxenes were generally clean, showed simple twinning, and optically indicated an augite composition (biaxial positive and middle second order maximum birefringence). Some primary quartz was present in some samples (i.e. in the upper right corner of Plate 5-8), but quartz and K-feldspar grains occur more commonly in association with increased hydrothermal alteration within the gabbro. Opaque mineral content is relatively minor in the freshest gabbros, consisting of skeletal magnetite-ilmenite. However, with increased alteration, the abundance of skeletal magnetite-ilmenite grains increases in association with chloritic alteration rims around pyroxene grains. When influenced by hydrothermal fluids, the magnetite can become preferentially sulphidized, producing a skeletal pyrite-ilmenite intergrowth, appearing reminiscent of a zebra skin pattern.

Plate 5-8 Photomicrograph of the least altered Ore Flow gabbro, showing anhedral to subhedral, tabular plagioclase and pyroxene grains, finer grained plagioclase matrix and a primary quartz grain. (Sample photographed under cross polarized light).

plag+ser



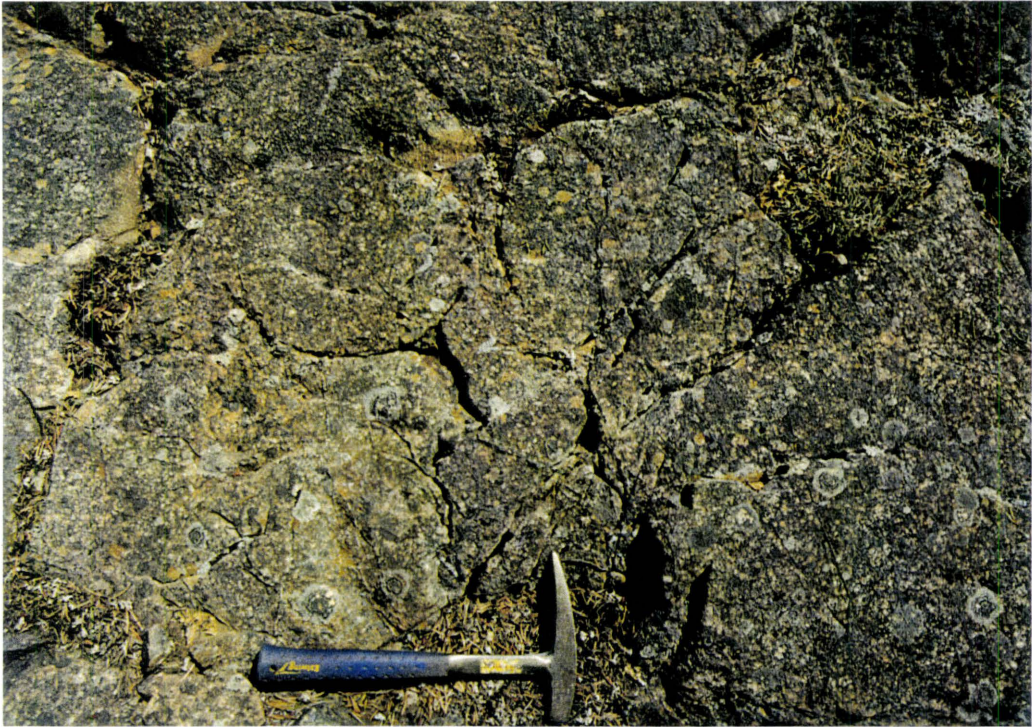
5.4.2 Ore Flow Basalts

The westward transition from massive gabbroic to pillowed phase of the Ore Flow tholeiites is very subtle in outcrop, but becomes much more evident further to the west. The first observable change from a massive gabbroic phase is indicated by a general decrease to a medium grain size and the appearance of delicate pillow structures (as seen in Plate 5-9) as well as glassy sheeted flow tops between line 300E to just east of line 400E (refer to Figure 4-2). Further to the west of line 300E, pillow selvages become much more evident and scattered varioles are noted in some pillows. Once line 200E has been reached, varioles has become very common (Plate 5-10) and can locally make up greater than 50% of the pillow volume. Vesiculation is fairly rare, but present (as seen in Plate 5-11a) in Ore Flow basalts, implying that water depth during extrusion was between 0.5 to 1.0 kilometres deep (pers. comm. Dr. Paul Clifford, 1995).

In thin section, the freshest tholeiitic pillowed flows of the Ore Flow are generally more strongly altered than the massive gabbroic flow facies. The majority of the chloritic and sericitic alteration observed in Ore Flow basalts is suspected to have occurred when the relatively thin flows were extruded onto the ocean floor, incorporating a large amount of water vapour into the crystallizing lava. The gabbroic portion of the flow, being much thicker and having a much smaller relative surface area in contact with sea water, incorporated much less water vapour and therefore experience much less alteration during extrusion.

Plate 5-9 Transitional phase between Ore Flow gabbro and basalt. Note homogenous medium grained texture and delicately developed pillow selvages.

Plate 5-10 Variolitic pillows at the western most end of the Ore Flow (note photo scale at bottom right and line picket for scale)



Ore Flow basalts are predominantly composed of chloritized clinopyroxene and sericitized plagioclase in roughly equal proportions. Within strongly variolitic basalts, the modal proportion of plagioclase to clinopyroxene within variolitic domains (2:1 to 3:1 plagioclase to pyroxene) is much higher relative to that in the non-variolitic domains (1:4 to 1:5 plagioclase to pyroxene). Minor amounts of quartz, calcite and sulphides are also noted in all Ore Flow basalts, but appear to have been introduced as secondary minerals during either metamorphism or by the late ore forming hydrothermal system. Mineral textures within the basalts vary significantly, but do not show any apparently spatial transitional trends. In the seven slides prepared from least altered Ore Flow basalts (i.e. basalts not effected by the late hydrothermal system), dominant mineral textures varied from plumose sericitized plagioclase (Plate 5-11a), to dendritic chloritized clinopyroxene (Plate 5-11b), to a fine acicular intergrowth of altered clinopyroxene and plagioclase. As a general summary for all examined Ore Flow basalts, it appears that almost all primary clinopyroxene has been altered to prochlorite and that plagioclase shows somewhat less intense pervasive sericitization. Absence of olivine and the abundance of varioles distinguish the Ore Flow pillowed basalts from the flow basalts of Theo's Flow. The less intense degree of alteration within Theo's Flow may also suggests that it has been subjected to significantly less hydrothermal activity than the Ore Flow.

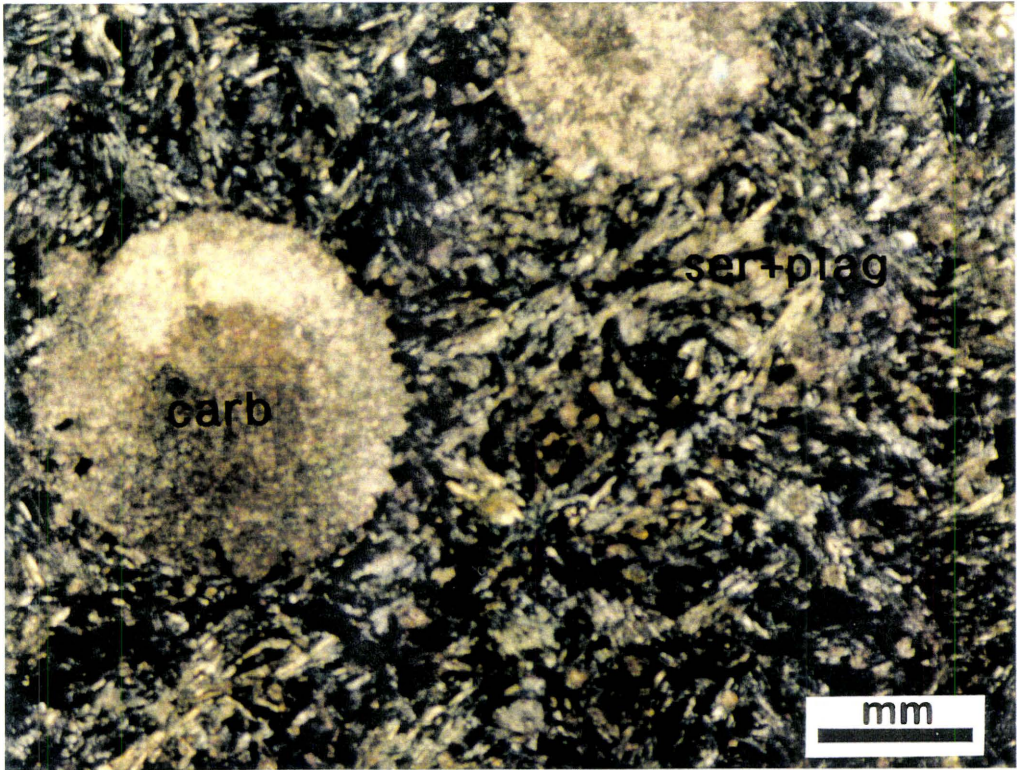
5.5 Sedimentary Rocks

Sedimentary rocks examined were primarily taken from the unit which overlies the Ore Flow. Two distinct sedimentary rock types are contained within this unit,

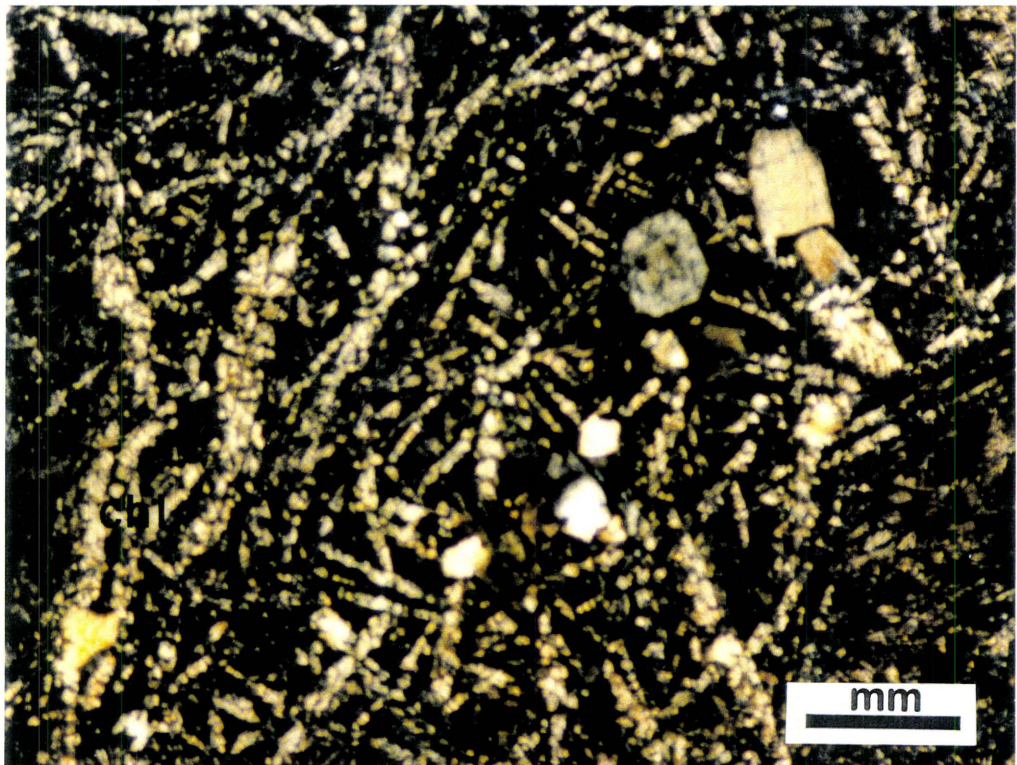
Plate 5-11a Photomicrograph of Ore Flow basalt showing plumose textured plagioclase and calcite filled vesicles. (Sample photographed under cross polarized light).

Plate 5-11b Photomicrograph of Ore Flow basalt showing dendritic textured, chloritized clinopyroxene. (Sample photographed under cross polarized

a)



b)

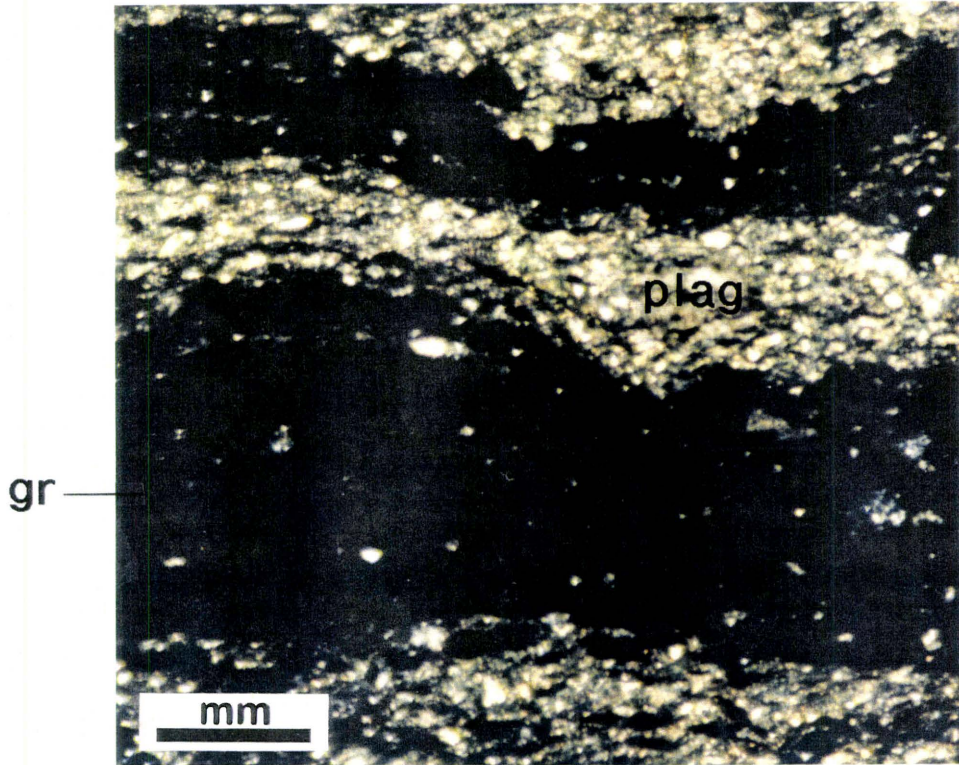


consisting of graphitic cherts and crystal tuffs. Tuffaceous rocks are significantly more abundant within the stratigraphy than the graphitic cherts, making up about 75% of the total sedimentary unit overlying the Ore Flow. The modest amount of surface and drill core information available on these inter-flow sediments shows very little evidence of consistent stratigraphy between the cherts and tuffs. Available information suggests that layering of cherts and tuffs appears fairly randomly, and may indicate accumulation within very subtle depressions located on a flat seafloor environment.

The graphitic cherts are not well exposed on surface within the map area, but are well represented in drill core. Texturally, these cherts vary from homogeneous black, to banded black and gray, to homogeneous black with varying amounts of pyritic nodules. In general, the presence of fairly thick accumulations of these siliceous sediments within the Potterdoal stratigraphy is a good indicator of quiescent periods of non-volcanism. In thin section, the homogeneous black graphitic cherts are quite opaque, owing to the high graphite content. In the banded graphitic cherts, the lighter gray bands are seen to be thin ash-rich layers which are interlayered with graphitic chert layers (Plate 5-12). Botryoidal to framboidal pyrite nodules found within many of the graphitic chert horizons (Plate 5-13), are suggested to have formed by a process of bacterial reduction of iron and sulphur within the unconsolidated siliceous chemical sediments. The implication of bacterial activity may also potentially explain the abundance of graphite, which in other similar rocks have been shown to have strongly negative carbon isotope values, indicative of a biochemical origin (Bowins and Crocket, 1994).

Plate 5-12 Photomicrograph of graphitic chert with narrow interlayered band of plagioclase-rich ash. (Sample photographed under cross polarized light).

Plate 5-13 Core samples showing framboidal pyrite nodules commonly found within graphitic cherts.



In outcrop, the crystal tuffs appear very clean, and shows rhythmic layering suggestive of active ash fall (Plate 5-14a). Often, these rhythmically layered tuff units show traces of cherty graphite at the top of centimeter-scale, fining-upward sequences (Plate 5-14b). In such cases the graphitic material probably indicates a short period of quiescence between very rapid accumulations of ash. Examination in thin section (Plate 5-14c) supports the field observations, predominantly showing smooth fining upwards sequences of very clean plagioclase crystals, with little or no “muddy” fine grained matrix. Even though layering within the tuff is primarily centimeter-scale normal graded bedding, smooth transitions into inversely-graded bedding can be found locally. This suggests that the grain size gradation is due to waxing and waning eruptions of air-fall ash, and not to Bouma-style turbidite deposition. This conclusion is backed up by the presence of graphitic chert within the tuffs, which indicates that deposition occurred in a low energy, deep oceanic environment. Since turbidites are most commonly associated with fairly energetic continental margin environments, the tuffs could not have been deposited by means of turbiditic sediment flows.

5.6 Komatiites

The komatiites which cap the stratigraphy are predominantly peridotitic, but do show a few interbedded units of more pyroxenitic affinity. In outcrop, the komatiitic flows show a characteristic rounded, reddish brown weathering surface (Plate 5-15). In thicker flows (greater than 2 m thickness), polygonal jointing as seen in Plate 5-16 is common. Plate 5-16 also shows the typical bluish green internal colour of the komatiitic

Plate 5-14a Crystal tuff in outcrop, showing fine rhythmic layering.

Plate 5-14b Core sample of crystal tuff, showing graded bedding and graphitic chert horizons, each indicating a short hiatus in ash fall. This sample also shows fault structure which were probably induced by seismic shocking while the tuff was still only semi-solidified.

Plate 5-14c Photomicrograph of graded bedding of the plagioclase crystal-rich tuff. Note the lack of any “muddy” interstitial material. (Sample photographed under cross polarized light).

a)



b)



c)

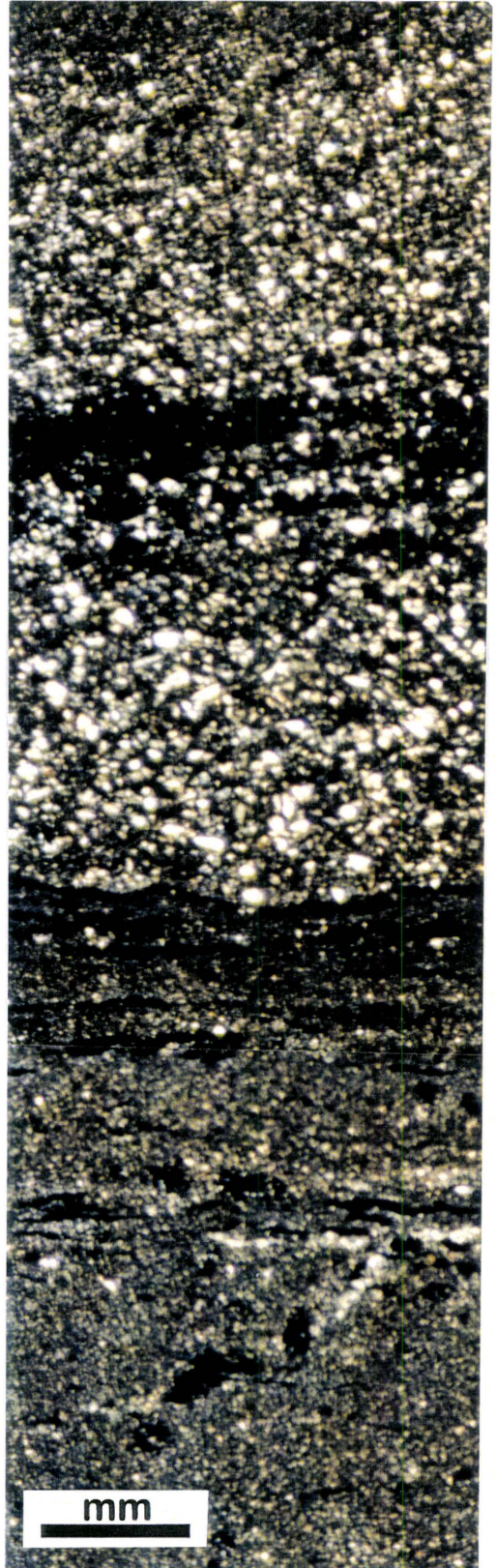
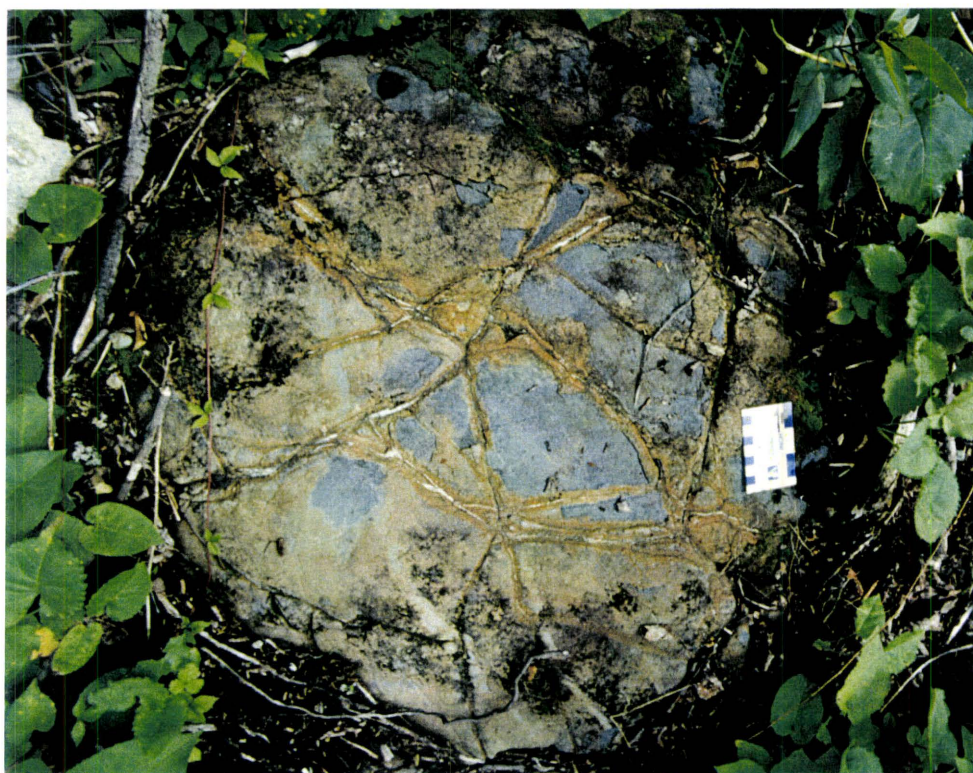


Plate 5-15 Peridotitic komatiites in outcrop, showing characteristic rounded erosion surface and reddish brown weathering.

Plate 5-16 Peridotitic komatiite showing polygonal jointing and internal bluish green colour where the weathered surface has spalled off.



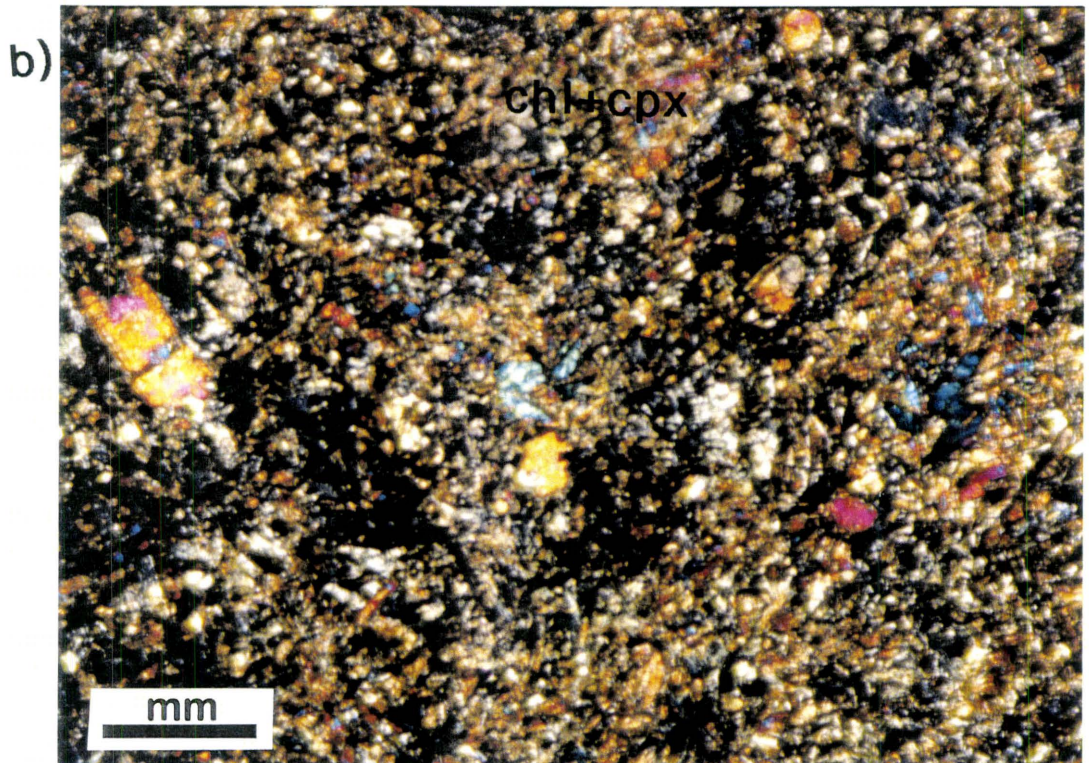
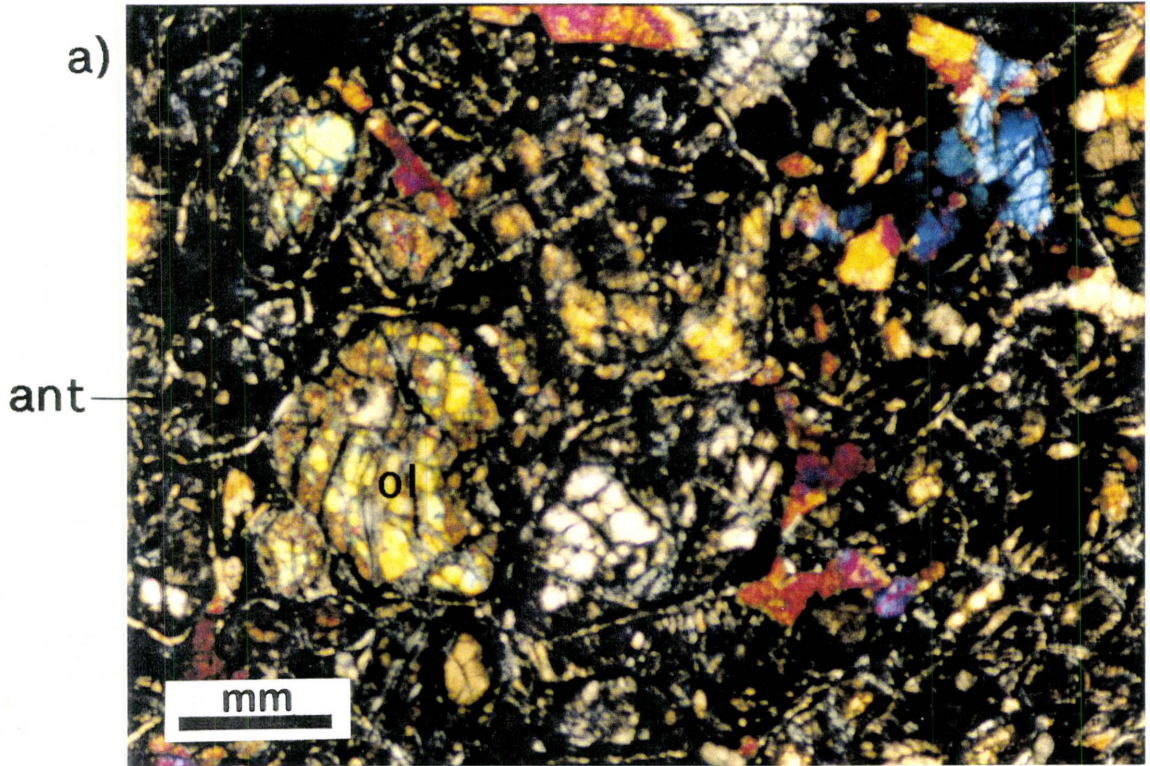
flows, exposed where the weathered surface has spalled off. Thinner flow units (0.5 to 1 m) within the map area sometime show skeletal "hopper" grains randomly distributed within the flow. These hopper grains appear as a cluster of radiating, bladed olivine crystals, and may represent an early or incomplete stage of the formation of the olivine spinifex texture.

The petrography of the peridotitic komatiites is dominated by medium to coarse grained olivine which shows strongly pervasive serpentinization. This serpentinization probably occurred during or shortly after the extrusion of the flow onto the sea floor. The effects of serpentinization are seen in Plate 5-17a, where the strongly birefringent, subhedral olivine crystals have largely been replaced by dirty, lower first order birefringent antigorite. Lesser amounts of fine grained, interstitial clinopyroxene also show minor to moderate replacement by chlorite. Opaque minerals are seen as thinly but evenly distributed, coarse grained (0.2 to 0.5 mm) euhedral to subhedral octahedrons, and as fine grained, dusty irregular patches of anhedral grains. No polished thin sections were prepared for these komatiites, so exact opaque mineral identification was not possible. However, it is suspected that the coarser grained octahedral crystals are primary chromite grains, and the dusty fine grained crystals are magnetite produced by the serpentinization of olivine grains.

The picritic komatiite consists mainly of a fine grained matrix of chloritized clinopyroxene, with a much lesser proportion of anhedral high birefringent olivine grains (Plate 5-17b). Opaques are also much less abundant than in the peridotitic komatiites, probably due to the limited production of magnetite from the serpentinization of olivine.

Plate 5-17a Photomicrograph of peridotitic komatiite, showing pervasive replacement of olivine by antigorite. (Sample photographed under cross polarized light).

Plate 5-17b Photomicrograph of picritic komatiite, showing the dominant intergrown matrix of chloritized clinopyroxene and lesser amounts of anhedral to irregular olivine. (Sample photographed under cross polarized light).



Chapter 6

Sulphide Petrography and Associated Alteration

6.1 Sulphide Mineralization

Sulphide mineralization is manifested in two principal styles within the Potterdoal deposit, consisting of an upper massive sulphide lens and underlying stockwork mineralization. The main massive sulphide lens is generally conformable to stratigraphy, and can be traced in the subsurface from line 400E to just west of line 0+00, where it appears to be terminated by the Buster Fault (Figures 4-2 and 4-5). This lens occurs along the top of the tectonic breccia which fills the fault scarp depression and appears to be relatively continuous along the entire length of the scarp. The stockwork mineralization transects both the Ore Flow gabbros as well as the tectonic breccias which underlie the massive sulphide lens. Within the Ore Flow gabbro stockwork alteration and mineralization is confined to narrow fault breccia zones and joint structures. However, once the stockwork reaches the highly permeable tectonic breccias, stockwork alteration and mineralization widens out rapidly (a conceptual diagram showing the relationships between these sulphide-bearing domains is illustrated in Figure 8-1). Strong chloritic alteration produced by the hydrothermal fluid is seen to intimately accompany all stockwork mineralization. Sulphide mineralogy is similar for both the massive sulphide

lens and stockwork, and consists of pyrrhotite, chalcopyrite, sphalerite and pyrite in decreasing order of relative abundance. The paragenetic sequence of sulphide minerals was determined in relation to increasing degree of hydrothermal alteration, and is summarized in Figure 6-1. This paragenetic sequence is interpreted as a response to mineral-fluid reactions in a regime of progressively increasing fluid temperatures (as suggested by Lydon, 1988). It is significant to note that the Potterdoal mineralization contains little to no associated Pb-sulphides. This observation applies to other VMS deposits of similar age.

6.2 Stockwork Mineralization

The sulphide paragenesis of stockwork mineralization was examined across alteration envelopes which surrounds narrow fault breccia zones within the Ore Flow gabbro. Sulphide mineralization within fault breccia range from disseminated grains to discrete, narrow veinlets, which make up at most 3 to 4 percent of the rock volume. Pyrite is the earliest sulphide mineral introduced in stockwork mineralization, and occurs as large (~ 1 mm) subhedral aggregates within fracture conduits, and as fine (< 0.01 mm), disseminated grains which replace iron oxides within domains of low intensity hydrothermal alteration. Sphalerite occurs with pyrite in slightly more altered rocks and can be found locally intergrown with pyrrhotite at higher degrees of alteration. Within moderately altered rocks, pyrrhotite corrodes and replaces pyrite while chalcopyrite becomes prevalent. Chalcopyrite shows mutual grain boundaries with pyrrhotite suggestive of equilibrium. Sphalerite also shows ragged irregular grain margins,

Figure 6-1 Sulphide paragenesis diagram showing the sequence of emplacement within the Ore Flow fault breccias related to increasing hydrothermal alteration.

—pyrite—

—sphalerite—

—pyrrhotite—

—chalcopyrite—

Progressive Mineralization →
(Increasing Alteration →)
(Increasing Temperature →)

suggesting disequilibrium with the hydrothermal fluid. At high intensities of alteration, chalcopyrite replaces pyrrhotite, and the sphalerite decreases or is absent. From these observations, it is concluded that sphalerite is an early constituent of the sulphide paragenesis and is progressively dissolved as the temperature of hydrothermal fluids increases. Chalcopyrite locally replaces pyrrhotite and can occur as massive veinlets up to 0.5 cm wide. The intensity of chloritic alteration and replacement of gangue minerals in vein selvages suggests that chalcopyrite formation is associated with the highest temperature alteration.

A significant observation in respect to stockwork mineralization notes that not all well developed fault breccias within the Ore Flow are mineralized. This implies that the hydrothermal regime responsible for creating the fault breccia textures is not necessarily the same one which introduced the sulphide ore. Many fault breccia zones (up to 1 m wide in core) show intense milling of fragments and strong marginal incipient brecciation, but relatively little dark chloritic alteration and sulphide mineralization which is typically associated with an ore-forming hydrothermal conduit. Hydrothermal mineralization seems to replace fault breccia textures and is associated with intense dark chloritic alteration. This suggests that fault breccias systems were utilized as preferred fluid conduits by hydrothermal fluids, due to their high permeability. These observations suggest that an early hot and highly pressurized hydrothermal fluid produced wide-spread fault breccias within many joint systems along the fault scarp. Later, a lower pressurized, but much longer lived hydrothermal system utilized the least resistant paths to the

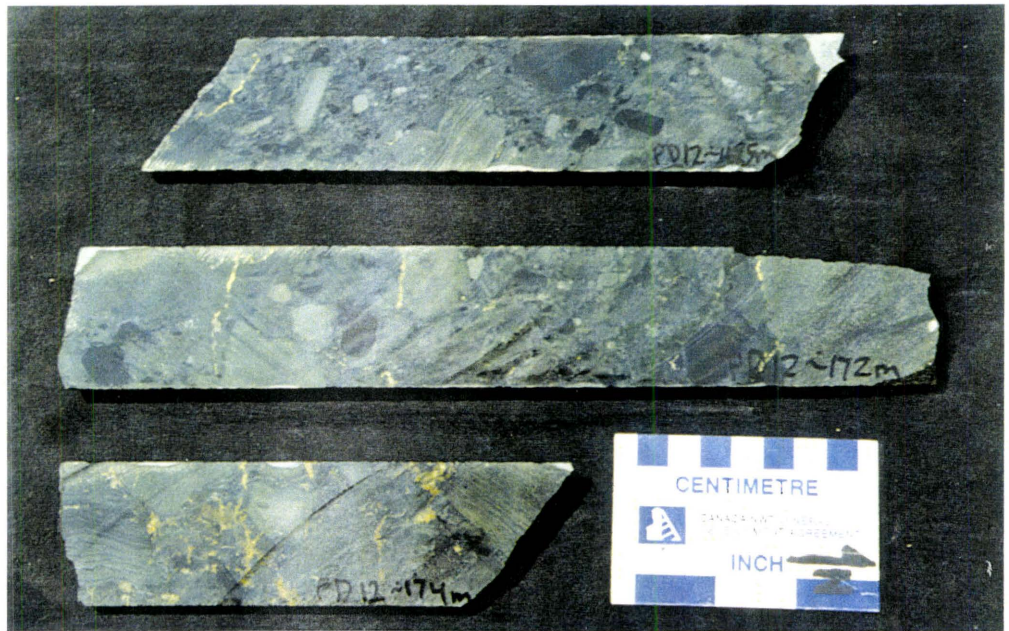
surface, selectively mineralizing and intensely altering only the most permeable fault breccias.

Stockwork within the tectonically brecciated sedimentary rocks displays the same sulphide paragenesis as seen in the Ore Flow fault breccia, although the style of mineralization differs significantly. Chloritic alteration is pervasive through much of the tectonic breccia. Base metal sulphides are more abundant than in stockworks where they are confined to fault breccias, and occur as discrete grains and complex networks of veinlets rather than discrete stringers (i.e. the lower two core samples shown in Plate 6-1). Sphalerite is significantly less abundant within the tectonic breccia, but chalcopyrite is common and can locally reach ore grades. Rare pyrrhotite pseudomorphs of pyrite framboids, partially replaced by chalcopyrite indicate the intense thermal conditions under which sulphide mineralization occurred within the tectonic breccias.

The change in style of stockwork mineralization reflects the transition between the highly constricted fault breccia pathways to the highly permeable tectonic breccias. The tectonic breccia was effective in diffusing the flow of the hydrothermal fluid, and thereby exposed a much larger volume of rock to hydrothermal alteration and mineralization. Pervasive chloritic alteration, extensive sulphide replacement dominated by chalcopyrite, and low proportions of sphalerite (suggestive of loss by resorption) are indicative of a significantly higher temperature environment than found within the majority of fault breccia stockwork. Elevated temperature seems to suggest that an efficient thermal barrier was present at the top of the tectonic breccia. Such a barrier may have been

Plate 6-1 Tectonic breccias showing varying degrees of sulphide veinlet formation.

Plate 6-2 A vertical transect of the sulphide ore lens, showing the transition of sulphide mineralogy from a yellowish-green chalcopyrite-rich base to a grayish-brown sphalerite-rich top.



generated by the massive sulphide lens itself, and by the gradual sealing of initial high porosity of the tectonic breccia domain.

6.3 Sulphide Lens Mineralization and The Vent Proximal Setting

The massive sulphide lens occurs within the uppermost portion of the tectonic breccia unit and accounts for the bulk of ore grade mineralization. The main lens is relatively undisturbed and retains much original texture, although the western margin is strongly tectonized where the Buster Fault intersects the ore horizon. The lens has a shallow westward pitch which follows the trace of the paleosurface fault scarp for at least 500 m. The width of this sulphide lens is generally greater than 100 m with thicknesses varying between 1 to 6 m.

Even though this large sulphide lens shows anomalously high base metal concentrations throughout, ore grade values occur only as broad sporadic centres, possibly representing localized hydrothermal vents. Drill core assays suggest that these ore centres grade outward laterally from chalcopyrite-rich centres to sphalerite-dominated peripheries as seen in Figure 6-2. A similar zonation of base metals is also noted for a vertical transect of the ore lens from the base to the top. This is seen in Plate 6-2 where the sulphide mineralogy varies from a yellowish-green chalcopyrite-rich base to a grayish-brown sphalerite-rich top. The base of the massive sulphide lens is usually difficult to distinguish from stockwork mineralization, since a large proportion (if not all) of the ore was deposited as a replacement of the tectonic breccia (Plate 6-3a and 6-3b).

Figure 6-2 Longsection projection of drill intersections for the Potterdoal sulphide lens, showing zoned centres with copper-rich cores and zinc-rich margins. Values displayed above drill intersections represents the percent volume of Cu and Zn respectively within the massive sulphide intersection.

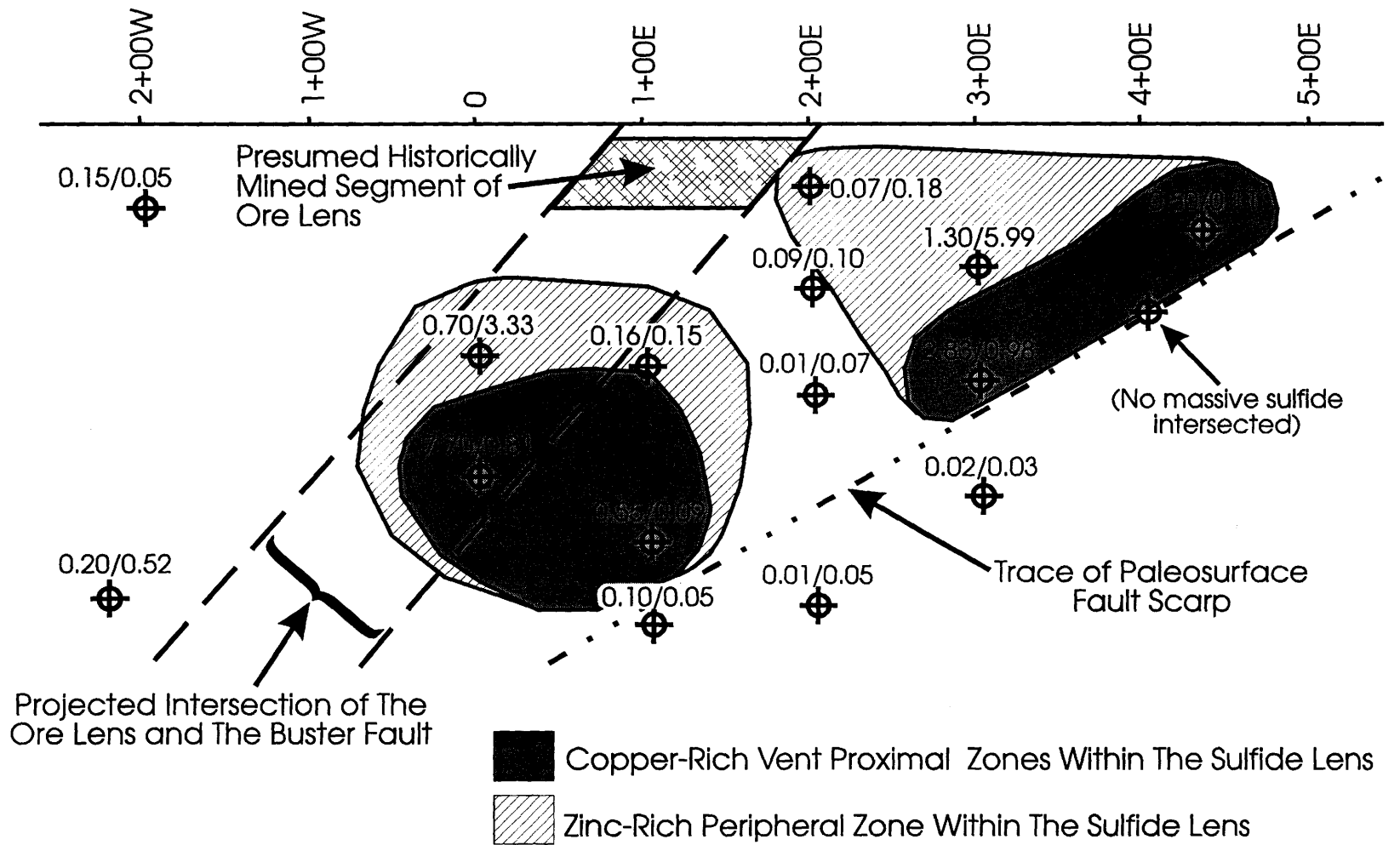
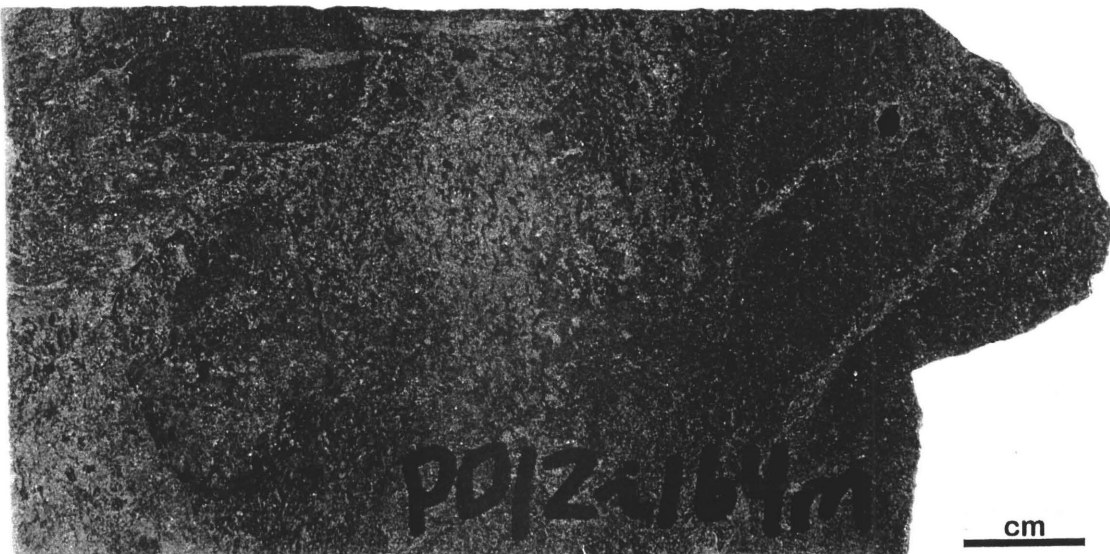
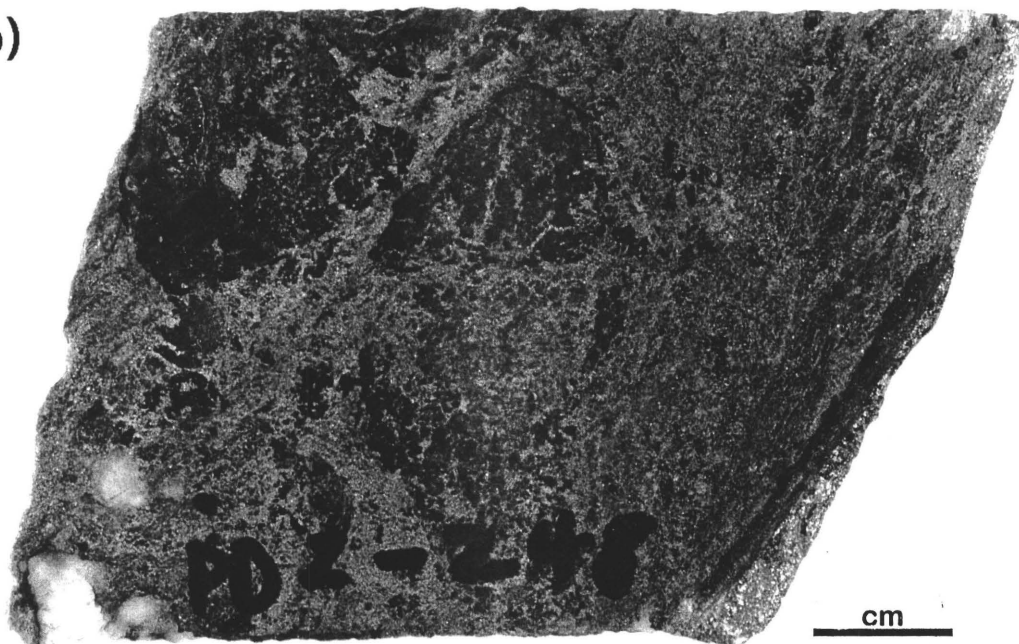


Plate 6-3a and b Massive sulphide samples showing indications of relict,
replaced tectonic breccia fragments. (Photograph is in black and white).

a)



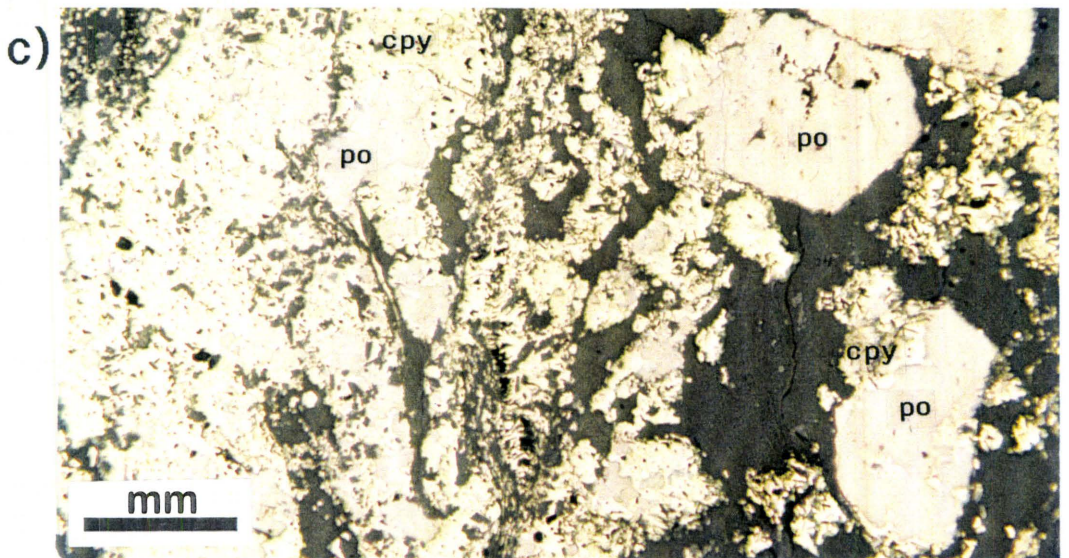
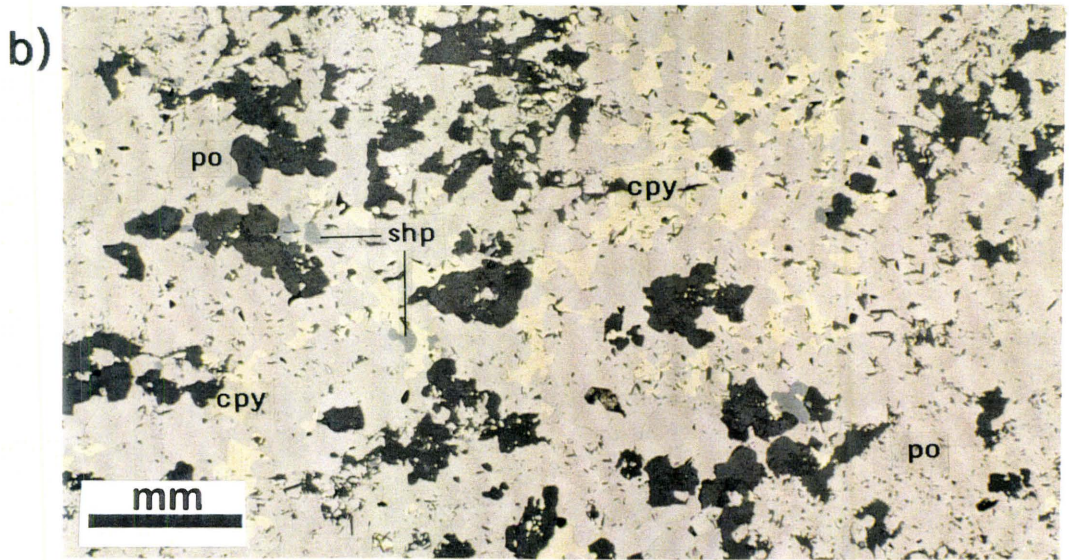
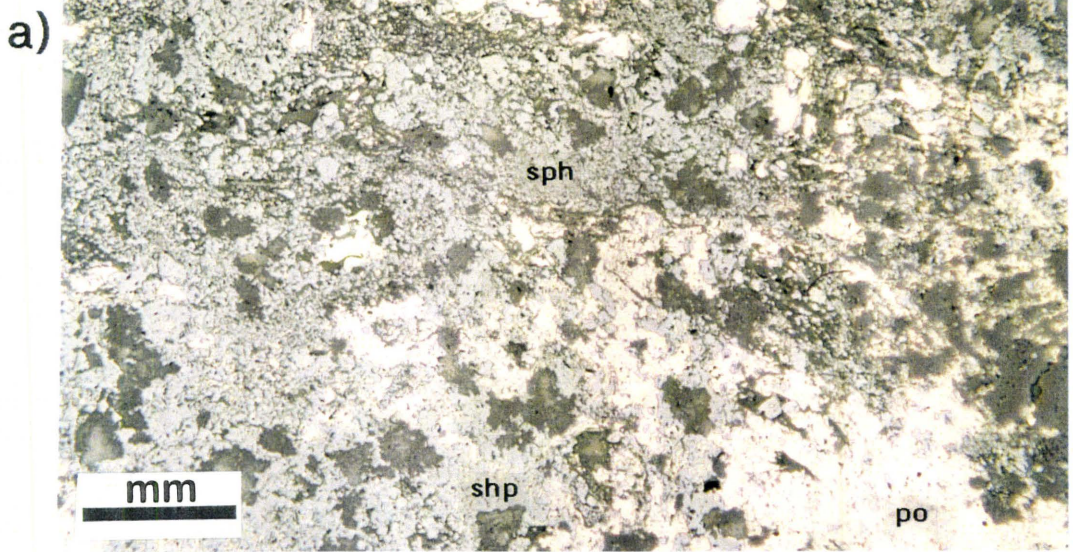
b)



As seen in polished sections, the sulphide mineralogy of a vertical section through a vent proximal ore centre is shown in Plates 6-4a, b and c. The polished thin sections, prepared from the three massive sulphide specimens shown in Plate 6-2, are largely dominated by pyrrhotite, which consistently comprises approximately 50% of the total sulphides of each sulphide specimen. Sphalerite and chalcopyrite show an inverse relationship in relative abundances, with sphalerite content increasing from 3% to 42% total volume and chalcopyrite decreasing from 57% to 5% from base to top of the lens. Gangue minerals comprise about 10% at most of the total volume, and change from fine granular penninite and acicular epidote at the base of the ore lens to patchy sericite, twinned albite and lesser penninite at the top.

Ore textures at the base of the lens are dominated by meandering coarse grained (> 1 mm) replacement veinlets of chalcopyrite, which have obscured most original textures. Sulphide grain sizes decrease noticeably from approximately 2.0 mm at the base to 0.5 mm at the top. Towards the top of the lens, sphalerite appears to have recrystallized, although grain size remains relatively fine (0.2 to 0.5 mm). Lamination within the fine grained sphalerite is locally defined by gangue minerals, and may represent exhalative sedimentation. However, there is no persuasive evidence from sulphide lens textures that any significant quantity of sulphides were accumulated by fall-out from sea floor vented hydrothermal fluid. Most sulphide accumulation represents direct replacement of the tectonic breccia, since the massive ore commonly shows "ghost" outlines of replaced chert fragments.

Plate 6-4 Photomicrographs of polished thin sections in cross-polarized, reflected light, each representing a portion of the vertical transect through an ore zone presented in Plate 6-2. **a)** Upper portion of the ore lens, showing relatively fine grained sphalerite (sph) and pyrrhotite (po). No chalcopyrite (cpy) is typically observed in ore from this stratigraphic level in the ore lens. **b)** The center of the ore lens, showing a fine to medium grained texture, with dominant chalcopyrite and pyrrhotite and lesser amounts of sphalerite. This slide shows the three main sulphide species existing in apparent equilibrium **c)** Lower portion of the massive sulphide lens, dominated solely by coarse grained chalcopyrite and pyrrhotite. The chalcopyrite shows a corrosive contact along and within the majority of pyrrhotite grains.



The upper contact of the massive ore with the overlying komatiite flows is typically sharp. The lack of any significant accumulations of exhalative chert overlying the massive ore suggests a brief hiatus between the termination of the hydrothermal ore system and the extrusion of the overlying komatiite. However, the komatiite flows probably did not smother or seal the hydrothermal system, since little evidence of hydrothermal alteration was noted within the komatiites.

Where the western edge of the sulphide lens is cut by the Buster Fault, the ore has been highly sheared, giving it a laminated appearance (see structural discussion in Chapter 4 and Plate 4-3). This section of shear laminated sulphides was originally misinterpreted to represent primary bedding (Ontario Dept. of Mines, 1928). Chalcopyrite tends to be more abundant within the sheared sulphides and was probably locally remobilized and concentrated by the shearing. This structural remobilization and reconcentration process likely explains why all past mining activity was focused only within the sheared portion of the deposit.

6.4 Hydrothermal Alteration and Metal Source

Hydrothermal alteration is primarily restricted to the top of the Munro-Warden Sill, the Ore Flow fault breccias, and the overlying tectonic breccias which host the main ore zone. Within both the upper Munro-Warden Sill and the tectonic breccias, alteration is pervasive but varies in intensity. The random nature of alteration within these two units makes it impossible to recognize any systematic alteration by the hydrothermal system. In contrast, Ore Flow fault breccias have well constrained marginal alteration

envelopes of several centimetres to several metres in scale, which demonstrate decreasing alteration away from the fluid conduits. A series of progressively altered Ore Flow gabbros, shown in Plate 6-5, were thin sectioned and studied to examine mineralogical changes associated with progressive hydrothermal alteration. A similar series of rock samples, specifically selected for their homogeneity and lack of sulphide mineralogy, were also used to assess the major element mass changes associated with the progressive hydrothermal alteration. The details of this mass balance study will be discussed in the following chapter.

6.4.1 Progressive Alteration of The Ore Flow Gabbro

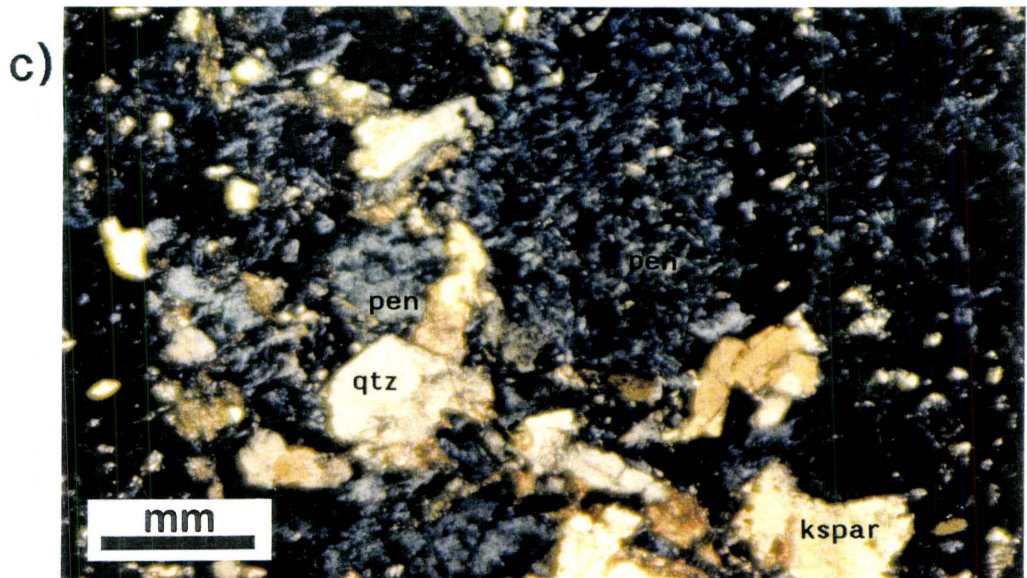
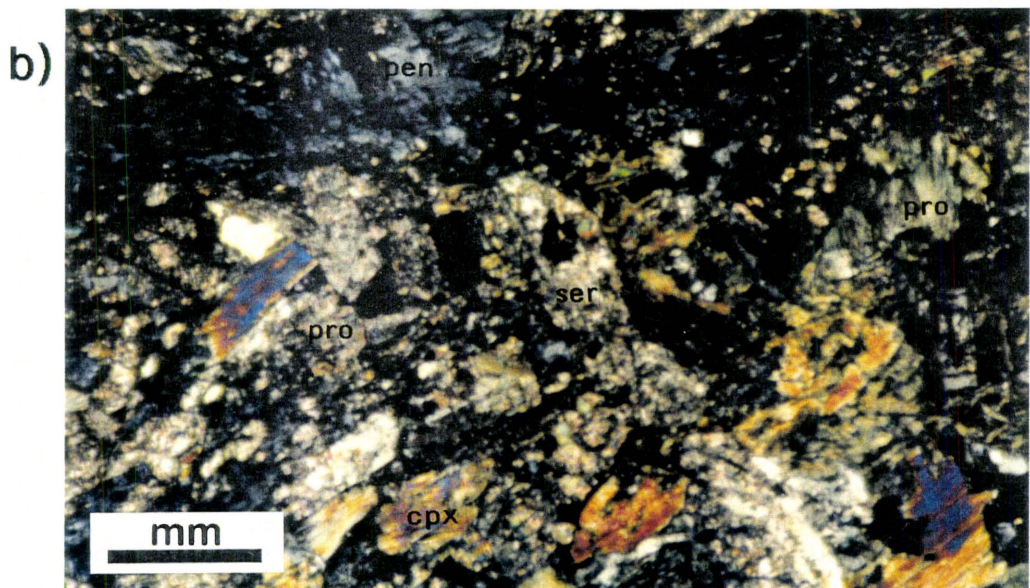
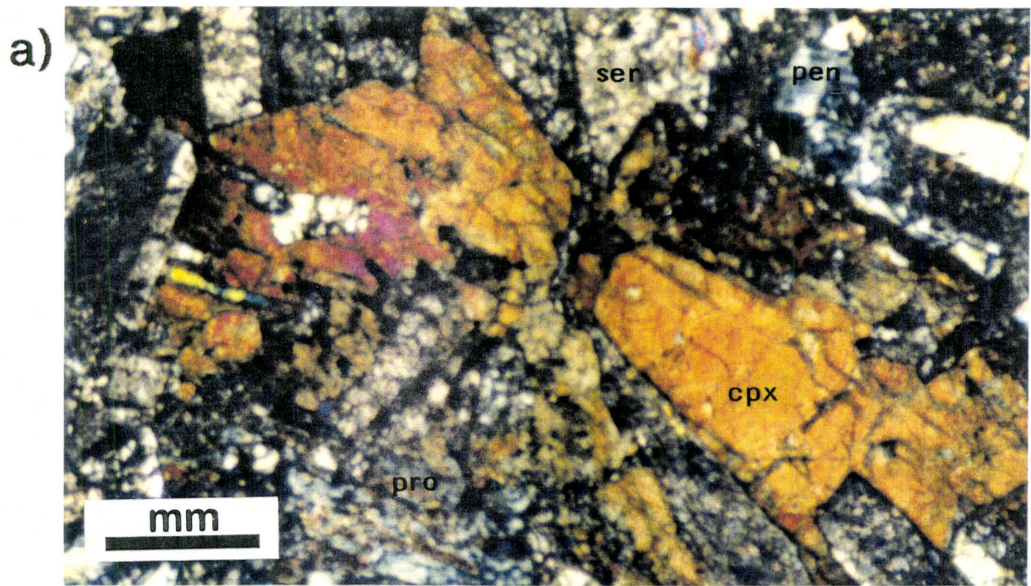
Examination of thin sections indicates that least altered Ore Flow gabbro consist of roughly equal proportions of plagioclase (45%) and clinopyroxene (45%), and minor titanite (2%; Refer to Plate 5-8 for photomicrograph of least altered gabbro). Quartz may constitute up to 8%, but is thought to be mainly of regional metamorphic origin (lower greenschist facies), since it typically appears as large irregularly shaped grains, which displace primary minerals. Macroscopic appearance of the least altered Ore Flow gabbro (top left core sample in Plate 6-5) is medium to pale green in colour with distinct plagioclase and pyroxene grain margins.

The lowest grade hydrothermal alteration on the margins of alteration envelopes is characterized by the initiation of pervasive replacement of clinopyroxene by prochlorite and magnetite, notable sericitization of the plagioclase, and replacement of subhedral titanite by leucoxene (Plate 6-6a). Locally, penninite can first be found replacing

Plate 6-5 Core samples showing progressive hydrothermal alteration of Ore
Flow gabbros.



Plate 6-6 Photomicrographs of progressive hydrothermal alteration of Ore Flow gabbros, taken from a fault breccia alteration envelope (all sample photographed under cross polarized light). a) Shows a mildly altered gabbro, with only limited break-down of clinopyroxene (cpx) into prochlorite (pro) and penninite (pen), and fairly pervasive replacement of plagioclase by sericite (ser). b) Moderate hydrothermally altered gabbro showing strong sericitization and near complete replacement of all clinopyroxene by near equal amounts of prochlorite and penninite. c) Highly altered gabbro showing predominant replacement of all previous mineral assemblages by hydrothermal penninite. Other residual minerals include quartz (qtz) and K-feldspar (kspar).



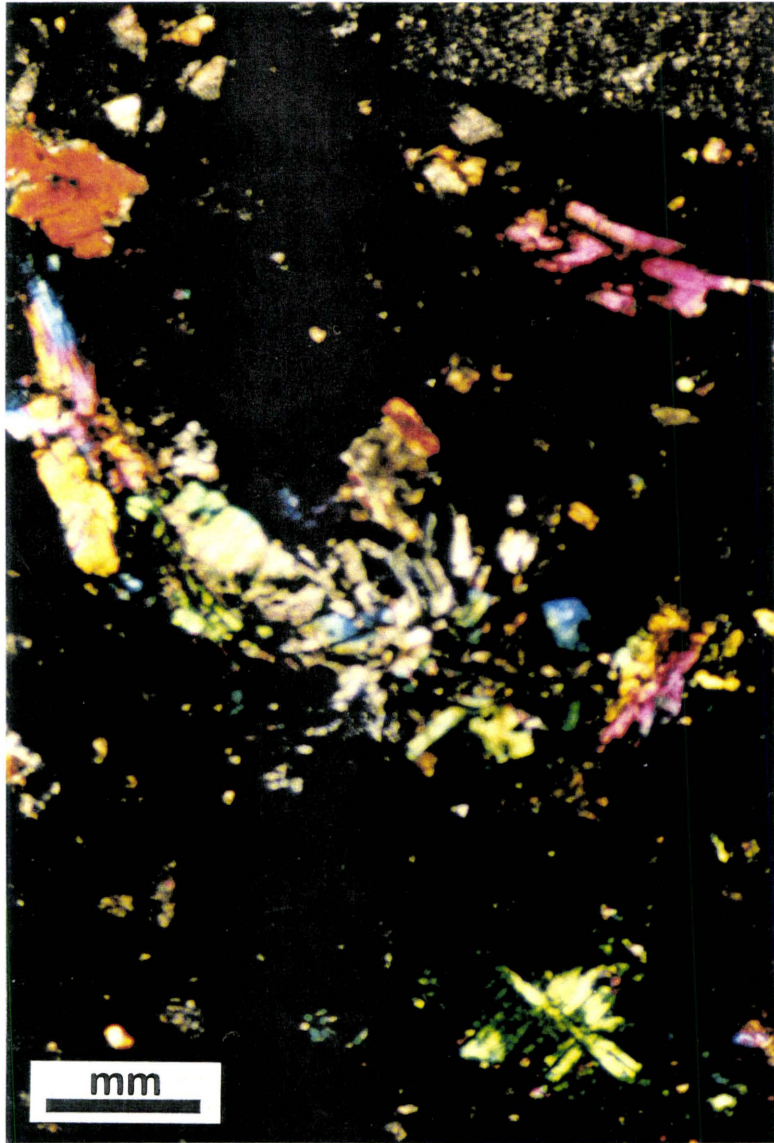
prochlorite and clinopyroxene in close proximity to fracture systems. In hand specimen, this rock shows a characteristic medium to dark olive green colour (top right core sample in Plate 6-5), and individual grains of plagioclase and clinopyroxene become less distinct along grain margins.

Intermediate alteration involves the progressive replacement of all pyroxene by prochlorite and penninite, pervasive sericitization of plagioclase, and conversion of leucoxene to titaniferous magnetite (Plate 6-6b). This rock has a peppered, black and white appearance (bottom left core sample in Plate 6-5), and individual grain boundaries have become very indistinct.

The most intense alteration along and within fault breccia conduits is dominated by extensive replacement of all minerals by hydrothermal penninite (plate 6-6c). Minor amounts of large, secondary quartz and K-feldspar grains are also present. The identification of the K-feldspar grains was not readily evident, since the grains were irregularly shaped, showed no twinning, and had irregular extinction. However, the grains were determined to be K-feldspar (possibly adularia) as indicated by elemental profiles (Figure 6-3) obtained from the EDS attachment of the McMaster University Life Sciences electron microscope. Locally within the highest altered fracture systems, epidote is also found (Plate 6-7) and appears to be replacing any residual feldspar. In hand specimen, very little primary textures appear are preserved, and the rock attains a dark black colour (bottom right core sample in Plate 6-5).

Figure 6-3 EDS elemental spectrum showing constituent elements of K-feldspar grains found within the highest hydrothermally altered fracture systems within the Ore Flow gabbros. Dominance of Si, Al and K indicates a K-feldspar composition.

Plate 6-7 Photomicrograph of epidote located within highly hydrothermally altered fractures within the Ore Flow gabbro. (Sample photographed under cross polarized light).



6.4.2 Metal Source

The exact source of metals found within the Potterdoal deposit has always been in question, since the immediate footwall rocks (i.e. the Ore Flow) shows only limited hydrothermal alteration. Upon more extensive examination of the Potterdoal footwall rocks, the Munro-Warden Sill is now thought to be the primary source of remobilized metals. The Munro-Warden Sill appears to have been the main heat source which drove the ore-forming hydrothermal system, and evidence supporting this hypothesis is found in the abundant alteration textures in the top of the sill. Specifically, gabbros in the upper sill show intense chloritic replacement of all pyroxene, strong sericitization of feldspars, and extensive fracturing along which the hydrothermal chlorite, penninite (see Plate 5-1 and 5-2), and high temperature sulphides occur (primarily pyrrhotite and traces of chalcopyrite). According to Pirajno (1992; p. 60-69), alteration textures of this nature are common in large sills emplaced at high structural levels into water-rich environments. Pirajno (1992) suggests that this alteration style is created by the contact of circulating sea water with hot, recently solidified intrusive rocks. Rapid cooling induced by the water creates a network of thermal contraction cracks, allowing convecting fluids to penetrate further into the intrusive along a "cracking front", which may advance downward at several meters per year. The propagation of this crack network continuously exposes a large surface area of rock ranging in temperature from 450 to 700°C. The alteration in the upper section of the Munro-Warden Sill suggests that these gabbros were exposed to such conditions, and were leached to produce a very hot hydrothermal fluid enriched in various metals. This metal-rich fluid quickly traveled through the permeable faults scarp

structure which transects the Ore Flow, causing only limited alteration and leaching of metal within the Ore Flow.

Chapter 7

Geochemistry

7.1 Introduction

As described in the chapter on methodology, major elements (expressed as oxides) and two suites of trace elements were determined by X-ray fluorescence (XRF) analysis. Rare earth elements, as well as a short list of other trace elements, were determined by instrumental neutron activation analysis (INAA). These data (compiled in Table 7-1) were used to help confirm parental magmatic affinities, probable tectonic setting of the volcanic suite, and to quantify the effects of alteration on mass changes in the Ore Flow gabbros. Elemental determinations of some lithologies (i.e. tuffs, komatiites and the upper Munro-Warden Sill gabbro) were based upon fairly small sample sets. While generalizations of chemistry from these small sample sets may not be truly representative of the full compositional variation for the lithology as found in the map area, the averages do appear consistent with those specific unit compositions established by Johnstone (1987), whose work was based on an extensive regional survey.

Table 7-1 Geochemical composition of surface and drill core rock samples.

Elements and oxides denoted by plain font indicates analysis by XRF, and elements denoted by italicized font indicates analysis by INAA. Pb was analyzed, however, most samples were below detection limits, and only one sample contained more than 7 ppm of Pb (SPD-23 contained 27 ppm Pb). Sc contents showed small variation for all samples, ranging between 18 to 40 ppm.

Table 7-1

Sample	Ore Flow Basalt				Ore Flow Gabbro						
	SPD-11	SPD-14	SPD-22	SPD-23	SPD-28	PD2-287	PD4-195	PD11-318	PD12-182	PD12-188	PD12-197
SiO2	47.35	47.15	51.80	49.10	52.89	53.14	45.93	52.98	54.32	54.05	53.19
TiO2	1.52	1.64	1.38	1.47	0.77	0.89	0.58	0.84	0.94	0.95	0.91
Al2O3	13.28	14.80	12.63	13.46	15.04	14.61	15.90	14.49	15.90	14.63	14.85
Fe2O3	17.85	15.21	15.19	17.02	9.86	10.58	20.36	12.28	12.80	11.99	15.56
MnO	0.27	0.29	0.25	0.34	0.15	0.15	0.25	0.17	0.13	0.16	0.18
MgO	6.18	6.41	5.26	6.37	6.35	5.51	8.16	6.12	6.58	5.94	5.87
CaO	8.75	7.02	9.08	7.34	8.12	8.71	2.41	8.98	3.35	4.73	2.92
Na2O	1.96	3.14	3.03	1.18	2.75	3.44	0.79	1.83	1.40	2.25	1.87
K2O	0.99	0.06	0.10	1.63	0.94	0.34	0.31	0.38	0.54	0.53	0.33
P2O5	0.13	0.14	0.11	0.13	0.07	0.10	0.08	0.09	0.10	0.09	0.10
L.O.I.	1.89	3.68	1.39	2.39	2.60	2.59	5.68	1.99	4.08	4.47	4.45
Total	100.17	99.54	100.22	100.43	99.54	100.06	100.45	100.15	100.14	99.79	100.23
Ni	60	31	56	57	58	44	116	43	43	40	40
Cu	160	123	154	156	44	0	807	66	21	20	200
Zn	142	150	121	266	42	63	124	72	94	158	67
Cr	40	15	31	35	167	36	303	51	46	26	34
Co	45	52	45	45	32	33	49	36	31	35	43
Ba	1133	76	102	387	242	141	57	109	105	86	79
Sr	288	207	306	186	242	199	50	131	119	150	123
Zr	115	128	102	110	66	67	46	82	83	77	72
Y	26	29	24	25	20	20	13	20	19	26	19
Rb	23	11	8	59	29	16	9	15	19	15	16
Ta	0.11	0.38	0.29	0.26	0.03	0.18	0.19	0.28	0.00	0.01	0.23
Hf	1.53	2.80	1.81	1.43	1.22	0.87	0.31	1.17	0.99	0.91	0.78
Cs	0.34	0.28	0.15	0.73	0.53	0.49	0.64	0.40	0.72	0.50	0.34
La	7.82	9.73	8.12	8.24	8.26	6.93	4.04	8.19	11.76	6.77	7.53
Ce	20.04	20.80	16.59	16.56	10.48	12.37	12.17	13.49	13.50	11.84	11.22
Nd	13.50	14.59	13.02	12.77	6.16	5.40	6.01	7.77	8.23	6.39	5.32
Sm	4.51	4.39	3.68	4.33	2.39	2.68	1.68	2.86	3.99	3.08	2.38
Eu	1.38	1.53	1.16	1.23	0.56	0.67	0.19	0.63	0.54	0.72	0.43
Tb	0.80	0.97	0.77	0.82	0.47	0.50	0.22	0.45	0.58	0.55	0.39
Yb	2.63	3.10	2.42	2.33	1.40	1.69	0.94	1.80	1.76	1.59	1.41
Lu	0.38	0.38	0.34	0.36	0.23	0.25	0.14	0.24	0.26	0.27	0.25

Table 7-1 (continued)

Sample	Theo's Flow Basalt		M-W Sill Gabbro		Komatiite			Tuff		
	SPD-7	SPD-8	SPD-32	SPD-34	SPD-3	SPD-12	PD1-105	SPD-24	SPD-31	PD4-108.5
SiO2	47.72	49.86	53.76	53.38	n/a	40.99	48.04	90.48	74.72	n/a
TiO2	1.16	1.53	0.76	0.76	n/a	0.25	1.31	0.05	0.71	n/a
Al2O3	9.76	13.33	16.51	15.70	n/a	5.33	12.77	4.33	11.95	n/a
Fe2O3	15.17	12.09	8.97	8.64	n/a	11.03	16.40	1.27	3.07	n/a
MnO	0.23	0.14	0.14	0.16	n/a	0.17	0.16	0.02	0.10	n/a
MgO	10.11	9.79	6.87	6.20	n/a	28.20	7.12	0.32	0.81	n/a
CaO	12.18	5.96	6.68	9.33	n/a	4.81	7.40	0.77	1.74	n/a
Na2O	1.12	4.26	2.69	2.08	n/a	0.05	3.62	0.45	4.12	n/a
K2O	0.53	0.05	0.97	0.48	n/a	0.00	0.04	0.82	0.91	n/a
P2O5	0.09	0.13	0.09	0.07	n/a	0.02	0.12	0.02	0.16	n/a
L.O.I.	1.79	2.98	2.29	3.09	n/a	8.27	3.09	1.20	1.19	n/a
Total	99.86	100.12	99.73	99.89	n/a	99.12	100.07	99.73	99.48	n/a
Ni	183	134	81	71	n/a	1432	78	13	25	n/a
Cu	154	141	63	123	n/a	0	138	25	31	n/a
Zn	98	132	48	52	n/a	43	323	6	178	n/a
Cr	599	286	288	218	2749	3924	126	24	52	103
Co	38	43	33	35	76	92	45	3	13	24
Ba	175	29	221	117	n/a	3	37	92	212	n/a
Sr	131	78	248	156	n/a	2	93	12	142	n/a
Zr	80	126	60	69	n/a	16	98	103	126	n/a
Y	23	32	10	12	n/a	6	21	33	20	n/a
Rb	20	8	34	28	n/a	9	8	27	20	n/a
Ta	0.04	0.40	0.07	0.33	0.00	0.00	0.32	0.88	0.38	0.38
Hf	0.82	2.29	1.22	1.19	0.47	0.26	2.15	4.00	3.01	2.85
Cs	0.12	0.39	0.36	0.24	0.93	0.55	0.33	0.26	0.23	0.96
La	5.58	9.40	6.24	9.09	0.52	0.93	7.54	21.30	10.53	15.61
Ce	12.49	20.79	11.34	13.30	8.29	3.07	19.95	57.73	29.05	28.76
Nd	7.48	17.46	6.60	6.57	0.00	2.08	14.24	29.46	17.58	17.28
Sm	3.52	4.81	2.23	2.71	1.02	0.56	3.17	4.97	2.48	3.70
Eu	0.70	1.30	0.55	0.58	0.40	0.24	1.22	0.42	1.01	1.70
Tb	0.48	1.10	0.44	0.46	0.19	0.09	0.76	1.23	0.69	0.68
Yb	1.85	2.97	1.23	1.32	1.39	0.71	2.72	4.75	2.75	2.27
Lu	0.24	0.44	0.18	0.23	0.11	0.07	0.32	0.57	0.35	0.26

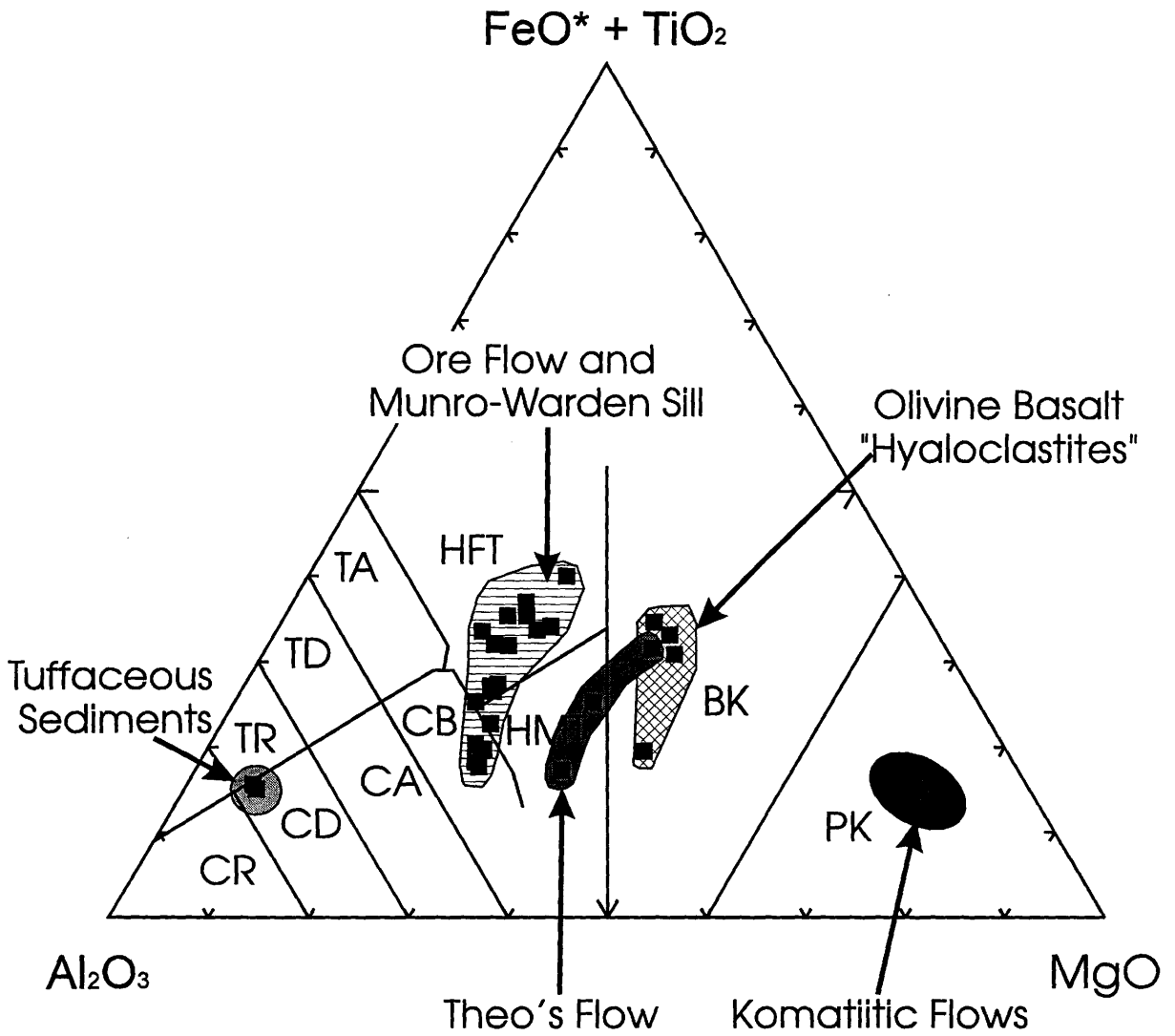
7.2 Major Element Discriminator Plots

Figure 7-1 shows the chemical affinities of various extrusive units from the map area on a Jensen cation plot (Jensen, 1976). This diagram emphasizes the iron tholeiite parentage of the Ore Flow in contrast to the magnesium tholeiite affinity of Theo's Flow. This supports the proposal that the Ore Flow and Theo's Flow represent different parental magma sources even though they are interpreted to be stratigraphically equivalent.

The Munro-Warden Sill gabbros (even though they are intrusive) plot at the calc-alkaline end of the linear array displayed by the Ore Flow basalts and gabbros. This calc-alkaline affinity appears to be the result of in situ fractional crystallization which significantly increased the relative proportion of plagioclase relative to other mafic minerals. The chemical similarity between the highly fractionated Munro-Warden Sill gabbros and the more felsic examples of Ore Flow gabbros suggests a similar parental magma composition and a possibly origin from the same deep-seated magma source.

Prior to this geochemical study, the emplacement of the hyaloclastites found within the map area were thought to be associated with one of the two main tholeiitic flow units. However, their distinct clustering on the Jensen plot suggests a unique composition unrelated to either the Ore Flow or Theo's Flow. The basaltic komatiitic composition of the local hyaloclastites is very similar to the olivine basalt composition (Johnstone, 1987) of breccias formed on top of the Centre Hill Complex, 1.5 km to the south. Since both these rock units are interpreted to exist along the same stratigraphic horizon, it is therefore probable that they were formed at the same source area (i.e. along the top of the seafloor-breached Centre Hill Complex), and was then distributed into the

Figure 7-1 Jensen cation plot (Jensen, 1976) showing rock type affinities for units within the Potterdoal deposit stratigraphy. The majority of the data shown on this diagram is summarized in Table 7-1 (PK, peridotitic komatiite; BK, basaltic komatiite; HFT, high iron tholeiite; HMT, high magnesium tholeiite; CB, calc-alkaline basalt; TA, tholeiitic andesite; CA, calc-alkaline andesite; TD, tholeiitic dacite; CD, calc-alkaline dacite; TR, tholeiitic rhyolite CR, calc-alkaline rhyolite). The plot illustrates the similar chemistry of the Ore Flow and The Munro-Warden Sill and the distinction of these units from Theo's Flow.



Potterdoal map area either by volcanic flow, or by some type of subaqueous pyroclastic fall-out.

Tuffaceous sedimentary rocks group tightly indicating a calc-alkaline dacite affinity. This supports the interpretation from mapping that the relatively thin beds of tuff had an origin outside the local tholeiitic dominated domain, and were introduced into the local stratigraphy by means of distal air-fall. Only one komatiitic sample from the map area was analyzed, and shows the expected peridotitic komatiite affinity.

A ternary plot (Figure 7-2), defined by Irvine and Baragar (1971), shows the variations of tholeiitic to calc-alkaline affinity within the Potterdoal suite. This figure shows that the majority of the suite fall within a tholeiitic affinity, as would be expected for rock extruded along a mid-oceanic ridge system. Samples which show a calc-alkaline affinity are either highly altered basalts and highly fractionated gabbros of original tholeiitic affinity, or are true calc-alkaline material, represented by the tuffs, which were derived from outside of the nearby stratigraphic area.

7.3 Trace Element Discriminator Plots

Tectonic setting of the deposit was examined using a Pearce and Cann (1973) plot shown in Figure 7-3. The majority of mafic flows plot within the ocean floor basalt (OFB) field, implying a rifted, mid-oceanic ridge environment. The tuffs generally fall within the calc-alkaline basalt (CAB) field, supporting an independent distal origin. The upper Munro-Warden Sill gabbros fall in the within-plate basalt field (WPB). However, since these sill gabbros are not extrusive rocks and may have easily incorporate some

Figure 7-2 A volcanic affinity plot (defined by Irvine and Barager, 1971), showing the dominant tholeiitic composition of the Potterdoal rock suite. Sample points plotting within the calc-alkaline are either true calc-alkaline, highly fractionated or strongly altered.

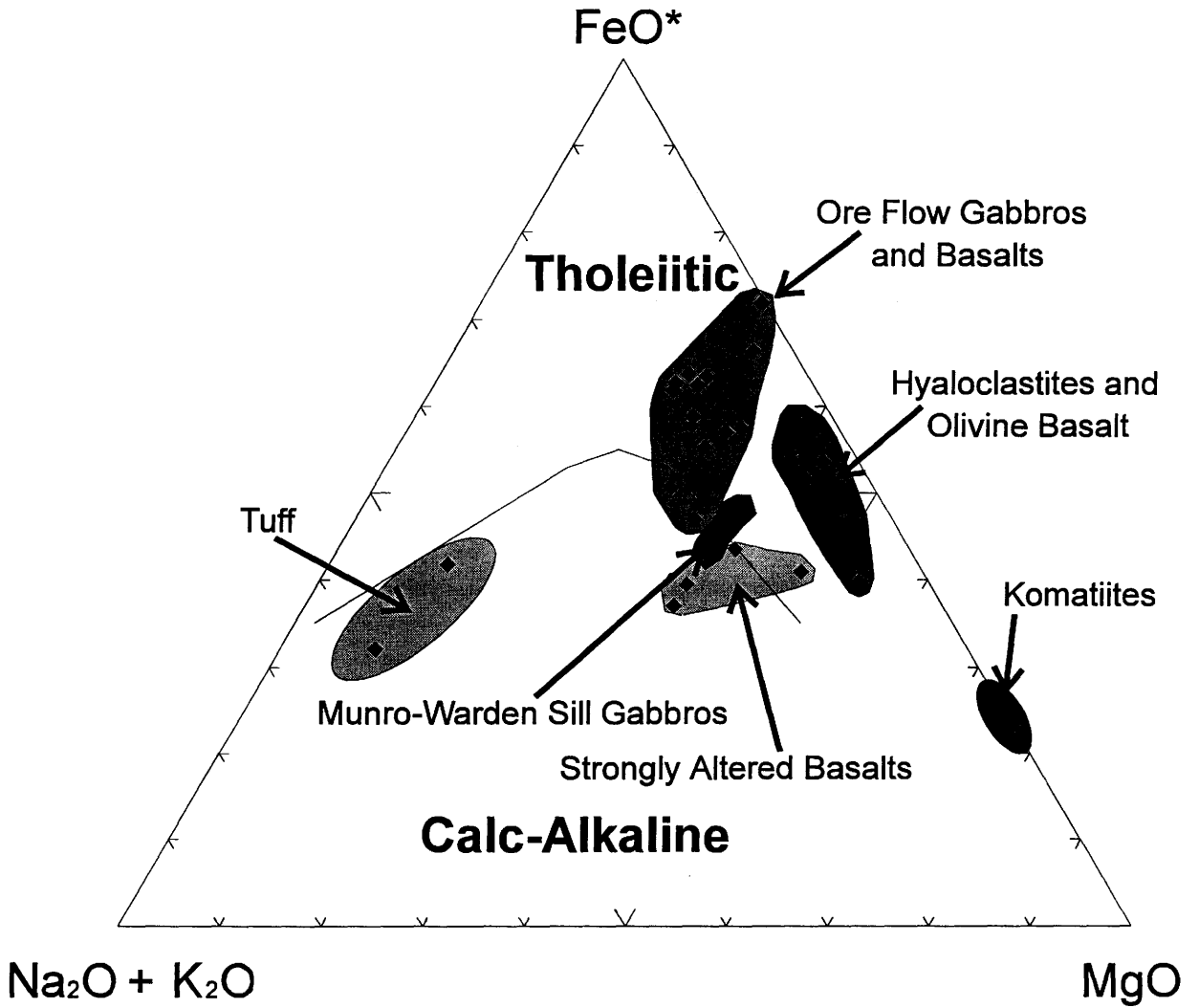
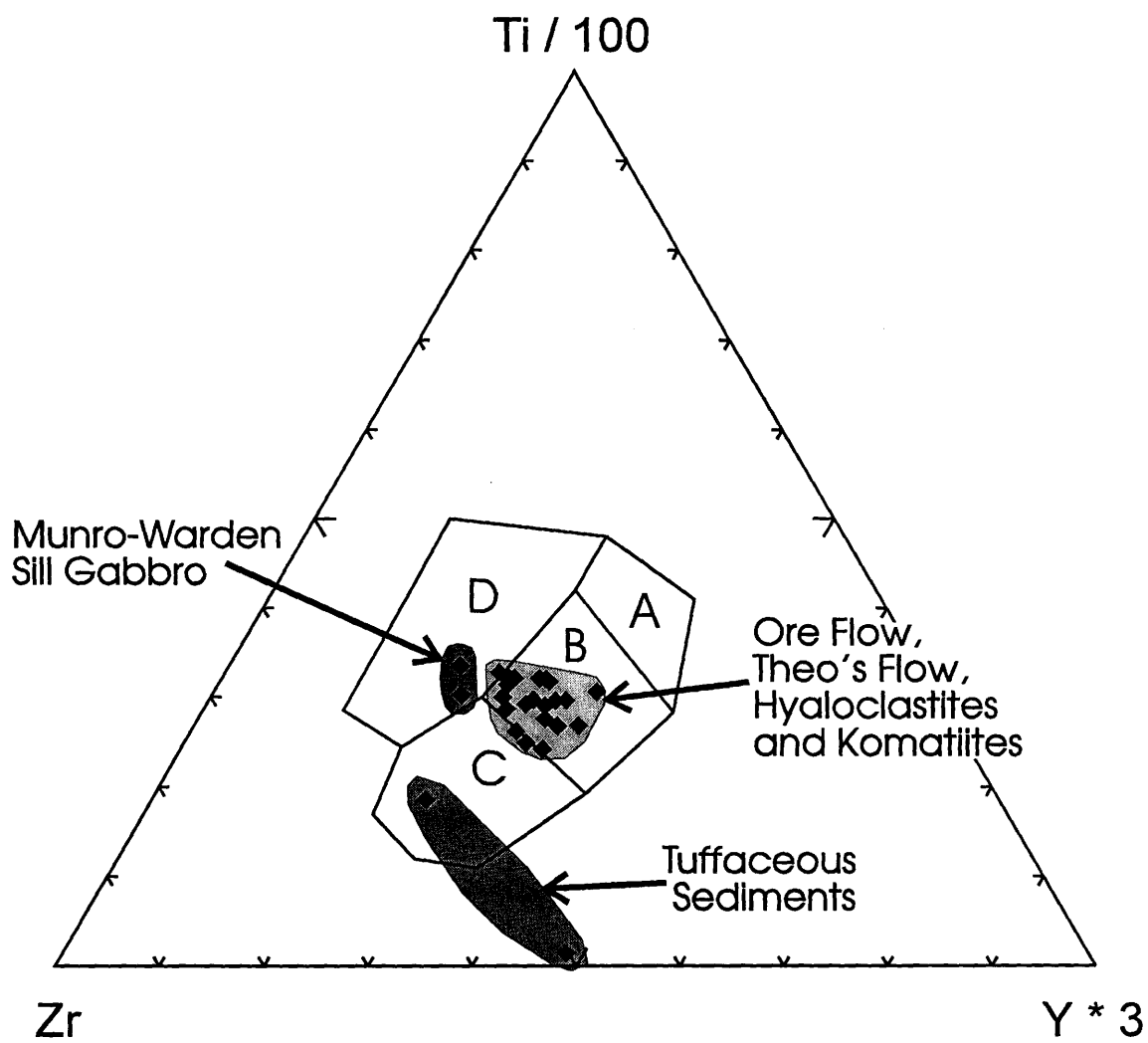


Figure 7-3 Pearce plot (Pearce and Cann, 1973) showing the dominant ocean floor basalt (OFB) tectonic setting of the principal mafic-ultramafic volcanic units of the Potterdoal stratigraphy. (A,B - LKT, low potassium tholeiite; B - OFB, ocean floor basalt; B,C - CAB, calc-alkaline basalt; D - WPB, within plate basalt)



crustal contamination, their designation as a WPB is not reliable and should therefore be ignored.

A similar ternary plot, shown in Figure 7-4 (Pearce and Cann, 1973), also displays a strong clustering of data points around the OFB envelope. This diagram does however show a strong linear dispersion trend along the axis defining Sr content. This dispersion of data points probably indicates high Sr mobility due to sea water interaction during extrusion, or during the subsequent hydrothermal alteration.

7.4 Rare Earth Elements

Rare earth element (REE) profiles are presented in Figure 7-5. Chondrite normalizing factors for each REE were taken from suggested average chondritic meteorite values defined by Boynton, 1989, and are summarized in Table 7-2. These REE profiles are generally compatible with an ocean ridge tectonic setting (as suggested by the Pearce-Cann plot, Figure 7-3), with the majority showing fairly flat profiles with slight negative slopes, indicative of a tholeiitic affinity. Normalized LaN/YbN ratios for tholeiitic Ore Flow basalts and gabbros vary between 1.00 to 3.60 with an average LaN/YbN of 2.57. This average value falls within the range of 0.8 to 3.0 defined by Barrie et al. (1993) for a Group I volcanic succession, which is the most likely volcanic succession type to host VMS deposits. The tholeiitic affinity of the Potterdoal stratigraphy, as indicated by REE, is also supported by immobile trace element contents. A Y-Zr plot (Figure 7-6) for rocks of the volcanic suite produces a regressed average Zr/Y value of 4.3. This value falls within the range of 3 to 5, representative of a tholeiitic

Figure 7-4 Another trace element Pearce plot (Pearce and Cann, 1973) showing a linear dispersion of data points centered around an ocean floor basalt (OFB) affinity. This dispersion is due to the relative high mobility of Sr caused by either sea floor alteration during extrusion, or by the alter hydrothermal system. (IAB - island arc basalts, CAB - calc-alkaline basalts).

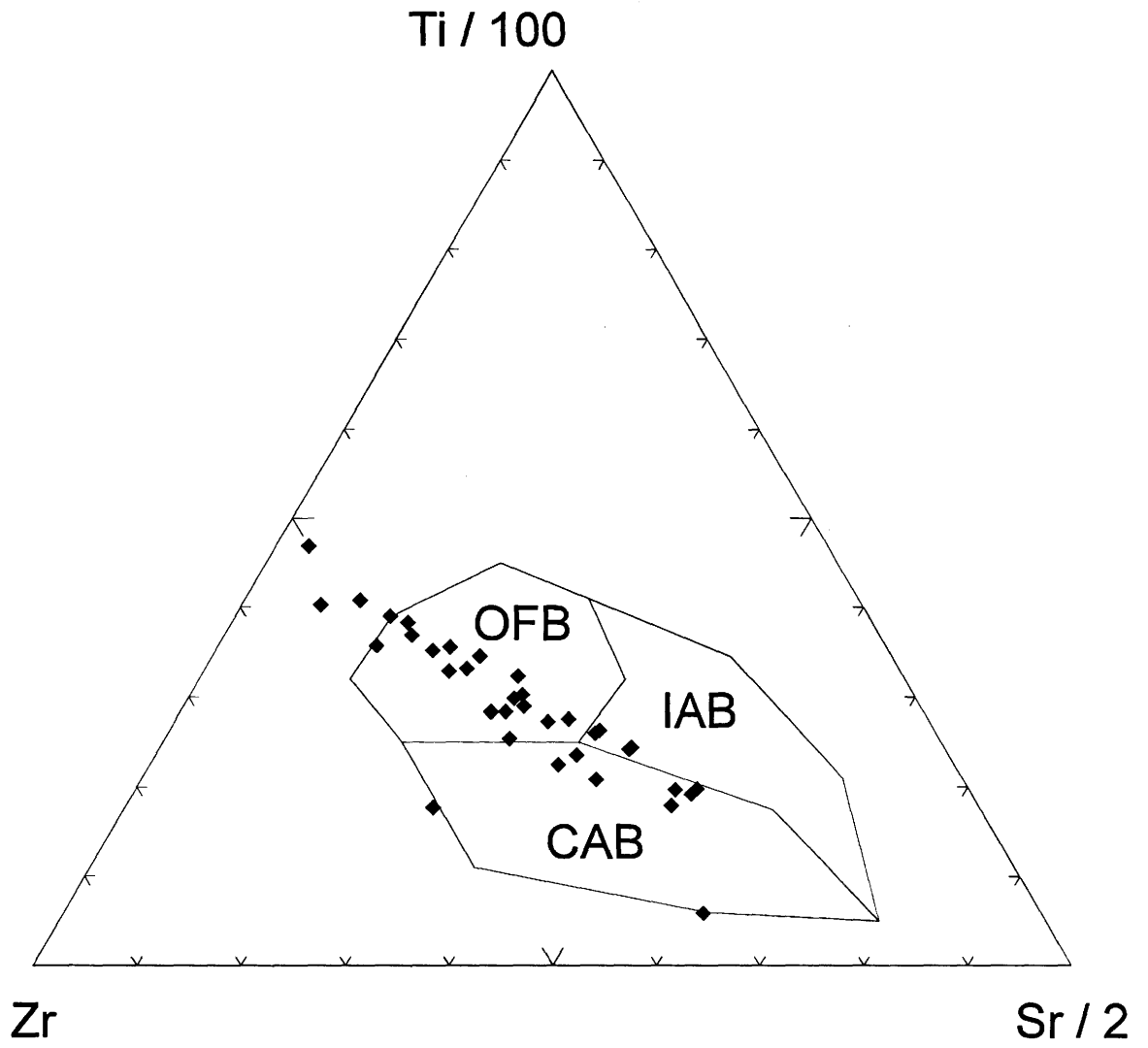


Figure 7-5 Normalized rare earth element profiles for various units within the Potterdoal stratigraphy. Normalization used recommended average chondrite values (Boynton, 1989; p.91).

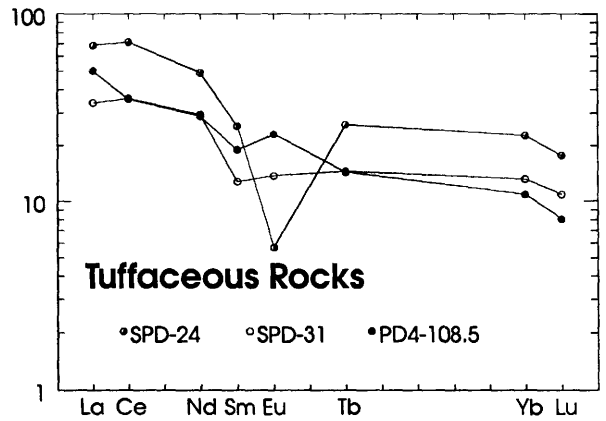
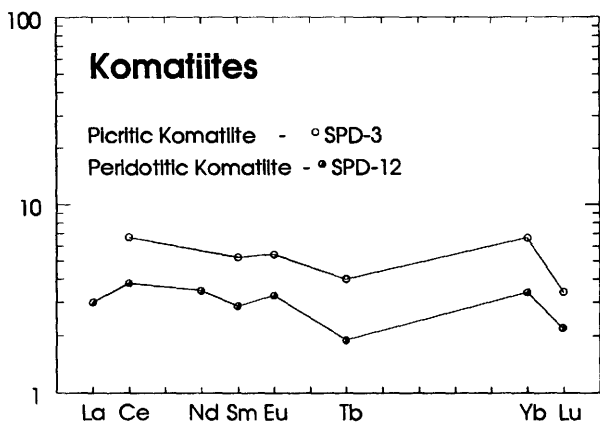
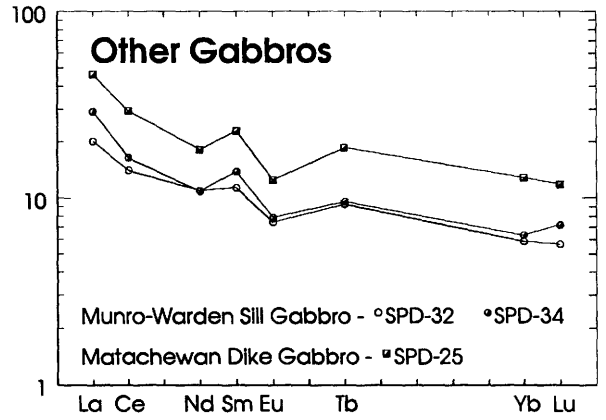
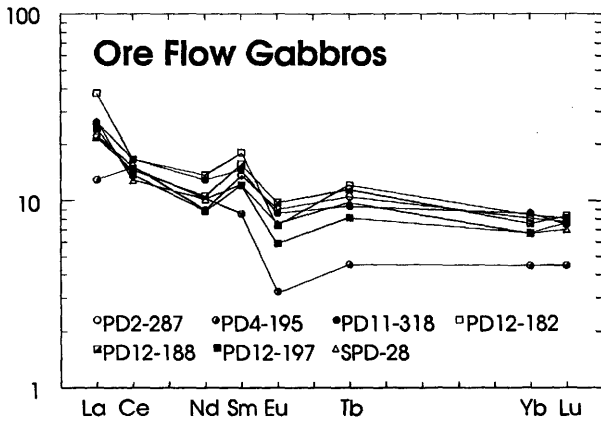
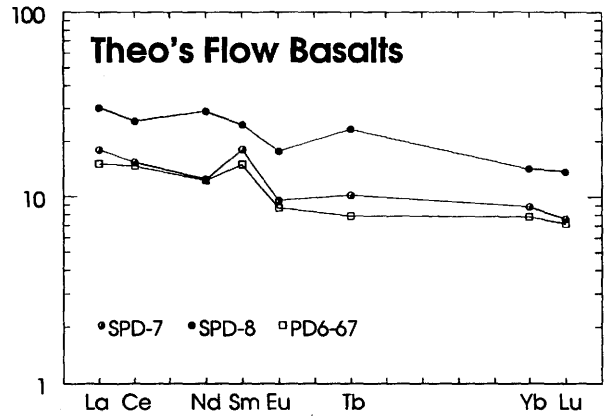
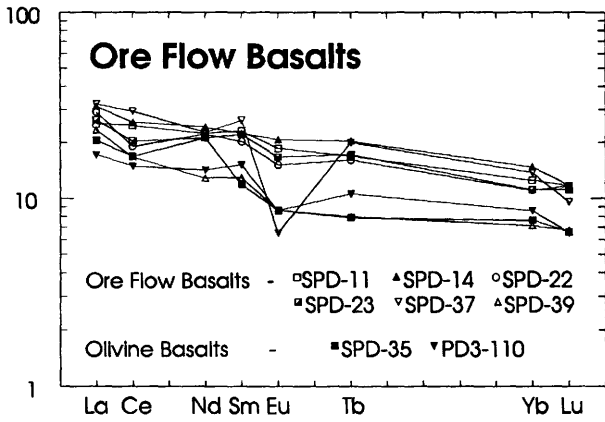
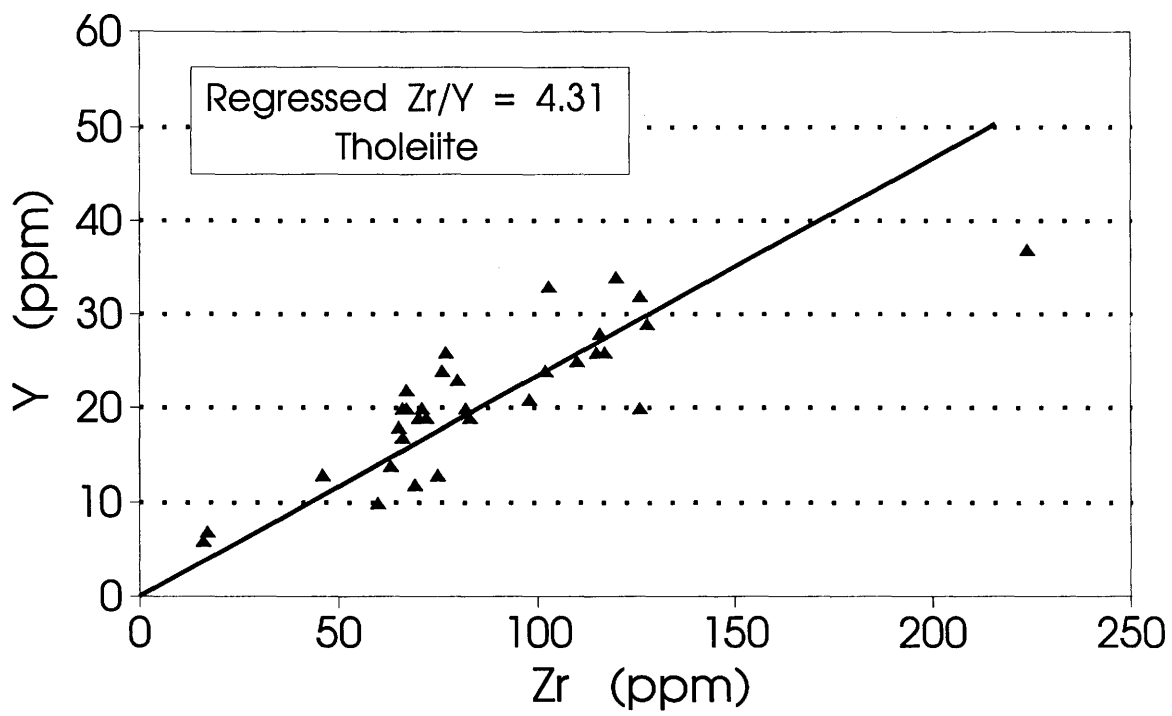


Table 7-2: Recommended Average rare earth element chondrite values (Boynton, 1989).

REE	Recommended Chondrite Values
La	0.310
Ce	0.808
Pr	0.122
Nd	0.600
Sm	0.195
Eu	0.0735
Gd	0.259
Tb	0.0474
Dy	0.322
Ho	0.0718
Er	0.210
Tm	0.0324
Yb	0.209
Lu	0.0322

Figure 7-6 Y vs. Zr plot of units making up the Potterdoal stratigraphy. The regressed average Zr/Y ratio indicates an overall tholeiitic affinity.



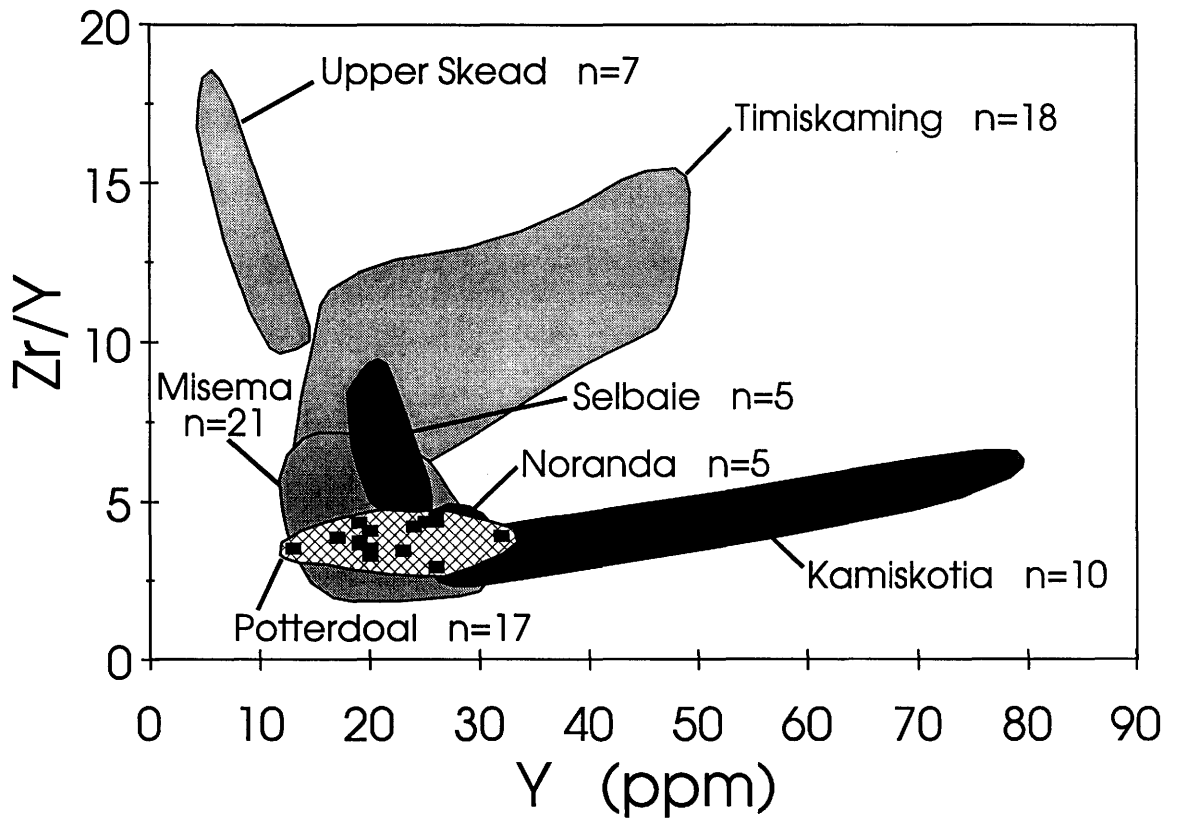
affinity, and is very distinct from the 7 to 30 range typical of a calc-alkaline suite (e.g. MacLean and Barrett, 1993). A Zr/Y against Y plot (Figure 7-7, after Barrie et al., 1993) also suggests a strong association of the Potterdoal tholeiites with ore-associated Group I tholeiites, as indicated by their similarity with ranges defined for Noranda and the lower Y end of the linear trend defined for Kamiskotia.

The REE patterns of extrusive flow basalts (Figure 7-5A and B) show relatively smooth profiles with slight negative dips indicative of tholeiitic compositioned rocks. REE profiles for the various local gabbros (Figure 7-5C and D) generally show small, but prevalent negative Eu and positive Sm anomalies. The depletion of Eu in these gabbros was most likely caused by Eu fractionation into early plagioclase soon after their emplacement. The slight enrichment in Sm may be due to mobilization and concentration into epidote, which was introduced by the late hydrothermal system.

Only two komatiitic were analyzed for REE, producing very flat profiles with low relative abundances of REE typical of ultramafic rocks. The observed roughness of the profiles is not so much a feature of the chemistry of the komatiites, but is a factor of the low concentration of these elements, which are only slightly above detectable limits.

The tuffaceous sediment profiles (Figure 7-5F) show a relatively steep, negatively dipping REE patterns, with high relative REE concentrations, typical of calc-alkaline rocks. The strong variability in Eu enrichment-depletion could indicate that the tuffs may have originated from a number of different calc-alkaline eruptive centres, each showing a different degree of magmatic evolution at the time of eruption.

Figure 7-7 Zr/Y vs. Y diagram showing the close association between Potterdoal tholeiites and other mafic tholeiitic suites (shaded in dark grey) associated with VMS occurrences. The lightly shaded ranges indicate tholeiitic suites which do not show an association to VMS occurrences (modified from Barrie et al., 1993).



7.5 Mass Balance Of Progressive Hydrothermal Alteration

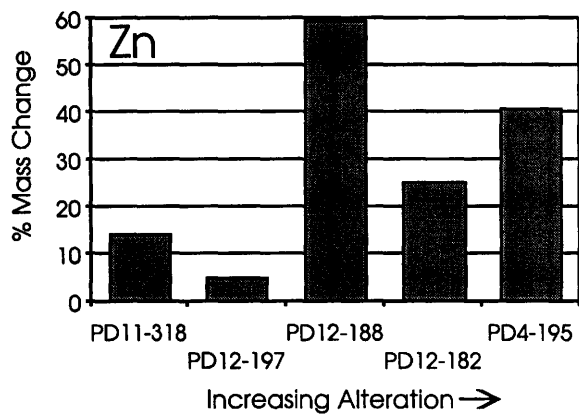
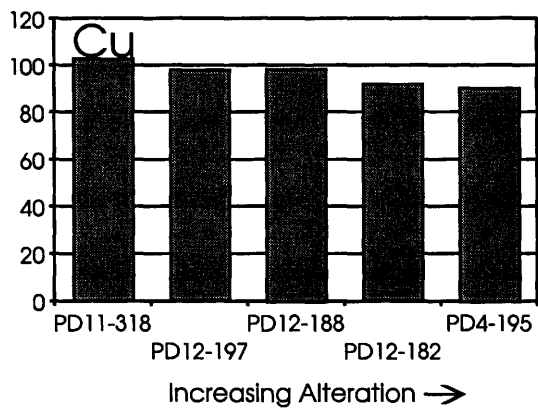
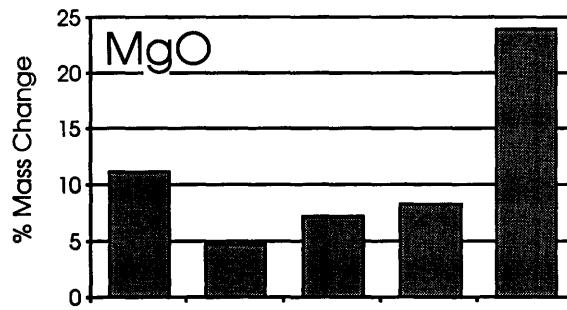
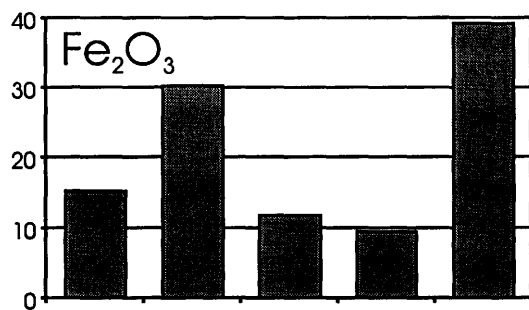
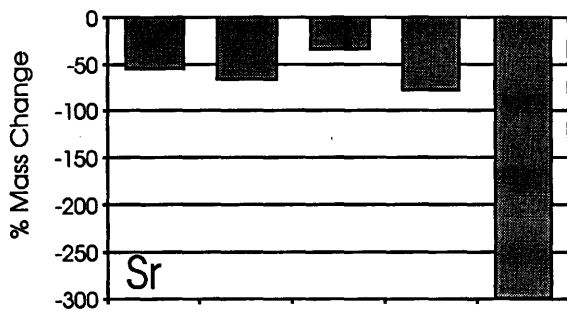
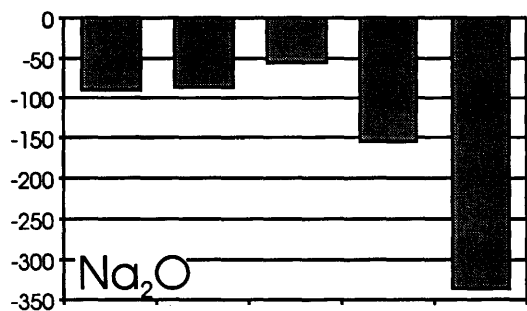
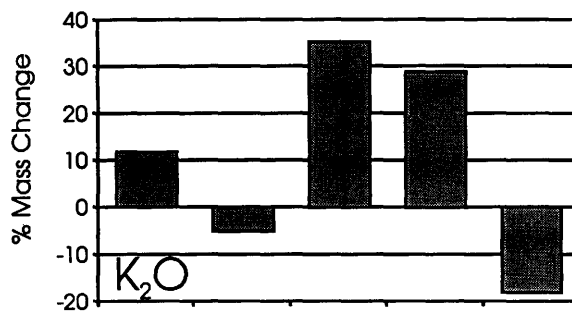
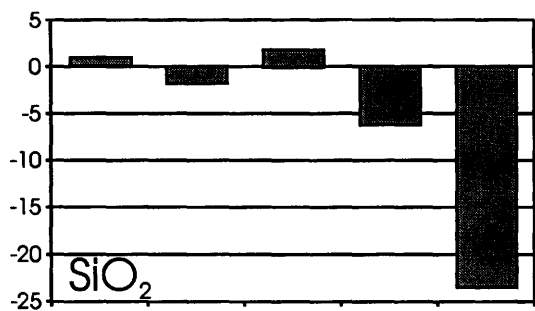
Progressive hydrothermal alteration within the footwall Ore Flow gabbros was examined using the mass change procedure of MacLean and Barrett (1993). Mass change in progressively altered samples was corrected to a least altered sample, which was then calibrated to the least mobile element. Alumina (Al_2O_3) was used as the preferred immobile “element” due to its high relative abundance in the rock suite, and because calculated mass change values were consistent with observed changes in relative abundances of the significant major elements for samples of the alteration suite (similar reasoning used by Lentz and Goodfellow, 1993). Using the formulae below, a reconstructed composition (R.C.), and then the relative mass change (M.C.) were determined:

$$\text{R.C.} = (\text{Al}_2\text{O}_3\text{precursor} / \text{Al}_2\text{O}_3\text{altered}) * (\% \text{ or ppm Component altered})$$

$$\text{M.C.} = \text{R.C.} - \text{Precursor Composition}$$

These calculated mass change values are shown in Figure 7-8, expressed as a relative percent mass change of the particular element or oxide within the sample. Sample PD2-287 was selected as the least altered sample because it is characterized by minimal alteration of clinopyroxene to chlorite and only minor sericitization of plagioclase, an assemblage typical of the local regional metamorphism. All mass change values are calculated with respect to this sample.

Figure 7-8 Mass change diagrams showing the mobility of specific elements with increasing alteration. The alteration is associated with hydrothermally altered envelopes surrounding fault breccia conduits within Ore Flow gabbro. (Mass change is expressed as a relative percentage).



The precursor composition of the Ore Flow gabbro is assumed, for the purposes of this assessment, to be homogeneous. This assumption is supported by the relatively consistent mineral proportions seen in thin sections of numerous gabbroic samples, and by the minimal lithological variation throughout the Ore Flow gabbros observed in outcrop and drill core. The suite of samples chosen to represent a typical progressive hydrothermal alteration suite were taken from alteration envelopes of 2 to 3 m maximum width, and ranging from a weakly altered periphery to the strongly altered core of a fault breccia conduit. The sample suite was taken from several different drill holes, since low sulphide content and homogeneity of alteration was required to optimize the probability that mass change would be due mainly to hydrothermal alteration, rather than hydrothermal mineralization.

Since the "least altered" gabbro sample, PD2-287, is representative of the background lower greenschist metamorphic grade, only the alteration attributable to hydrothermal fluid-rock reactions should be indicated by the mass change diagrams (Figure 7-8). Weak alteration on these diagrams is represented by sample PD11-318, which shows weak chloritization of clinopyroxene and moderate sericitization of plagioclase. Sample PD4-195 is representative of strong hydrothermal alteration with almost complete replacement of all primary minerals by hydrothermal chlorite. The remaining samples found on the mass change diagrams (PD12-197, PD12-188 and PD12-182), represent gradational alteration steps in between the weakly altered and most altered samples described above. The designation and ranking of these intermediately

altered samples were assessed visually using macroscopic features, since at the time of sample preparation no thin sections had been prepared.

For SiO_2 , mass change is relatively insignificant except in the most intensely altered rocks. Loss of Si is probably due to large-scale destruction of original feldspars under intense hydrothermal conditions. Similar mass losses of Na_2O and Sr, as well as by CaO (not shown in Figure 7-8), occur in conjunction with SiO_2 loss. Persistent losses of Na, Sr and Ca during the early stages of alteration are due to sericitization and conversion of primary plagioclase to K-feldspar. As noted before, the K-feldspar composition was confirmed by optical crystallographic properties and by energy dispersive X-ray spectrometry, which indicated the presence of only K, Al, Si and trace Na. The colourless, translucent character of the mineral, the lack of any twinning and its irregular anhedral habit suggests this mineral is adularia. As noted for Si, the major decrease in mass of these three elements under extreme alteration is due to the pervasive destruction of precursor silicates and replacement by the hydrothermal chlorite, penninite.

The erratic behaviour of K in weakly altered samples appears to be due to minor local variations in sericitization, generated during the subsequent regional lower greenschist metamorphism. However, with increasing alteration, sericitization along with more persistent replacement by K-feldspar (probably adularia) explains the mass gain in K. The final rapid drop in K content in highly altered samples is due to the wholesale replacement of all minerals by hydrothermal chlorite.

Mass change for Fe_2O_3 and MgO indicate addition of both Fe and Mg related to the incremental replacement of in-situ chlorite and clinopyroxene by hydrothermal

chlorite. The substantial mass gain in the most altered sample is related to the large increase in modal abundance of hydrothermal chlorite which replaces of all other minerals.

Both Cu and Zn show mass gains through all levels of alteration. Cu shows fairly consistent addition in all samples, but Zn enrichment is erratic, possibly due to variable resorption by the hydrothermal fluid.

Using the information covered above, the footwall alteration associated with the emplacement of the Potterdoal deposit can be summarized as follows. With increasing degree of alteration, Fe, Mg, Cu and Zn show moderate mass gain, whereas Si, Na, Ca and Sr show strong mass loss. Mass change for K is erratic, but generally there is a positive mass gain. These chemical mobility systematics found within the alteration features of the Potterdoal deposit are generally consistent with those of alteration pipes associated with many Archean VMS deposits (Lydon, 1984).

Chapter 8

Discussion

8.1 Tectonic Setting

The discriminator plots described above place the Potterdoal volcanic succession within an ocean ridge tectonic setting, and indicate a general tholeiitic ocean floor basalt affinity. This interpretation appears applicable to the majority of the rocks in the eastern end of the Kidd-Munro assemblage within Munro Township (Johnstone, 1991). The Y-Zr plot (Figure 7-6) supports a tholeiitic affinity, and further suggests that a chemistry closely related to that of bimodal tholeiitic mafic volcanic and high silica rhyolite successions (i.e. Group I type volcanic succession shown in Figure 7-7, Barrie et al., 1993) which are most often associated with large VMS deposits. The chemical similarities between the mafic volcanic of the Potterdoal sequence and those at Kidd Creek and Kamiskotia suggest that these rocks may have had a similar petrogenesis. However, the critical difference is the nearly complete absence of any felsic component within and surrounding the Potterdoal stratigraphy. This observation has led some authors (Barrie et al., 1993) to a comparison with currently active volcanism along the Icelandic ocean ridge system. Sigmarsson et al. (1991) determined that the production of high silica rhyolites associated with the East Iceland Rift results from partial melting at

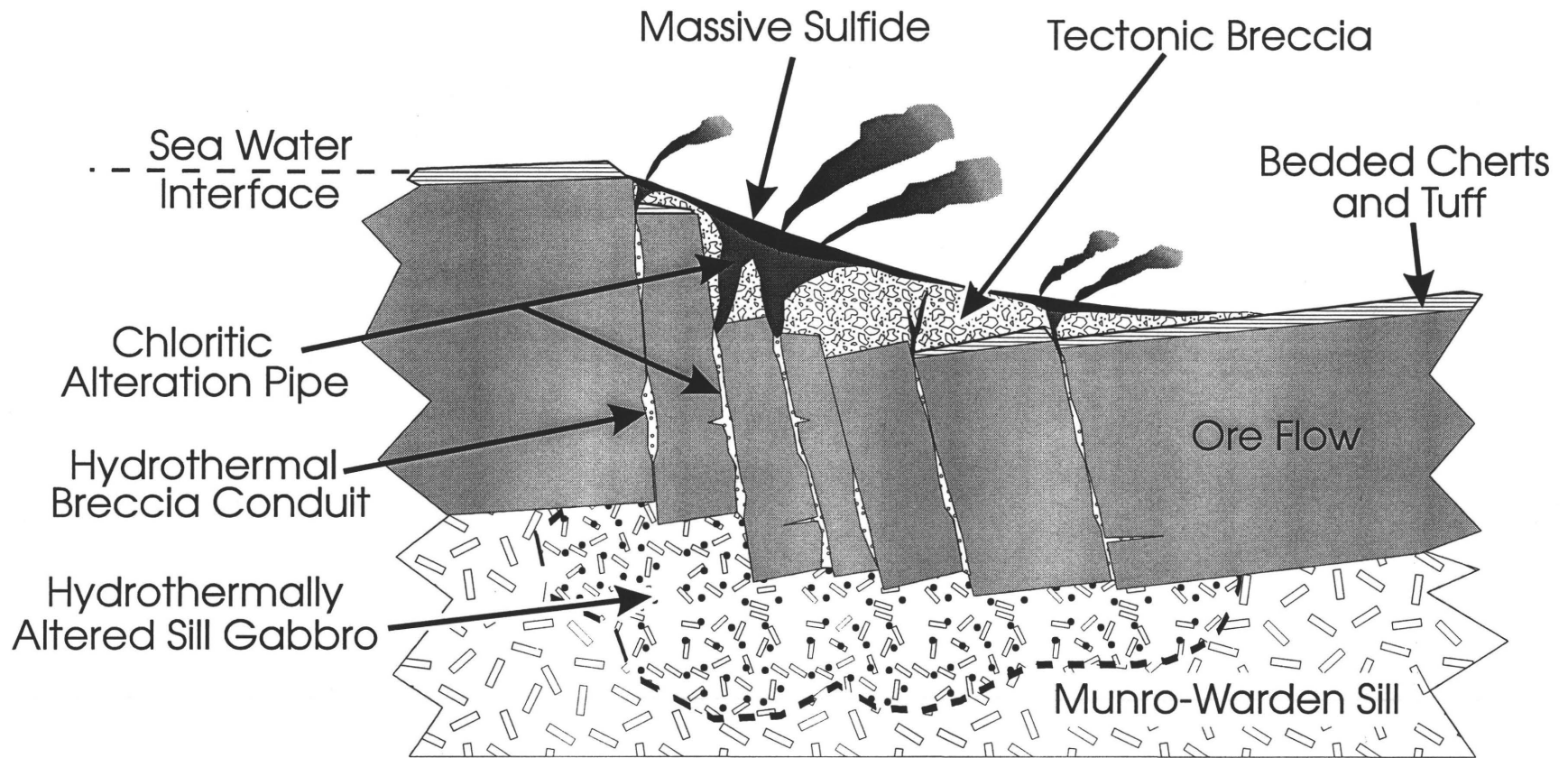
the base of a thick tholeiitic basalt assemblage. To attain the crustal thicknesses required to generate such partial melting, an off-axis setting away from the high heat flux and rapid spreading about an oceanic ridge is required. This type of off-axis setting has recently been suggested (Fyon et al., 1992; Barrie et al., 1993) as a plausible interpretation of the bimodal character of the western Kidd-Munro assemblage, as well as other assemblages which host major VMS deposits. Tholeiitic successions produced in a ridge-proximal environment do not attain sufficient crustal thickness to permit the production of high silica rhyolites by partial melting, and therefore do not show successions with a bimodal rhyolite component. Such a ridge-proximal environment may explain the general lack of bimodal felsic volcanism within the eastern end of the Kidd-Munro assemblage.

8.2 Ore Deposit Model -- A Genetic Summary

The shallow emplacement of thick, hot synvolcanic sills is considered the main thermal energy source for the formation of many Archean VMS deposits (Campbell et al., 1981; Fyon et al., 1992; Barrie et al., 1993). The shallow emplacement of the Munro-Warden Sill within the Potterdoal stratigraphy is proposed as an example of such an energy source.

Figure 8-1 is a diagrammatic representation of the ore-forming system responsible for the emplacement of the Potterdoal deposit. The upper portion of the Munro-Warden Sill was intruded under a relatively thin (100 to 200 m) cover of the tholeiitic Ore Flow. The fault scarp structure which cuts across the Ore Flow tholeiites is interpreted to have

Figure 8-1 Conceptual illustration showing interpreted relationships of rock units, the hydrothermal system and sulfide mineralization. Percolating seawater, which has reacted with the upper portion of the Munro-Warden Sill, rises through constricted fault breccia zones through the Ore Flow, and then disperses throughout the overlying tectonic breccia causing intense alteration pipes under a capping lens of massive sulfide.



formed primarily during the intrusion of the Munro-Warden Sill. The precise origin of this scarp structure is uncertain, but two possibilities exist. The scarp may have formed during ocean ridge synvolcanic rifting. The subsequent intrusion of the Munro-Warden Sill then initiated the formation of a hydrothermal system within the highly permeable fault zone, and thus localized the sulphide deposit. Evidence which supports this interpretation is found in the shallowly plunging, west-northwest trending fault scarp orientation, which conforms closely with the regional rifting orientation suggested by Johnstone (1987). A second possibility is that the fault scarp formed after the extrusion of the basaltic stratigraphy, concurrent with the intrusion of the Munro-Warden Sill. Dilational forces, induced by the lateral intrusion of the sill, would cause the thin overlying stratigraphy to break into fault-bounded blocks, with local subsidence to form the scarp.

The tectonic breccia (composed primarily of angular chert and tuffaceous rock fragments) which fills the fault scarp depression is considered to have formed during the tectonic disruption accompanying the initial intrusion of the sill. At approximately the same time, the hydrothermal fault breccias were also formed by the first high pressure/temperature fluids generated by heat loss from the sill magma. Once the sill was fully emplaced, channellized hydrothermal convection was established within the fault and overlying tectonic breccia systems. Hydrothermal fluids coming in contact with the hot sill created a rapid downward-propagating crack front, which caused the pervasive hydrothermal alteration and leaching of the upper portion of the sill. The metal-rich hydrothermal fluids were then rapidly channelled through the thin overlying tholeiitic

skin and exited at localized vent sites, depositing the entrained metals just below the seafloor interface.

Hydrothermal alteration within the overlying Ore Flow tholeiites was restricted to a few meters width along the margins of fault breccia conduits. The narrowness of these alteration envelopes along with the pervasive mass gains of Fe, Mg and base metals, suggest that very little (if any) of the Potterdoal sulphide mineralization was derived directly from the Ore Flow tholeiites. Hence, most of the metals must have been derived from other source rocks, of which the pervasively altered upper Munro-Warden Sill is the strongest candidate. Another possible source might be residual, metal-rich deuteritic fluids resulting from crystallization of the sill. However, input from such a source appears to be limited since precious metals which are often concentrated in deuteritic fluids (see, for example, Good and Crocket, 1994, with respect to the Coldwell Complex) are in very low concentrations in the deposit. A similar conclusion was reached for the nearby Potter Mine deposit (Coad, 1976), where sulphide mineralization occurs within the mafic fragmental cap of the Centre Hill Complex.

Due to the high permeability of the joint and fault breccia systems to downward percolation of seawater, the thin layer of Ore Flow tholeiites provided very little thermal insulation to the underlying Munro-Warden Sill. Hence, the sill would have cooled rapidly and thus shortened the time during which the associated hydrothermal system was active. The short duration of hydrothermal activity appears to be the most important factor leading to the relatively small size of the Potterdoal deposit (estimated at approximately 200,000 tons).

Metal zonation within the Potterdoal deposit shows strong evidence that sulphide deposition was controlled by the thermal stability of individual sulphide minerals within a cooling hydrothermal fluid. Hydrothermal circulation was restricted to specific highly permeable routes through the fault and tectonic breccias, and therefore only a relatively small proportion of these breccias have ore grade mineralization. The cooling rate of the hydrothermal fluid within the breccia conduits was relatively slow, owing to the insulating effect of the wall rocks, and thermal gradients were probably very steep. Sulphide mineralization within these breccia conduits was therefore dominated by the higher temperature assemblage of chalcopyrite and pyrrhotite. Migrating upwards towards the tectonic breccia/seawater interface, the hydrothermal fluid eventually came in contact and mixed with downward-moving seawater. Mixing caused rapid cooling and the subsequent deposition of all remaining dissolved lower temperature sulphides (predominantly sphalerite) within the interstitial pore space between tectonic breccia fragments. Where the hydrothermal flow was more intense, partial to complete replacement of sedimentary rock fragments is observed. This sulphide precipitation should have reduced the permeability of the tectonic breccias, causing isotherms to rise under the massive sulphide lens. Evidence which suggests the rising of ore system isotherms is indicated by the upwards and outwards zonation within the ore lens from a Cu-rich core to Zn-rich peripheries. This zonation was controlled by the preferential precipitation of progressively lower temperature minerals, as the cooling hydrothermal fluid migrated away from vent sites just below the seafloor interface. Following the

mineralizing event, the accumulated massive sulphide were probably buried quickly by the relatively unaltered komatiitic units of Fred's Flow.

The rotation of the Potterdoal stratigraphy into its present subvertical orientation was then initiated by marginal tilting, related to basinal subsidence along the regional rifting centre, as proposed by Johnstone (1987). A similar process was proposed by Jensen and Langford (1985), where initial up-turning of the rapidly extruded stratigraphy is accomplished by ridge proximal subsidence along ridge parallel listric faults.

This subsidence formed an open synclinal structure which was later compressed into the tight isoclinally folded McCool Hill Syncline during the late Kenoran transpressional event. This isoclinal folding require a significant amount of bedding-parallel thrust faulting for the conservation of local stratigraphic volume. One of these bedding-subparallel faults includes the Buster Fault, which was produced the small scale stratigraphic repetition represented by Theo's Flow and the ore bearing Ore Flow, exposed along the current erosional surface.

8.3 Comparison Of The Potterdoal Deposit with the Potter Mine Deposit

As previously noted, the Potterdoal and Potter deposits are closely related owing to their similar tectonic setting and general position within the regional stratigraphy. Both deposits appear to occupy the same stratigraphic horizon on opposite sides of the McCool Hill syncline; however, small local variations in the regional stratigraphy has produced two deposits of very different formational style.

Correcting for the structural repetition found within the Potterdoal area, the local stratigraphy of the Potterdoal deposit is seen to consist of a thick layered tholeiitic sill (Munro-Warden Sill) overlain by a tholeiitic flow (the Ore Flow), and capped by a thick komatiitic succession (Fred's Flow). The Potter Mine deposit shows a similar stratigraphy, with a thick, cyclically layered tholeiitic gabbro base (the Centre Hill Complex), overlain by the basaltic komatiitic "hyaloclastite" layer, and capped by a thick sequence of komatiitic flows (Coad, 1976). For both deposits, sulphide mineralization roughly occurs along the top of the extrusive unit which is sandwiched between the thick footwall gabbroic unit and the capping komatiites.

Aside from the above noted similarities in general deposit stratigraphy, the role which key units played during the transport and emplacement of sulphide ore within each stratigraphy varies significantly. As noted in the genetic model of the Potterdoal deposit, the main heat engine driving the ore forming hydrothermal system was the Munro-Warden Sill. This sill intruded under a thin skin of extrusive tholeiites (approximately 150 m thick), forcing the hydrothermal system to circulate through the pre-existing tholeiitic layer before the contained sulphides could be precipitated within the overlying tectonic breccias, just below the sea water interface. Economic deposits of base metal sulphides are concentrated above highly permeable hydrothermal conduits which transect the tholeiitic unit.

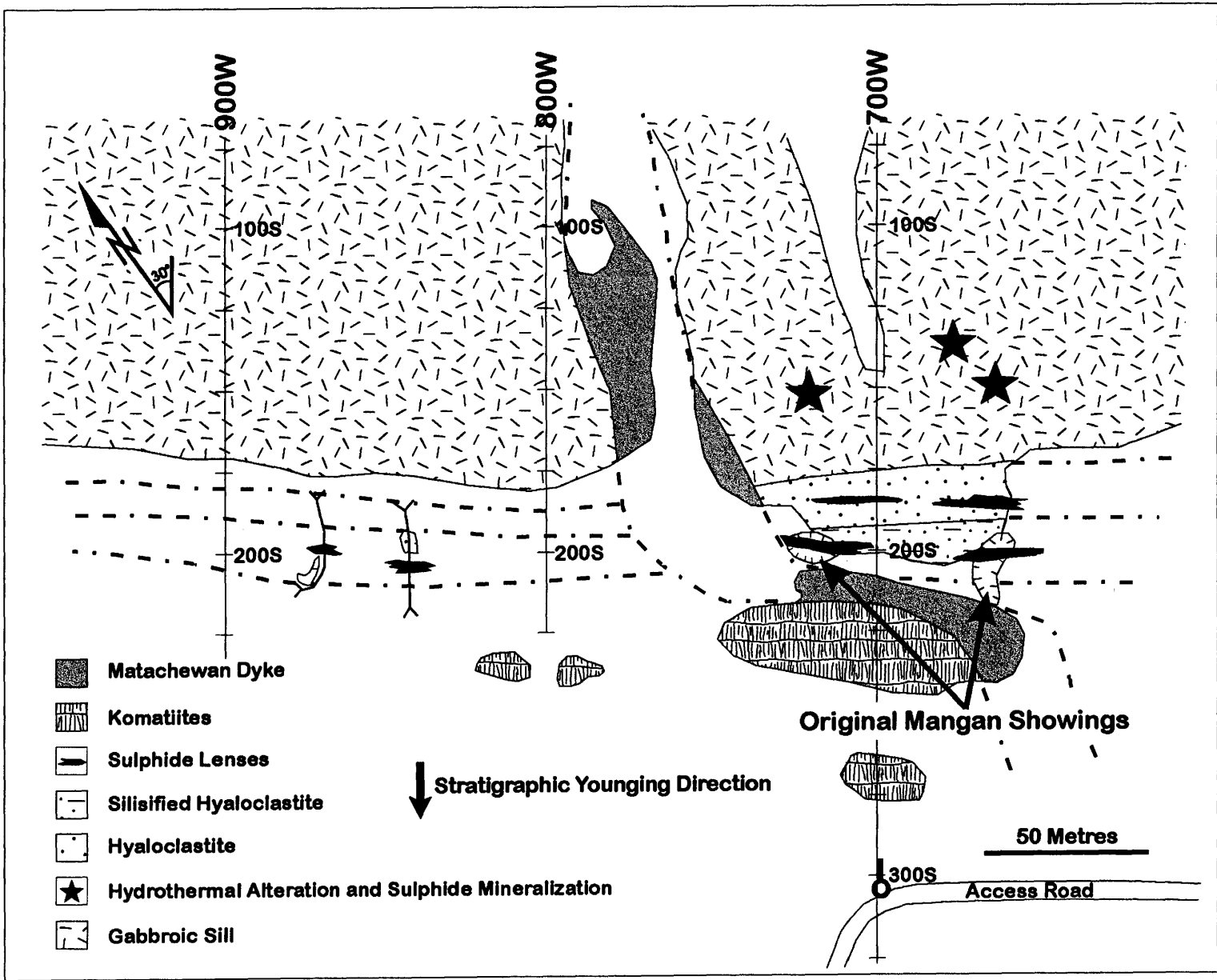
A genetic model for the Potter Mine deposit was first proposed by Coad (1976), however, some inconsistencies existed with this model. Currently, no expression of the Potter Mine mineralization exists on surface and all available stored diamond drill core

had been vandalized, making the direct examination of the Potter Mine deposit difficult. However, from the examination of available footwall outcrops within the mine site area and by using Coad's (1976) thorough petrographic descriptions of drill core, other local occurrences like the Mangan showing can be seen to have experienced very similar genetic processes.

Figure 8-2 shows a surface map of the area surrounding the Mangan showing, located roughly east of the Potter Mine deposit (see Figure 1-2). Being on the north limb of the McCool Hill Syncline, the stratigraphic younging direction is towards the south, similar to the Potterdoal deposit. The Mangan showing shows a near identical stratigraphic profile as is found at the Potter mine, consisting of a thick, footwall gabbroic unit overlain by a fragmental "hyaloclastite", and capped by komatiites.

Personal field observations and personal communications with several other geologists (primarily Andy Fyon, James Crocket and Tucker Barrie, 1995) support the interpretation that the Mangan and Potter Mine stratigraphies were created by the breaching of a large sill above the sea floor interface. This breached sill would then have appeared as a large subaqueous lava lake, which formed a thick breccia cap by quench shattering and phreatic activity along the top of the ponded magma. This breccia cap is represented by the fragmental unit overlying the gabbro at the Mangan showing, and by the hyaloclastite horizon, identified by Coad (1976), which directly overlies the Centre Hill Complex in the Potter Mine area. Escaping heat from the ponded lava then initiated a convecting hydrothermal system through the breccia cap, leaching the recently crystallized gabbro and depositing the entrained metals within the breccia cap. Alteration

Figure 8-2 Geology map of the Mangan showing. The Mangan showing shares a very similar stratigraphy with the Potter Mine deposit, however, since the Mangan showing is on the opposite limb of the McCool Hill Syncline, the younging direction is opposite (i.e. towards the south) to the Potter Mine.



and sulphide mineralization probably occurred initially at some depth within the breccia cap owing to the high permeability of the breccia. However, as the porosity decreased within the breccia cap (due to the interstitial precipitation of sulphide and gangue minerals), the effects of alteration and mineralization would have moved upwards within the breccia. The highest degree of alteration and sulphide mineralization would have developed along the upper contact of the breccia cap where the hydrothermal gradient was the most intense. These processes could explain why there are a number of irregular mineralized horizons within the breccias of the Mangan showing, and why silicification is so intense within the upper portion of the breccia unit. Initial hydrothermal convection within the breccia cap would have generally been unfocused, leading to wide spread but limited mineralization of the bulk of the breccia cap. However, as the permeability of the breccias decreased, hydrothermal convection would have become more focused, allowing for the concentration and deposition of economic base metal grades. Evidence supporting the late stage concentration of hydrothermal flow can be seen underlying the main Mangan showing, where hydrothermal chlorite veins and sulphide mineralization is much more evident within the upper portion of the footwall gabbros.

Both the Potterdoal and Potter deposits show strong chloritic alteration pipes associated with the main hydrothermal conduits which emplaced the massive sulphides. The most intense hydrothermal alteration is indicated by a pervasive replacement of all other minerals by chlorite (penninite), epidote and varying amounts of sulphides. Silicification of the hyaloclastite horizon, surrounding and along the flanks of the massive sulphide mineralization, also seems to be a prevalent alteration style associated with the

Potter and Mangan deposits. The presence of widespread silicification of the tectonic breccias is not as obvious within the Potterdoal deposit. However, due to highly focused venting found beneath the Potterdoal deposit, it is likely that overlying silicified breccias would have been replaced by massive sulphides as the thermal regime rose within the tectonic breccia pile.

Sulphide mineralogies for both deposits are very simple and are virtually identical. The predominant sulphide assemblage (in descending order of abundance) for the Potterdoal is pyrrhotite-chalcopyrite-sphalerite-pyrite, whereas the Potter has a pyrrhotite-pyrite-chalcopyrite-sphalerite assemblage. The higher abundance of pyrite in the Potter Mine deposit may be due to the rapid, less restricted convection of meteoric sea water, producing a relatively less reducing environment which would have allowed pyrite to be more stable.

As noted before, the small size of the Potterdoal and Potter Mine deposits (approximately 200,000 tons and 600,000 tons respectively) are a direct result of the rapid cooling of the underlying, shallowly emplaced gabbros. The somewhat larger size of the Potter Mine deposit may be explained by the cyclic layering within the Centre Hill Complex, which suggests multiple injections of new magma. This extended period of periodic magma injection could have prolonged the activity of the hydrothermal system which formed the Potter Mine deposit, allowing significantly more sulphides to accumulate relative to the other occurrences like the Potterdoal deposit and the Mangan showing.

Chapter 9

Conclusions

9.1 Genetic Summary Of The Potterdoal Deposit

This study provides a new interpretation for the poorly understood tholeiite/komatiite dominated VMS occurrences (e.g. Potterdoal and Potter Mine deposits) of the Kidd-Munro assemblage. Whole rock geochemistry demonstrates an iron tholeiitic affinity for the rocks which host the Potterdoal deposit. These tholeiites have geochemical properties consistent with ocean floor basalts, erupted in a mid-ocean ridge tectonic setting. The Potterdoal deposit was emplaced into this stratigraphy by a hydrothermal system driven by heat from the Munro-Warden Sill which was intruded at a high stratigraphic level. The relatively small size of the deposit probably resulted from the rapid cooling of the sill, and consequent short duration of the hydrothermal system. The cooling of the sill was accelerated by the lack of sufficient stratigraphic cover, along with an efficient convecting hydrothermal system. The primary source of metals for the deposit was the upper portion of the Munro-Warden Sill, as indicated by the high degree of pervasive hydrothermal alteration of gabbros.

A three dimensional interpretation of subsurface geology of the Potterdoal deposit, based largely on new drill core data, shows a typical VMS cross-section,

consisting of a mineralized footwall stockwork zone overlain by an extensive massive sulphide lens, with local ore grade Cu-Zn values. The lower stockwork mineralization is confined to narrow, highly altered joints and fault breccia conduits within the massive Ore Flow gabbros, footwall to the main mineralization. Above the Ore Flow gabbros, the mineralized stockwork rapidly widens into a tectonic breccia which fills the fault scarp structure defined in the paleosurface. Intense chloritic alteration surrounded by a halo of sericitic alteration accompanies the stockwork mineralization, and mass changes observed within these altered rock are consistent with mass change associated with alteration pipes of other VMS deposits. However, it is important to note that the alteration aureole surrounding a typical Potterdoal hydrothermal fault breccia conduit measure only several meters wide, whereas alteration pipes underlying a typical major VMS deposit typically show widths of 100 m. The massive sulphide lens at the top of the tectonic breccia stockwork formed by the wholesale replacement of the tectonic breccia just below the seawater interface, and shows an upward and outward gradation from a Cu-rich core to Zn-rich margins.

Drill core information demonstrates the importance of bedding subparallel thrusting along the Buster Fault, during the Kenoran compressional event (~ 2.6 Ga). This thrusting was responsible for the local repetition of stratigraphically equivalent tholeiitic flows, and has effectively removed the deep footwall rocks originally associated with the Potterdoal deposit.

References

- Arndt, N. T., 1975, Ultramafic rocks of Munro Township and their volcanic setting: Unpub. Ph.D. thesis, University of Toronto, 192 p.
- , 1977, Thick, layered peridotitic-gabbro lava flows in Munro Township, Ontario: *Can. J. Earth Sci.*, v. 14, p. 2620-2637.
- Arndt, N. T., Naldrett, A. J., and Pyke, D. R., 1977, Komatiitic and iron-rich tholeiitic lavas of Munro Township, northeast Ontario: *J. Petrol.*, v. 18, p. 316-369.
- Barrie, C. T., and Davis, D. W., 1990, Timing of magmatism and deformation in the Kamiskotia-Kidd Creek area, Western Abitibi Subprovince, Canada: *Precamb. Res.*, v. 46, p. 217-240.
- Barrie, C. T., Ludden, J. N., and Green, T. H., 1993, Geochemistry of volcanic rocks associated with Cu-Zn and Ni-Cu deposits in the Abitibi Subprovince: *Ec. Geol.*, v. 88, p. 1341-1358.
- Bath, A. C., 1990, Mineral occurrences, deposits, and mines of the Black River-Matheson area: Ontario Geological Survey, Open File Report 5735, p. 336-344.
- Bowins, R. J., and Crocket, J. H., 1994, Sulphur and carbon isotope in Archean banded iron formation: Implication for sulphur sources: *Chemical Geology*, V. 111, p. 307-323.
- Boynton, W. V., 1989, Cosmochemistry of the rare earth elements: Meteorite studies, *in* Henderson, P., ed., *Rare Earth Element Geochemistry*. London, Elsevier, p. 63-114.
- Campbell, I. H., Franklin, J. M., Gorton, M. P., Hart, T. R., and Scott, S. D., 1981, The role of subvolcanic sills in the generation of massive sulphide deposits: *Econ. Geol.*, v. 76, p. 2248-2253.
- Coad, P. R., 1976. The Potter Mine, Ontario, Unpub. M.Sc. thesis. Univ. Toronto. 239p.

- Corfu, F., Jackson, S. L., and Sutcliffe, R. H., 1991, U-Pb ages and tectonic significance of late Archean alkalic magmatism and non-marine sedimentation: Timiskaming Group, southern Abitibi belt, Ontario: *Can. J. Earth Sci.*, v. 28, p. 489-503.
- Corfu, F., Krough, T. E., Kwok, Y. Y., and Jensen, L. S., 1989, U-Pb zircon geochronology in the southwestern Abitibi greenstone belt, Superior Province: *Can. J. Earth Sci.*, v. 26, p. 1747-1763.
- Cotnoir, A., 1993, Granges Inc. Potterdoal option project #535, Report of 1992 geophysical surveys and diamond drilling, Warden and Munro Townships, Larder Lake mining division. 20 p.
- Dept. of Energy, Mines and Resources, 1974, Potterdoal Mine mineral inventory assessment: Mineral Resource Branch, Department of Energy, Mines and Resources. File #503143.
- Epp, M. S., and Crocket, J. H., Geology and geochemistry of the Potterdoal Cu-Zn deposit, Munro Township, Ontario, *in* Hannington, M., Barrie, C. T., and Bleeker, W., eds., *The Giant Kidd Creek Volcanogenic Massive Sulphide Deposit, Western Abitibi Subprovince, Canada: Economic Geology, Monograph 10*, in press.
- Fahrig, W. F., and West, T. D., 1986, Diabase dyke swarms of the Canadian Shield: Geological Survey of Canada, Map 1627A.
- Franklin, J. M., Lydon, J. W., and Sangster, D. F., 1981, *Ec. Geol.*, 75th Anniversary Volume, p. 485-627.
- Fyon, J. A., Breaks, F. W., Heather, K. B., Jackson, S. L., Muir, T. L., Stott, G. M., and Thurston, P. C., 1992, Metallogeny of metallic mineral deposits in the Superior Province of Ontario *in* Ontario Geological Survey Spec. Vol. 4, Pt 2, p. 1091-1103.
- Gates, T. M., and Hurley, P. M., 1973, Evaluation of Rb-Sr dating methods applied to the Matachewan, Abitibi, MacKenzie and Sudbury dike swarms in Canada: *Can. J. Earth Sci.*, v. 10, p. 900-919.
- Goodwin, A. M., and Ridler, R., 1970, The Abitibi orogenic belt: *in* Symposium on Basins and Geosynclines of the Canadian Shield, A.J. Bear (ed.), Geological Survey of Canada, Paper 70-40, p. 1-30.
- Irvine, T. N., and Barager, W. R. A., 1971, A guide to the chemical classification of the common volcanic rocks: *Can. J. of Earth Sci.*, v. 8, p. 523-548.

- Jackson, S. L., and Fyon, J. A., 1991, The western Abitibi subprovince in Ontario *in* Ontario Geological Survey Spec. Vol. 4, Pt 1, p. 404-482
- Jackson, S. L., Fyon, J. A., and Corfu, F., 1994, Review of Archean supracrustal assemblages of the southwest Abitibi greenstone belt in Ontario, Canada: products of microplate interaction within a large-scale plate-tectonic setting: *Precambrian Res.*, v. 65, p. 183-205
- Jacobs, J. W., Korotev, R. L., Blanchard, D. P., and Haskin, L. A., 1977, A well tested procedure for instrumental neutron activation analysis of silicate rocks and minerals: *J. Radioanal. Chem.*, v. 40, p. 93-114.
- Jensen, L.S., 1976, A new cation plot classifying subalkalic volcanic rocks: Ontario Geological Survey, Misc. Paper 66, 22 p.
- Jensen L. S., and Langford, F. F., 1985, Geology and petrogenesis of the Archean Abitibi belt in the Kirkland Lake area, Ontario: Ontario Geological Survey, Misc. Paper 123, 130 p.
- Jolly, W. T., 1980, Development and degradation of Archean lavas, Abitibi area, Canada, in light of major element geochemistry: *J. Petrol.*, v. 21, p. 323-363.
- Johnstone, R. M., 1987, Geology of the Stoughton-Roquemaure group, Beatty and Munro Townships, northeastern Ontario: Unpub. M.Sc. thesis, Univ. Toronto, 290 p.
- , 1991, The geology of the northwestern Black River-Matheson area, District of Cochrane: Ontario Geological Survey, Open File Report 5785, 288 p.
- Lentz, D. R., and Goodfellow, W. D., 1993, Petrology and mass-balance constraints on the origin of quartz-augen schist associated with the Brunswick massive sulfide deposit, Bathurst, New Brunswick: *Can. Mineral.*, v. 31, p. 877-903.
- Leshner, C. M., Goodwin, A. M., Campbell, I. H., and Gorton, M. P., 1986, Trace-element geochemistry of ore-associated and barren, felsic metavolcanic rocks in the Superior Province, Canada: *Can. J. Earth Sci.*, v. 23, p. 222-237.
- Lydon, J. W., 1984, Ore deposit models - 8. Volcanogenic massive sulphide deposits part I: A descriptive model: *Geoscience Canada*, v.11, p. 195-202.
- , 1988, Ore deposit models - 14. Volcanogenic massive sulphide deposits part 2: Genetic models: *Geoscience Canada*, v. 15, p. 43-65.

- MacLean, W. H., and Barrett, T. J., 1993, Lithogeochemical techniques using immobile elements: *J. Expl. Geochem.*, v. 48, p. 109-133.
- MacRae, N. D., 1965, Petrology and geochemistry of ultramafic intrusions in the Abitibi area, Ontario: Unpub. Ph.D. thesis, McMaster University, Hamilton.
- Ontario Dept. of Mines, 1927, Ontario Dept. of Mines Annual Report 36: Part 1, p. 88-89.
- , 1928, Ontario Dept. of Mines Annual Report 37: Part 1, p. 84.
- , 1952, Ontario Dept. of Mines Annual Report 60: Part 8, p. 42-43.
- Pearce, J. A., and Cann, J. R., 1973, Tectonic setting of basic volcanic rocks determined using trace element analyses: *Earth Planet. Sci. Letters*, v. 19, p. 290-300.
- Pirajno, F., 1992, *Hydrothermal Mineral Deposits: Principles and Fundamental Concepts For The Exploration Geologist*. Berlin, Springer-Verlag, 709 p.
- Satterly, J., 1952, Geology of Munro Township, Ontario Department of Mines, Annual Report for 1951, v. 60, Part 8, 60 p. Accompanied by Map 1951-1, scale 1:12000.
- Schwartz, T. C., 1995, Petrology and geochemistry of felsic volcanoclastic rocks along the Sherman Mine road, Temagami Greenstone Belt, Strathy Township, Ontario: Unpub. M.Sc. thesis, McMaster University, 180 p.
- Sigmarsson, O., Hemond, C., Condomines, M., Fourcade, S., and Oskarsson, N., 1991, Origin of silicic magma in Iceland revealed by Th isotopes: *Geology*, v. 19, p. 621-624.
- Sillitoe, R. H., 1985, Ore-related breccias in volcanoplutonic arcs: *Econ. Geol.*, v. 80, p. 1467-1514.
- Spence, C. D., and De Rosen-Spence, A. F., 1975, The place of sulfide mineralization in the volcanic sequence at Noranda, Quebec: *Econ. Geol.*, v. 70, p. 90-101.
- Walker, F. W., Kirouac, J., and Rourke, F. M., 1977, Chart of the nuclides, Knolls Atomic Power Laboratory, Schenectody, N.Y., General Electric Company.

Appendix A

Sample Descriptions and Locations

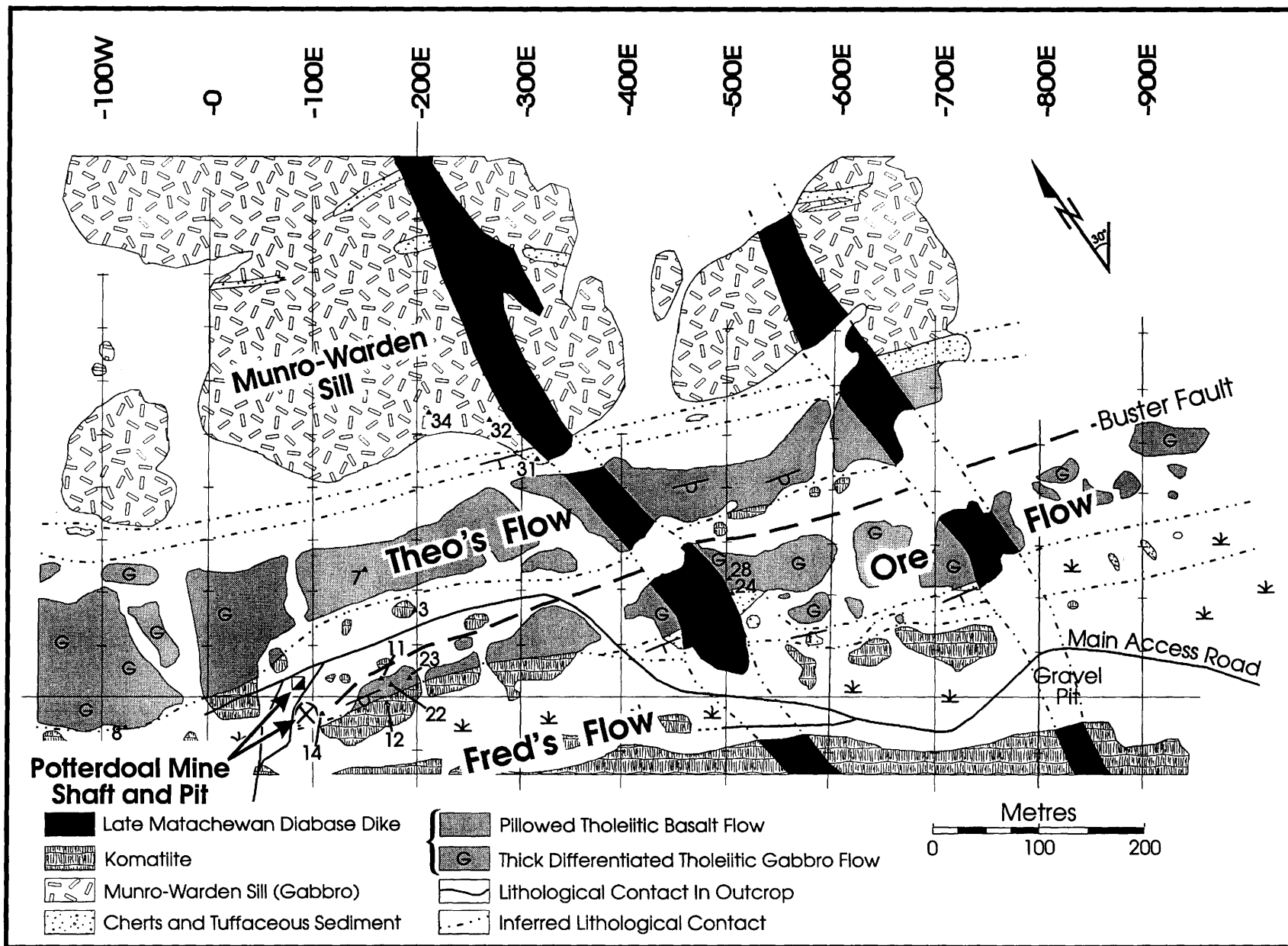
Sample Descriptions and Locations

Samples preceded by “SPD” are surface samples, and are located on the field map shown in Figure A-1. Samples preceded by only “PD” are diamond drill core samples. The number following the “PD” is the drill hole number, and the number after the dash is the depth into the hole (measured in metres) at which the sample was located. Diamond drill core samples are located within abbreviated diamond drill logs summarized in Table A-1.





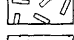
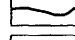
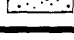
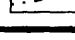
<u>Sample</u>	<u>Rock Type</u>	<u>Alteration</u>
<u>Ore Flow Basalts</u>		
SPD-11	Variolitic basalt	Moderately altered (spilitization)
SPD-14	Massive basalt	Strongly altered (hydrothermal alteration)
SPD-22	Variolitic basalt	Moderately altered (spilitization)
SPD-23	Variolitic basalt	Moderately altered (spilitization)
<u>Ore Flow Gabbros</u>		
SPD-28	Medium grained gabbro	Weakly altered, nearby sulphides (hydrothermal alt.)
PD2-287	Coarse grained gabbro	Relatively fresh (regional metamorphic alteration)
PD4-195	Gabbro	Very strongly altered, most primary texture destroyed (hydrothermal alteration)
PD11-318	Medium grained gabbro	Weak to moderately altered (hydrothermal alt.)
PD12-182	Medium grained gabbro	Strongly altered (hydrothermal alteration)
PD12-188	Coarse grained gabbro	Moderately altered (hydrothermal alteration)
PD12-197	Medium grained gabbro	Moderately altered (hydrothermal alteration)
<u>Theo's Flow Basalts</u>		
SPD-7	Sheeted flow basalt	Moderately altered (spilitization)
SPD-8	Pillowed basalt	Moderately altered (spilitization)

Sample	Rock Type	Alteration
<u>Munro-Warden Sill Gabbros</u>		
SPD-32	Leucogabbro	Weak to moderately altered (hydrothermal alt.)
SPD-34	Leucogabbro	Moderate to strongly altered (hydrothermal alt.)
<u>Komatiites</u>		
SPD-3	Picritic komatiite	Moderately altered (spilitization)
SPD-12	Peridotitic komatiite	Moderately altered (spilitization)
PD1-105	Hyaloclastite	Moderately altered (spilitization)
<u>Tuffs</u>		
SPD-24	Cherty tuff	Weakly altered (regional metamorphic alteration)
SPD-31	Laminated tuff	Weakly altered (regional metamorphic alteration)
PD4-108.5	Laminated tuff	Weakly altered (regional metamorphic alteration)

Figure A-1 Potterdoal area surface sample location map.



Potterdoal Mine
Shaft and Pit

- | | | | |
|---|--------------------------------|---|---|
|  | Late Matachewan Diabase Dike |  | Pillowed Tholeiitic Basalt Flow |
|  | Komatiite |  | Thick Differentiated Tholeiitic Gabbro Flow |
|  | Munro-Warden Sill (Gabbro) |  | Lithological Contact In Outcrop |
|  | Cherts and Tuffaceous Sediment |  | Inferred Lithological Contact |

Metres
0 100 200

Table A-1: Abbreviated diamond drill logs showing sample locations.

Hole ID: PD1 Dip: -60°N Collar Location: 1+00E / 0+75S

From	To	Rock Type	Comments
0.0	5.7	-----	Casing
5.7	105.4	Komatiite	Fred's Flow *** PD1-105 Komatiite Sample
105.4	159.9	Variolitic Basalt	
159.9	171.8	Mineralized Basalt Breccia	Ore Flow Gabbro
171.8	172.0	Fault	Buster Fault
172.0	193.6	Komatiite	Komatiite Overlying Theo's Flow
193.6			End Of Hole

Hole ID: PD2 Dip: -70°N Collar Location: 1+00E / 1+50S

From	To	Rock Type	Comments
0.0	3.0	-----	Casing
3.0	235.8	Komatiite	Fred's Flow
235.8	236.8	Fault	
236.8	238.3	Komatiite	Fred's Flow
238.3	247.6	Variolitic Basalt	Locally brecciated and mineralized
247.6	248.7	Massive Sulphide	
248.7	268.4	Tuff/Chert Breccia	Tectonic Breccia
268.4	291.0	Gabbro	Ore Flow Gabbro *** PD2-287 Ore Flow Gabbro Sample
291.0			End Of Hole

Hole ID: PD4 Dip: -60°N Collar Location: 3+00E / 0+50S

From	To	Rock Type	Comments
0.0	3.5	-----	Casing
3.5	90.8	Komatiite	Fred's Flow
90.8	91.4	Fault	
91.4	93.4	Massive Sulphide	
93.4	159.9	Tuff/Chert Breccia	Tectonic Breccia *** PD4-108.5 Tuff Sample
159.9	234.8	Gabbro	Ore Flow Gabbro *** PD4-195 Ore Flow Gabbro Sample
234.8	235.8	Fault	Buster Fault
235.8	315.0	Basalt	Theo's Flow Basalts
315.0			End Of Hole

Hole ID: PD11 Dip: -65°N Collar Location: 1+00E / 1+29S

From	To	Rock Type	Comments
0.0	1.8	-----	Casing
1.8	285.3	Komatiite	Fred's Flow
285.3	350.0	Gabbro	Ore Flow Gabbro *** PD11-318 Ore Flow Gabbro Sample
350.0			End Of Hole

Hole ID: PD12 Dip: -60°N Collar Location: 2+92E / 1+12S

From	To	Rock Type	Comments
0.0	2.0	-----	Casing
2.0	161.8	Komatiite	Fred's Flow
161.8	162.3	Tuff	
162.3	166.3	Massive Sulphide	
166.3	176.9	Tuff/Chert Breccia	Tectonic Breccia
176.9	206.0	Gabbro	Ore Flow Gabbro ***PD12-182 Ore Flow Gabbro Sample ***PD12-188 Ore Flow Gabbro Sample ***PD12-197 Ore Flow Gabbro Sample
206.0			End Of Hole

Appendix B

Precision and Accuracy Calculations

For XRF and INAA Data

Table B-1: Precision and accuracy calculations for XRF data.

R.V.	—	Recommended value
S.D.	—	Standard deviation about the mean
Prec%	—	Precision or "reproducibility" = (S.D./Mean)*100
Var.	—	Variance = ((X1-R.V.) ² +(X2-R.V.) ² +...+(Xn-R.V.) ²)/n
Dev.	—	Standard deviation about the recommended value = SQRT(Var.)
Accu1.%	—	Accuracy 1 = (Dev./R.V.)*100
Accu2.%	—	Accuracy 2 = (Mean-R.V.)/R.V.*100

Sample	SiO2	TiO2	Al2O3	Fe2O3	MnO	MgO	CaO	K2O	P2O5	Na2O
PCC-1	41.34	0.01	0.46	8.49	0.12	43.76	0.51	0.00	0.01	0.00
PCC-1	41.63	0.00	0.49	8.43	0.11	43.63	0.52	0.00	0.01	0.00
R.V.	41.67	0.01	0.67	8.25	0.12	43.43	0.52	0.00	0.00	0.00
Mean	41.49	0.01	0.48	8.46	0.12	43.70	0.52	0.00	0.01	0.00
S.D.	0.145	0.005	0.015	0.030	0.005	0.065	0.005	0.000	0.000	0.000
Prec. %	0.35	100.00	3.16	0.35	4.35	0.15	0.97	0.00	0.00	0.00
Var.	0.055	0.000	0.038	0.045	0.000	0.074	0.000	0.000	0.000	0.000
Dev.	0.235	0.007	0.196	0.212	0.007	0.273	0.007	0.000	0.010	0.000
Accu1.%	0.56	70.71	29.19	2.57	5.89	0.63	1.36	0.00	0.00	0.00
Accu2.%	-0.44	-50.00	-29.10	2.55	-4.17	0.61	-0.96	0.00	0.00	0.00

Sample	SiO2	TiO2	Al2O3	Fe2O3	MnO	MgO	CaO	K2O	P2O5	Na2O
JB-1A	52.06	1.26	14.51	8.91	0.14	7.85	9.10	1.43	0.25	2.51
JB-1A	51.98	1.27	14.63	9.02	0.14	8.00	9.12	1.42	0.25	2.53
JB-1A	52.13	1.25	14.52	8.93	0.14	8.03	9.15	1.43	0.25	2.54
R.V.	52.16	1.30	14.55	9.10	0.15	7.75	9.23	1.42	0.26	2.74
Mean	52.06	1.26	14.55	8.95	0.14	7.96	9.12	1.43	0.25	2.53
S.D.	0.061	0.008	0.054	0.048	0.000	0.079	0.021	0.005	0.000	0.012
Prec%	0.12	0.65	0.37	0.53	0.00	0.99	0.23	0.33	0.00	0.49
Var.	0.014	0.002	0.003	0.024	0.000	0.050	0.012	0.000	0.000	0.046
Dev.	0.120	0.041	0.054	0.154	0.010	0.224	0.109	0.008	0.010	0.214
Accu1.%	0.23	3.14	0.37	1.70	6.67	2.89	1.18	0.57	3.85	7.80
Accu2.%	-0.20	-3.08	0.02	-1.61	-6.67	2.71	-1.16	0.47	-3.85	-7.79

Sample	SiO2	TiO2	Al2O3	Fe2O3	MnO	MgO	CaO	K2O	P2O5	Na2O
MRG-1	39.23	3.75	8.48	18.06	0.17	13.57	14.66	0.16	0.06	0.82
MRG-1	38.99	3.75	8.44	18.16	0.17	13.62	14.69	0.16	0.07	0.73
R.V.	39.09	3.77	8.46	17.93	0.17	13.55	14.71	0.18	0.06	0.74
Mean	39.11	3.75	8.46	18.11	0.17	13.60	14.68	0.16	0.07	0.78
S.D.	0.120	0.000	0.020	0.050	0.000	0.025	0.015	0.000	0.005	0.045
Prec%	0.31	0.00	0.24	0.28	0.00	0.18	0.10	0.00	7.69	5.81
Var.	0.015	0.000	0.000	0.035	0.000	0.003	0.001	0.000	0.000	0.003
Dev.	0.122	0.020	0.020	0.187	0.000	0.051	0.038	0.020	0.007	0.057
Accu1.%	0.31	0.53	0.24	1.04	0.00	0.38	0.26	11.11	11.79	7.70
Accu2.%	0.05	-0.53	0.00	1.00	0.00	0.33	-0.24	-11.11	8.33	4.73

Table B-1: Precision and accuracy calculations for XRF data (continued).

Sample	Zr	Y	Sr	Rb	Zn	Cu	Ni	
BHVO-1	180	27	404	12	102	137	123	
BHVO-1	179	28	405	12	104	134	119	
R.V.	179	27.6	403	11	105	136	121	
Mean	179.5	27.5	404.5	12.0	103.0	135.5	121.0	
S.D.	0.50	0.50	0.50	0.00	1.00	1.50	2.00	
Prec. %	0.3	1.8	0.1	0.0	1.0	1.1	1.7	
Var.	0.50	0.26	2.50	1.00	5.00	2.50	4.00	
Dev.	0.71	0.51	1.58	1.00	2.24	1.58	2.00	
Accu1.%	0.40	1.85	0.39	9.09	2.13	1.16	1.65	
Accu2.%	0.28	-0.36	0.37	9.09	-1.90	-0.37	0.00	
Sample	Zr	Y	Sr	Rb	Sample	Zn	Cu	Ni
G-2	313	12	492	169	BIR-1	65	127	157
G-2	319	12	488	168	BIR-1	63	124	158
R.V.	309	11	478	170	R.V.	71	126	166
Mean	316.0	12.0	490.0	168.5	Mean	64.0	125.5	157.5
S.D.	3.0	0.0	2.0	0.5	S.D.	1.0	1.5	0.5
Prec. %	0.9	0.0	0.4	0.3	Prec. %	1.6	1.2	0.3
Var.	58.00	1.00	148.00	2.50	Var.	50.00	2.50	72.50
Dev.	7.62	1.00	12.17	1.58	Dev.	7.07	1.58	8.51
Accu1.%	2.46	9.09	2.55	0.93	Accu1.%	9.96	1.25	5.13
Accu2.%	2.27	9.09	2.51	-0.88	Accu2.%	-9.86	-0.40	-5.12
Sample	Zr	Y	Sr	Rb	Sample	Zn	Cu	Ni
BE-N	268	28	1378	48	MRG-1	189	129	191
BE-N	266	30	1374	47	MRG-1	191	133	190
R.V.	265	30	1370	47	R.V.	191	134	193
Mean	267.0	29.0	1376.0	47.5	Mean	190.0	131.0	190.5
S.D.	1.0	1.0	2.0	0.5	S.D.	1.0	2.0	0.5
Prec. %	0.4	3.4	0.1	1.1	Prec. %	0.5	1.5	0.3
Var.	5.00	2.00	40.00	0.50	Var.	2.00	13.00	6.50
Dev.	2.24	1.41	6.32	0.71	Dev.	1.41	3.61	2.55
Accu1.%	0.84	4.71	0.46	1.50	Accu1.%	0.74	2.69	1.32
Accu2.%	0.75	-3.33	0.44	1.06	Accu2.%	-0.52	-2.24	-1.30
Sample	Zr	Y	Sr	Rb	Sample	Zn	Cu	Ni
NIM-G	295	144	11	316	NIM-P	105	18	563
NIM-G	298	141	10	319	NIM-P	103	17	564
R.V.	300	143	10	320	R.V.	100	18	560
Mean	296.5	142.5	10.5	317.5	Mean	104.0	17.5	563.5
S.D.	1.5	1.5	0.5	1.5	S.D.	1.0	0.5	0.5
Prec. %	0.5	1.1	4.8	0.5	Prec. %	1.0	2.9	0.1
Var.	14.50	2.50	0.50	8.50	Var.	17.00	0.50	12.50
Dev.	3.81	1.58	0.71	2.92	Dev.	4.12	0.71	3.54
Accu1.%	1.27	1.11	7.07	0.91	Accu1.%	4.12	3.93	0.63
Accu2.%	-1.17	-0.35	5.00	-0.78	Accu2.%	4.00	-2.78	0.63

Table B-2: Precision and accuracy calculations for INAA data. Elemental determinations for the SCo-1 and MRG-1 standards where calculated relative to the BHVO-1 standard.

R.V. — Recommended value
 S.D. — Standard deviation about the mean
 Prec% — Precision or "reproducibility" = (S.D./Mean)*100
 Var. — Variance = ((X1-R.V.)²+(X2-R.V.)²+...+(Xn-R.V.)²)/n
 Dev. — Standard deviation about the recommended value = SQRT(Var.)
 Accu1.% — Accuracy 1 = (Dev./R.V.)*100
 Accu2.% — Accuracy 2 = (Mean-R.V)/R.V.*100

Sample	Sm	La	Nd	Lu	Yb	Sc	Ce	Tb	Hf	Rb	Co	Ta	Eu
SCo-1	5.63	31.52	33.29	0.47	2.63	13.61	147.07	2.02	8.89	149.66	17.05	1.53	1.92
SCo-2	4.94	29.72	34.78	0.47	2.92	14.44	124.51	1.64	7.95	56.43	17.12	1.04	1.75
SCo-3	5.57	29.91	33.77	0.44	2.46	13.76	74.66	1.46	6.02	269.55	13.92	1.16	1.48
R.V.	5.30	29.50	26.00	0.34	2.27	10.80	62.00	0.70	4.60	112.00	10.50	0.92	1.19
Mean	5.38	30.38	33.95	0.46	2.67	13.93	115.41	1.70	7.62	158.55	16.03	1.25	1.72
S.D.	0.310	0.808	0.621	0.016	0.191	0.364	30.250	0.235	1.196	87.235	1.491	0.211	0.178
Prec%	5.77	2.66	1.83	3.55	7.16	2.61	26.21	13.77	15.69	55.02	9.30	16.93	10.40
Var.	0.103	1.435	63.534	0.014	0.195	9.959	3767.996	1.062	10.561	9776.546	32.815	0.150	0.308
Dev.	0.321	1.198	7.971	0.119	0.442	3.156	61.384	1.030	3.250	98.876	5.728	0.387	0.555
Accu1.%	6.05	4.06	30.66	35.03	19.45	29.22	99.01	147.21	70.65	88.28	54.56	42.11	46.63
Accu2.%	1.52	3.00	30.56	34.70	17.54	29.03	86.15	143.34	65.69	41.56	52.68	35.33	44.16
Sample	Sm	La	Nd	Lu	Yb	Sc							
MRG-1	4.46	9.88	13.37	0.09	0.62	44.80							
MRG-2	4.03	9.65	10.97	0.11	0.72	42.20							
MRG-3	4.60	9.29	13.82	0.07	0.38	44.25							
R.V.	4.5	9.8	19.2	0.12	0.6	55							
Mean	4.36	9.60	12.72	0.09	0.57	43.75							
S.D.	0.244	0.241	1.250	0.013	0.142	1.117							
Prec%	5.59	2.51	9.83	14.16	24.84	2.55							
Var.	0.079	0.097	43.578	0.001	0.021	127.809							
Dev.	0.280	0.311	6.601	0.032	0.145	11.305							
Accu1.%	6.23	3.17	34.38	26.50	24.14	20.55							
Accu2.%	-3.07	-2.01	-33.76	-24.23	-4.57	-20.45							

Table B-3: Precision calculations for triplicate samples.

S.D. — Standard deviation about the mean
 Prec% — Precision or "reproducibility" = (S.D./Mean)*100

Samples	Sm	La	Nd	Lu	Yb	Sc	Ce	Tb	Hf	Co	Ta	Eu
SPD-22-1	3.97	9.10	13.37	0.38	2.32	24.56	8.11	0.35	1.54	43.51	0.26	1.12
SPD-22-2	3.77	8.76	10.70	0.34	2.05	26.37	8.77	0.49	1.83	44.28	0.34	1.15
SPD-22-3	3.31	6.50	15.01	0.29	2.82	24.72	15.98	0.70	2.07	46.27	0.28	1.18
Mean	3.68	8.12	13.02	0.34	2.40	25.22	10.95	0.51	1.81	44.68	0.29	1.15
S.D.	0.28	1.15	1.78	0.04	0.32	0.82	3.56	0.14	0.21	1.16	0.03	0.02
Prec%	7.53	14.21	13.65	10.72	13.40	3.26	32.52	27.74	11.87	2.60	11.90	1.97